Theory of transport in lowdimensional nanostructures

Wozny, Simon

2025

Theory of transport in lowdimensional nanostructures

SIMON WOZNY
DEPARTMENT OF PYSICS | FACULTY OF ENGINEERING | LUND UNIVERSITY

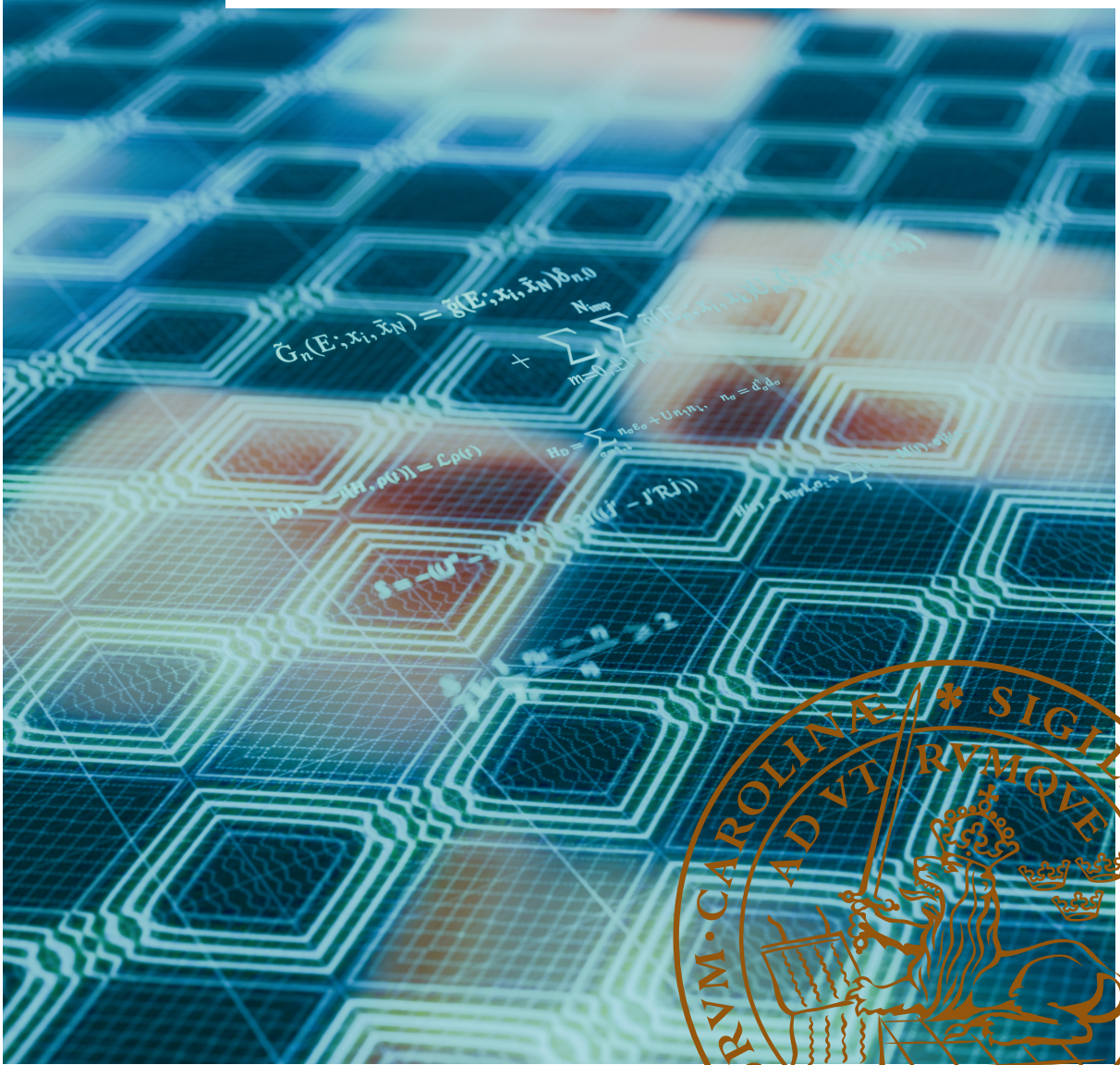

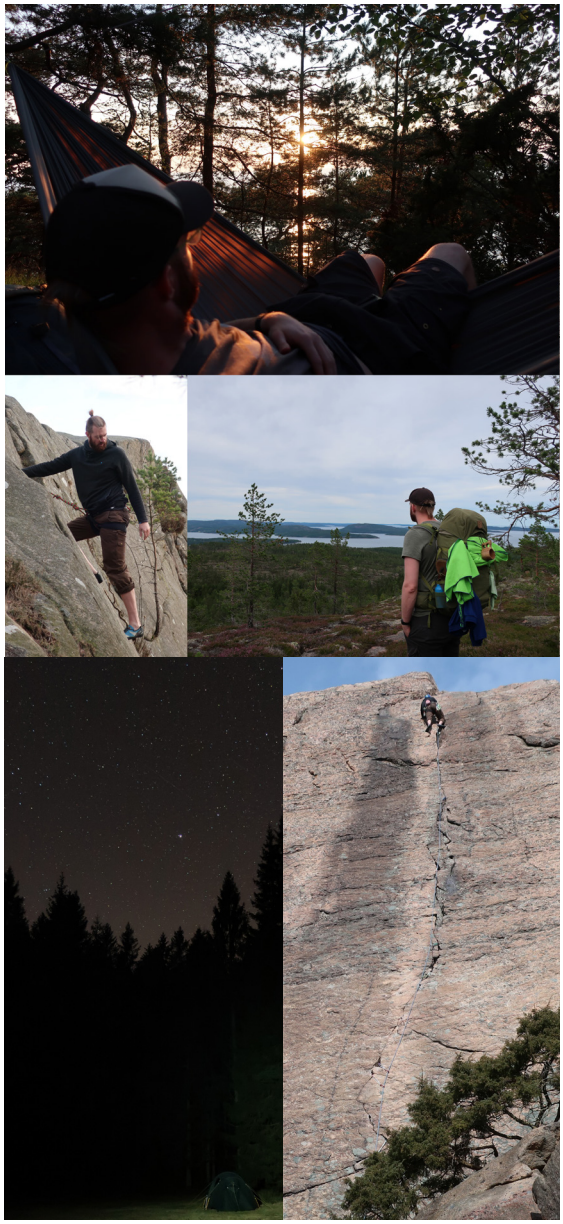

In my free time I enjoy hiking, climbing and all being out in nature. Here are a few highlights from the adventures during my PhD time.

Printed by Media-Tryck, Lund 2025 NORDIC SWAN ECOLABEL 3041 0903

LUND UNIVERSITY

Faculty of Engineering
Department of Pysics
Division of Solid State Physics

ISBN 978-91-8104-511-6

Theory of transport in lowdimensional nanostructures

Theory of transport in lowdimensional nanostructures

by Simon Wozny

LUND
UNIVERSITY

Thesis for the degree of Doctor of Philosophy
To be presented, with the permission of the Faculty of Engineering of Lund University, for public criticism at the Rydberg lecture hall (Rydbergsalen, H418) at the Department of Pysics on
Friday, the 13th of June 2025 at 13:00.

Thesis advisor: Prof. Martin Leijnse
Supporting advisor: Prof. Peter Samuelsson

Faculty opponent: Fabio Taddei, Senior researcher at CNR-NANO & NEST, Scuola Normale Superiore, Pisa, Italy

Organization
LUND UNIVERSITY

Department of Pysics
Box 124
SE–221 00 LUND
Sweden

Document name
DOCTORAL DISSERTATION

Date of disputation
2025-06-13

Sponsoring organization

Author(s)
Simon Wozny

Title and subtitle
Theory of transport in lowdimensional nanostructures

Abstract
This thesis theoretically investigates electronic transport in different low dimensional nanostructures. The miniaturization of electronics means that we reach a limit where quantum effects play a role in electronic devices. To understand and improve electronics at this level it is important to understand the transport properties. Excellent control over the nanostructures also makes them a great platform for exploring fundamental physics aspects.

In this thesis we investigate two different types of low dimensional system. It contains three peer-reviewed studies that have been published in scientific journals.

Papers I and II investigate different quantum dot systems coupled to electronic leads. To treat theses systems we use master equations and counting statistics, which are introduced before summarizing the papers. In paper I we explore a parallel double quantum dot and its application as a charge sensor. We compare to a more conventional single dot charge sensing setup and show that the double dot sensor is not limited by temperature. Paper II investigates a single spinful quantum dot in a thermoelectric engine configuration. Here we investigate the so-called thermodynamic uncertainty relations, a trade off between power, fluctuations and efficiency of the engine. In principle, including transport processes up to cotunneling order allows for violations of these relations. However, in the heat engine regime we cannot find violations at the maximum the power point of the engine.

Paper III investigates edge states in two dimensional topological insulators. In these systems the quantum spin Hall effect leads to so-called helical edge states that are robust to scattering on non-magnetic impurites. We investigate the density of states and transmission though these edge states in the presence of rotating magnetic impurites. We use Green's functions and scattering theory, which are both introduced in the preceding sections. We identify different driving regimes and find that the electric potential can not screen the imputities in a way that prevents backscattering.

Key words
quantum transport, master equations, quantum thermodynamics, quantum dot, quantum dot thermoelectric engine, topological insulators, impurities, greens function

Classification system and/or index terms (if any)

Supplementary bibliographical information

Language
English

ISSN and key title

ISBN
978-91-8104-511-6 (print)
978-91-8104-512-3 (electronic)

Recipient's notes

Number of pages
143

Price

Security classification

Theory of transport in lowdimensional nanostructures

by Simon Wozny

LUND
UNIVERSITY

A doctoral thesis at a university in Sweden takes either the form of a single, cohesive research study (monograph) or a summary of research papers (compilation thesis), which the doctoral student has written alone or together with one or several other author(s).

In the latter case the thesis consists of two parts. An introductory text puts the research work into context and summarizes the main points of the papers. Then, the research publications themselves are reproduced, together with a description of the individual contributions of the authors. The research papers may either have been already published or are manuscripts at various stages (in press, submitted, or in draft).

Cover illustration front: Artistic illustration using simulation results and formulas from the thesis by Alina Wozny

Cover illustration back: Collage of pictures from some adventures during my PhD time

Diviaion of Solid State Physics
Department of Pysics
Faculty of Engineering
Lund University

Box 124
SE–221 00 LUND
Sweden

ISBN: 978-91-8104-511-6 (print)
ISBN: 978-91-8104-512-3 (electronic)

Printed in Sweden by Media-Tryck, Lund University, Lund 2025

Dedicated to my family
Für meine Familie

Contents

List of publications (with author contributions)

This thesis is based on the following publications, referred to by their Roman numerals:

I **Metastability and quantum coherence-assisted sensing in interacting parallel quantum dots**

S. Matern, K. Macieszczak, **S. Wozny**, M. Leijnse
Physical Review B 107, 125424 (2023)
I participated in developing the theory for section V and was responsible for the signal and noise simulations in that section. I took part in writing the respective sections and appendices of the manuscript. I also read and commented on the remaining parts of the paper and discussed them with the other authors.

II **Current noise in quantum dot thermoelectric engines**

S. Wozny, M. Leijnse
Physical Review B 111, 075422 (2025)
I was main responsible for developing the theory, simulations and writing the manuscript.

III **Dynamic impurities in two-dimensional topological-insulator edge states**

S. Wozny, M. Leijnse, S. I. Erlingsson
Physical Review B 104, 205418 (2021)
I was main responsible for developing the theory, simulations and writing the manuscript.

Acknowledgments

In the last years I have encountered many helpful people and they are ultimately the reason why this work exists. Here I would like to like to thank the most important people that I had the pleasure to share my time with.

First I would like to thank my supervisor Martin. You for took me in for the master thesis and even allowed me to stick around and be one of your PhD students. I have not only learned a lot of physics from you, but also many other things about academic life and life in general. Thank you for keeping an open door and making time for me, when it was needed.

I also want to thank my co-supervisor Peter. Your sometimes slightly anarchistic view on university life was greatly appreciated.

Another thank you goes to all collaborators, in particular to Siggi. You were basically with me from my bachelor thesis time until now and I am grateful for the support and encouraging words throughout this time.

Thank you to all (former) members of the group: Florinda, Martin J., Ruben, Thanos, Stephanie, Max, Konstantin, Morten, Ola, Viktor, William, Ferdinand, Elna, Alva, Agnes, Quinn. Be it group meetings, coffee breaks, group barbecues, after works, without you I wouldn't have made it. Having a good group of people around to discuss physics and many things beyond that really made the time what it was.

While the group was quite big, it was of course not all of FTF. Thank you to everyone else at FTF (current and former) that made coming to the office more than coming to work. Thank you for lunches in the sun, freezing in k-space and some other shenanigans. Here I also want to include the MatFys and NanoLund people that I had the pleasure to hang out with.

Of course there is not only work. However, I was lucky enough to meet a group of people there, that I could spend my time with in other exciting ways. Thank you to the whole climbing gang, Stephanie, Bengt, Jason, David, Ville, Jonatan. With you climbing turned into a part of my life that I don't want to miss. I'm looking forward to many more adventures with you! Another shout out goes to the golfers (we play golf!). I might have learned more while golfing with you than studying and it certainly played a large role in staying sane in crazy times.

Going beyond my time in Sweden, I would also like to thank the friends I made before and during my studies. There are way to many to name all of them, so here I'll just name some groups and a few specific ones: my flatmates from Konstanz, specifically Jan, Lu and Eva, the physics gang and Firlefanz. Matthis, thank you for always being there for me and

giving me a place to stay every year. And finally Max, thanks for being there since before I could think. You all helped me in one way or another to get me to where I am now.

Thank you also to my family. Mama und Papa, danke, dass ihr es mir so leicht gemacht habt zu tun was ich will.

Last, but not least I would like to thank Franzi for everything! Without you I would not be who and where I am today and I certainly couldn't enjoy hiking, vacationing and simply existing nearly as much as I can with you! Thank you for taking care of me!

Abstract

This thesis theoretically investigates electronic transport in different low dimensional nanostructures. The miniaturization of electronics means that we reach a limit where quantum effects play a role in electronic devices. To understand and improve electronics at this level it is important to understand the transport properties. Excellent control over the nanostructures also makes them a great platform for exploring fundamental physics aspects.

In this thesis we investigate two different types of low dimensional system. It contains three peer-reviewed studies that have been published in scientific journals.

Papers I and II investigate different quantum dot systems coupled to electronic leads. To treat theses systems we use master equations and counting statistics, which are introduced before summarizing the papers. In paper I we explore a parallel double quantum dot and its application as a charge sensor. We compare to a more conventional single dot charge sensing setup and show that the double dot sensor is not limited by temperature. Paper II investigates a single spinful quantum dot in a thermoelectric engine configuration. Here we investigate the so-called thermodynamic uncertainty relations, a trade off between power, fluctuations and efficiency of the engine. In principle, including transport processes up to cotunneling order allows for violations of these relations. However, in the heat engine regime we cannot find violations at the maximum the power point of the engine.

Paper III investigates edge states in two dimensional topological insulators. In these systems the quantum spin Hall effect leads to so-called helical edge states that are robust to scattering on non-magnetic impurites. We investigate the density of states and transmission though these edge states in the presence of rotating magnetic impurites. We use Green's functions and scattering theory, which are both introduced in the preceding sections. We identify different driving regimes and find that the electric potential can not screen the imputities in a way that prevents backscattering.

Popular summary in English

Contrary to what teachers used to say, we are carrying a calculator with us at almost all times. With the computing power of many times what was used for the moon landing our mobile phones are more than overpowered for double and triple checking the calculations we do in our heads. This power is to a large extent based on our ability to create smaller and smaller electric circuits and components. We are reaching length scales, where important parts of these components are only made up of a few atoms. At these length scales the classical picture of an electric current is not necessarily a full description of what is happening anymore. We have to take into account quantum mechanical effects to fully understand what is happening. Quantum mechanics is the theory used to described the strange world of single electrons and atoms. Of course, this can also be turned around: the ability to create and control tiny systems allows us to look for new and interesting quantum mechanical effects that we would not see otherwise, and perhaps use these effects to make better devices. In this thesis we theoretically investigate two examples of what can happen when the systems get small in all three or only one spatial dimension, respectively.

To make this summary a little more fun, we will tell a story about electrons and how they travel the world. Electrons share a surprising amount of properties with us humans. For example, they have a strong desire for personal space. They are negatively charged, so they do not like to be close to each other. This is called *Coulomb repulsion*. When the electrons go on vacation to a nice little tropical island, the first one hops on it quite easily. The second electron however will need a lot of convincing to share the space with the one that is already there. We call these little islands *quantum dots*. The larger landmasses, where the electrons spend their non-vacation time, are the *electric contacts* and an incredibly large amount of electrons lives on these contacts. When two of these big landmasses are close to the island, some electrons will occasionally jump onto the island, this is the famous *tunnel effect*. Sometimes they also hop to the other side, as you can see in Fig. A. If enough electrons jump across in one direction, we have a current that we can measure. The current

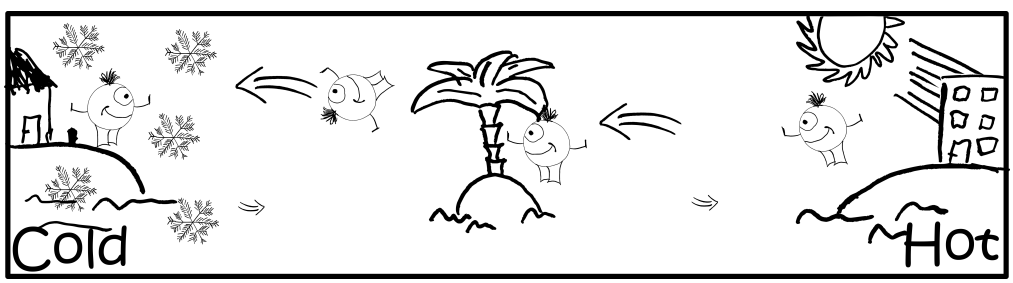

Figure A: Electrons hopping between main landmasses, cold (left) and hot (right), and the island in the middle.

can depend on many things, for example how far it is between the island and the main land, so how easy it is for the electrons to jump. This is called the *tunnel coupling*. Other factors can be how high the island is, the energy of the so-called *dot level*, and also how many electrons are on the main land, the *chemical potential* of the contact. When one of the main landmasses has a lot more electrons on it, electrons on the island are more likely to jump to the less populated side. The difference in population between the main landmasses is called *potential difference* or *voltage*.

We can modify this setting in many ways. What happens if we put two islands between the main lands? This is called a *double quantum dot*. How does this setup react, if we slightly alter the distance to the main land or the height of the islands? This corresponds to changing the tunnel couplings and the dot level, respectively. By sitting on the main land and counting how many electrons come from the island, can we learn something about a third island, that sits close by? If we for example find out, whether there are electrons on the third island, this is called *charge sensing*. This is the topic of paper I, where we investigate a parallel double dot and potential applications as a charge sensor.

So far we have not really cared about the weather. Which way will electrons go if it is very hot on one side of the island and really cold on the other, like the situation in Fig. A? If we can convince electrons to jump to the side with more electrons, we have used *heat* from the hot side to do *electrical work*. This is the concept of a *heat engine*. What if we bring the island and mainlands close enough together, so two electrons can shout at each other and coordinate their jumps, or one of them can jump twice in a very short time? The processes that involve two coordinated jumps are called *cotunneling* events. Allowing these arrangements between electrons does not only change how many electrons jump on average, the *current*, but also how the number of electrons that jump fluctuates around the average This is called the *noise*. It also affects the *efficiency* of the heat engine. In paper II we investigate these effects and also look at a trade-off between the current, noise and the efficiency in the so-called *thermodynamic uncertainty relations*.

Of course, not all electrons hang out close to these little island in the sea all the time. Some of them have regular jobs and have to commute along a coastal highway, the sea on one side and a impassable landscape on the other, as sketched in Fig. B. The highway also has somewhat special traffic rules: in one direction only blue cars are allowed and in the other direction only red cars. They call this rule *spin-momentum locking* and the countries where that happens *topological insulators*. In these very special countries the electrons are also very environmentally friendly and have to carpool. They also have somewhat funny cars. Depending on which of the seats in the car are occupied the color of the car is either red or blue. This property is called the *spin projection* and determines which way the electrons are allowed to go. When the car hits a speed bump, they call them *magnetic impurities*, the electrons are sometimes thrown up from their seats. If after this *scattering event* they sit in different places the car can change color. If they hit a speed bump on the highway and

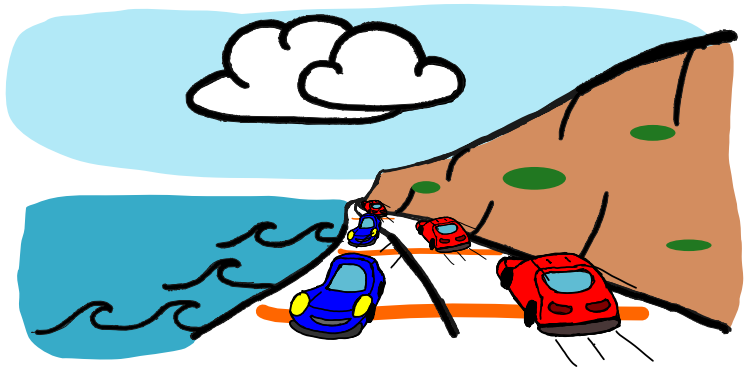

Figure B: Illustration of the coastal highway with the strange traffic rules: red cars can only go on the right, blue cars on the left in the opposite directions. The speed bumps are drawn in orange.

the car changes color they of course have to turn around. This can make the traffic quite challenging. If a car enters on one end of the coastal highway, the likelihood of making it to the other side is called the *transmission*. In paper III we look at how the speed bumps affect the traffic and how likely it is for electrons to arrive where they had planned to go. And since that is not strange enough already, we also let the speed bumps rotate.

With this thesis we hope to contribute to the understanding of the travel habits of electrons, so they can be used in this strange and wonderful quantum world that we and the electrons live in. The vacation and car pooling habits of electrons could in the future be used in many technical applications. From using quantum effects to make existing electronics more efficient, to using them to measure things we could not before or even develop entirely new types of computers, a huge number of things seem possible.

Populärwissenschaftliche Zusammenfassung auf Deutsch

Im Gegensatz zu dem, was Lehrer früher sagten, tragen wir fast immer einen Taschenrechner bei uns. Mit einer Rechenleistung, die ein Vielfaches dessen beträgt, was für die Mondlandung verwendet wurde, sind unsere Mobiltelefone für das Überprüfen unserer Kopfrechenaufgaben, mehr als ausreichend. Diese Leistung beruht zu einem großen Teil auf unserer Fähigkeit, immer kleinere elektrische Schaltkreise und Komponenten herzustellen. Wir erreichen Größenskalen, bei denen wichtige Teile dieser Komponenten nur noch aus wenigen Atomen bestehen. Bei diesen Größenskalen ist das klassische Bild eines elektrischen Stroms nicht mehr unbedingt eine vollständige Beschreibung des Geschehens. Wir müssen quantenmechanische Effekte berücksichtigen, um die Vorgänge vollständig zu verstehen. Die Quantenmechanik ist die Theorie, die verwendet wird, um die seltsame Welt der einzelnen Elektronen und Atome zu beschreiben. Natürlich lässt sich dies auch umkehren: Die Fähigkeit, winzige Systeme zu schaffen und zu kontrollieren, ermöglicht es uns, nach neuen und interessanten quantenmechanischen Effekten zu suchen, die wir sonst nicht sehen würden. Vielleicht lassen sich diese Effekte auch nutzen, um bessere Geräte zu bauen. In dieser Arbeit untersuchen wir theoretisch zwei Beispiele dafür, was passieren kann, wenn die Systeme in allen drei bzw. nur einer räumlichen Dimension klein werden.

Um diese Zusammenfassung ein wenig unterhaltsamer zu gestalten, erzählen wir eine Geschichte über Elektronen und wie sie durch die Welt reisen. Elektronen haben überraschend viele Eigenschaften mit uns Menschen gemeinsam. Zum Beispiel haben sie ein starkes Bedürfnis nach persönlichem Freiraum. Da sie negativ geladen sind, stehen sie nicht gern dicht beieinander. Dies wird als *Coulomb-Abstoßung* bezeichnet. Wenn die Elektronen auf eine nette kleine tropische Insel in den Urlaub fahren, hüpft das erste Elektron ganz einfach darauf. Das zweite Elektron braucht jedoch viel Überzeugungsarbeit, um den Platz mit dem bereits vorhandenen Elektron zu teilen. Wir nennen diese kleinen Inseln *Quantenpunkte*. Die größeren Landmassen, auf denen die Elektronen ihre Nichturlaubszeit verbringen, sind die *elektronischen Kontakte*. Auf diesen Kontakten lebt eine unglaublich große Anzahl von

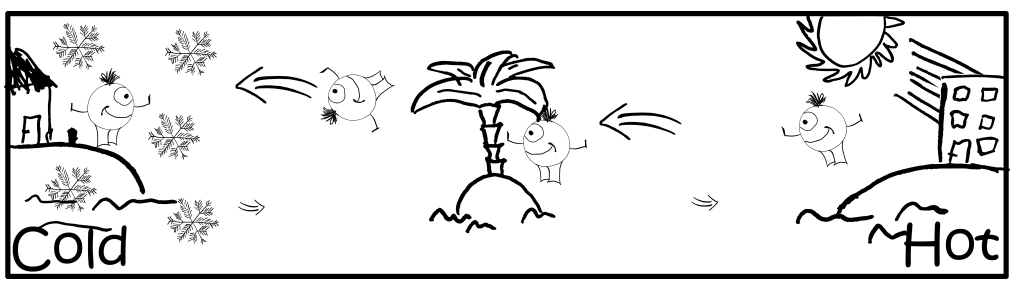

Abbildung A: Elektronen hüpfen zwischen den kalten (links) und heißen (rechts) Hauptlandmassen und der Insel in der Mitte.

Elektronen. Wenn sich zwei dieser großen Landmassen in der Nähe der Insel befinden, springen gelegentlich einige Elektronen auf die Insel, dies ist der berühmte *Tunneleffekt*. Manchmal springen sie auch auf die andere Seite, wie man in Abb. A sehen kann. Wenn genügend Elektronen in eine Richtung springen, entsteht ein Strom, den wir messen können. Der Strom kann von vielen Dingen abhängen, z. B. davon, wie weit die Insel vom Festland entfernt ist, also wie leicht es für die Elektronen ist, zu springen. Dies nennt man die *Tunnelkopplung*. Weitere Faktoren sind die Höhe der Insel, die Energie des so genannten *Punktlevels*, und auch die Anzahl der Elektronen auf dem Festland, das chemische Potenzial des Kontakts. Wenn sich auf einer der Hauptlandmassen viel mehr Elektronen befinden, springen die Elektronen auf der Insel mit größerer Wahrscheinlichkeit auf die weniger bevölkerte Seite. Der Unterschied in der Bevölkerung zwischen den Hauptlandmassen wird als *Potentialdifferenz* oder *Spannung* bezeichnet.

Wir können die Ausgangssituation auf viele Arten verändern. Was passiert, wenn wir zwei Inseln zwischen die Hauptländer setzen? Das wird als *Doppelquantenpunkt* bezeichnet. Wie reagiert diese Anordnung, wenn wir den Abstand zum Hauptland oder die Höhe der Inseln leicht verändern? Dies entspricht einer Änderung der Tunnelkopplungen bzw. des Punktlevels. Wenn wir auf dem Festland sitzen und zählen, wie viele Elektronen von der Insel kommen, können wir dann etwas über eine dritte Insel erfahren, die sich in der Nähe befindet? Wenn wir zum Beispiel herausfinden, ob sich auf der dritten Insel Elektronen befinden, nennt man das einen *Ladungssensor*. Dies ist das Thema des Artikels I, in dem wir einen parallelen Doppelpunkt und mögliche Anwendungen als Ladungssensor untersuchen.

Bislang haben wir uns nicht wirklich um das Wetter gekümmert. Welchen Weg werden die Elektronen einschlagen, wenn es auf der einen Seite der Insel sehr heiß und auf der anderen Seite sehr kalt ist, wie in Abb. A? Wenn wir die Elektronen überzeugen können, auf die Seite mit mehr Elektronen zu springen, haben wir die Wärme der heißen Seite genutzt, um elektrische Arbeit zu verrichten. Dies ist das Konzept eines Wärmemotors. Was wäre, wenn wir die Insel und das Festland nahe genug zusammenbringen, so dass sich zwei Elektronen gegenseitig absprechen und ihre Sprünge koordinieren können, oder eines von ihnen in sehr kurzer Zeit zweimal springen kann? Die Prozesse, bei denen zwei koordinierte Sprünge stattfinden, werden als *cotunneling*-Ereignisse bezeichnet. Wenn man diese Anordnungen zwischen Elektronen zulässt, ändert sich nicht nur die durchschnittliche Anzahl der springenden Elektronen, der *Strom*, sondern auch das *Rauschen* um diesen Mittelwert. Das Rauschen wird auch als *Fluktuationen* bezeichnet. Es wirkt sich auch auf den *Wirkungsgrad* der Wärmekraftmaschine aus. In Papier II untersuchen wir diese Effekte und betrachten auch ein Zusammenspiel zwischen dem Strom, dem Rauschen und dem Wirkungsgrad in den sogenannten *thermodynamischen Unschärferelationen*.

Natürlich halten sich nicht alle Elektronen die ganze Zeit in der Nähe dieser kleinen Insel im Meer auf. Einige von ihnen haben einen festen Arbeitsplatz und müssen entlang einer Küstenstraße pendeln, mit dem Meer auf der einen und einer unwegsamen Landschaft

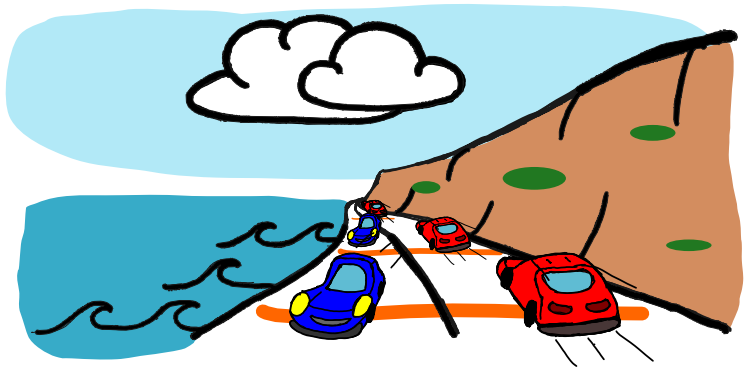

Abbildung B: Illustration der Küstenautobahn mit den seltsamen Verkehrsregeln: rote Autos dürfen nur rechts fahren, blaue Autos links in die entgegengesetzte Richtung. Die Bodenwellen sind orange eingezeichnet.

auf der anderen Seite, wie in Abb. B skizziert. Auf dem Highway gelten auch besondere Verkehrsregeln: In der einen Richtung dürfen nur blaue Autos fahren, in der anderen nur rote. Man nennt diese Regel *Spin-Impuls-Kopplung* und die Länder, in denen das passiert, *topologische Isolatoren*. In diesen ganz besonderen Ländern sind die Elektronen auch sehr umweltbewusst und müssen Fahrgemeinschaften bilden. Sie haben auch etwas komische Autos. Je nachdem, welche Sitze im Auto besetzt sind, ist die Farbe des Autos entweder rot oder blau. Diese Eigenschaft wird als *Spinprojektion* bezeichnet und bestimmt, in welche Richtung sich die Elektronen bewegen dürfen. Wenn das Auto auf eine Bodenwelle stößt, man nennt sie *magnetische Verunreinigungen*, werden die Elektronen manchmal von ihren Sitzen hochgeschleudert. Wenn sie sich nach diesem *Streuungsereignis* an verschiedenen Orten niederlassen, kann das Auto seine Farbe ändern. Wenn sie auf der Autobahn auf eine Bodenwelle stoßen und das Auto seine Farbe ändert, müssen sie natürlich umdrehen. Das kann den Verkehr ziemlich herausfordernd machen. Wenn ein Auto an einem Ende der Küstenautobahn einfährt, wird die Wahrscheinlichkeit, es auf die andere Seite zu schaffen, als *Transmission* bezeichnet. In Papier III sehen wir uns an, wie sich die Bodenwellen auf den Verkehr auswirken und wie wahrscheinlich es ist, dass die Elektronen dort ankommen, wo sie eigentlich hinwollen. Und weil das noch nicht seltsam genug ist, lassen wir die Bodenwellen auch noch rotieren.

Mit dieser Arbeit hoffen wir, einen Beitrag zum Verständnis der Reisegewohnheiten von Elektronen zu leisten, damit sie in dieser seltsamen und wunderbaren Quantenwelt, in der wir und die Elektronen leben, genutzt werden können. Die Urlaubs- und Fahrgemeinschaftsgewohnheiten von Elektronen könnten in Zukunft in vielen technischen Anwendungen genutzt werden. Von der Nutzung von Quanteneffekten, um die bestehende Elektronik effizienter zu machen, bis hin zur Verwendung von Quanteneffekten, um Dinge zu messen, die wir bisher nicht messen konnten, oder sogar zur Entwicklung völlig neuer Arten von Computern - vieles scheint möglich.

Populärvetenskaplig sammanfattning på svenska

Till skillnad från vad lärarna brukade säga har vi nästan alltid en miniräknare med oss. Med en datorkraft som är många gånger större än den som användes vid månlandningen räcker våra mobiltelefoner mer än väl till för att dubbel- och trippelkolla de beräkningar vi gör i huvudet. Denna prestanda beror till stor del på vår förmåga att tillverka allt mindre elektriska kretsar och komponenter. Vi håller på att nå längdskalor där viktiga delar av dessa komponenter består av endast några få atomer. På dessa längdskalor är den klassiska bilden av en elektrisk ström inte längre nödvändigtvis en fullständig beskrivning av vad som händer. Vi måste ta hänsyn till kvantmekaniska effekter för att till fullo förstå processerna. Kvantmekanik är den teori som används för att beskriva den märkliga värld som enskilda elektroner och atomer lever i. Naturligtvis kan detta ses från det omvända perspektivet: Möjligheten att skapa och kontrollera små system gör att vi kan leta efter nya och intressanta kvantmekaniska effekter som vi annars inte skulle se, och kanske använda dessa effekter för att förbättra eller uppfinna nya komponenter. I den här artikeln undersöker vi teoretiskt två exempel på vad som kan hända när systemen blir små i alla tre eller bara en rumslig dimension.

För att göra denna sammanfattning lite mer underhållande berättar vi en historia om elektroner och hur de färdas genom världen. Elektroner har förvånansvärt många egenskaper gemensamt med oss människor. Till exempel har de ett starkt behov av personligt utrymme. Eftersom de är negativt laddade tycker de inte om att vara nära varandra. Detta kallas för *Coulombrepulsion*. När elektronerna åker på semester till en fin liten tropisk ö är det bara för den första elektronen att hoppa på. Den andra elektronen behöver dock en hel del övertalning för att dela utrymmet med den elektron som redan är där. Vi kallar dessa små öar för *kvantprickar*. De större landmassorna där elektronerna tillbringar sin icke-semestertid är de *elektriska kontakterna*, och ett otroligt stort antal elektroner lever på dessa kontakter. När två av dessa stora landmassor är nära ön, hoppar ibland några elektroner till ön, detta är den berömda *tunneleffekten*. Ibland hoppar de också till andra sidan, vilket kan ses i

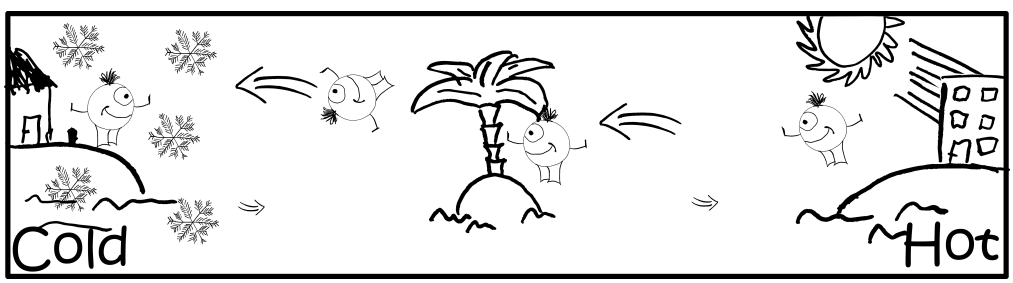

Figur A: Elektronerna studsar mellan de kalla (vänster) och varma (höger) landmassorna och ön i mitten.

Fig. A. Om tillräckligt många elektroner hoppar i en riktning uppstår en ström som vi kan mäta. Strömmen kan bero på många saker, t.ex. hur långt ön ligger från fastlandet, dvs. hur lätt det är för elektronerna att hoppa. Detta kallas för *tunnelkoppling*. Andra faktorer är öns höjd, energin i den s.k. *kvantpricknivån*, och även antalet elektroner på fastlandet, den *kemiska potentialen* i kontakten. Om det finns många fler elektroner på en av de stora landmassorna är det mer sannolikt att elektronerna på ön hoppar till den mindre befolkade sidan. Skillnaden i befolkning mellan de stora landmassorna kallas *potentialskillnad* eller *spänning*.

Det finns många varianter av ovanstående bild man kan fundera på. Vad händer om vi lägger två öar mellan landmassorna? Detta kallas för en *dubbel kvantprick*. Hur reagerar detta arrangemang om vi ändrar avståndet till fastlandet eller höjden på öarna något? Detta motsvarar en förändring av tunnelkopplingarna eller punktens nivån. Om vi sitter på fastlandet och räknar hur många elektroner som kommer från ön, kan vi då ta reda på något om en tredje ö som ligger i närheten? Om vi till exempel tar reda på om det finns elektroner på den tredje ön kallas detta för *laddningsavkänning*. Detta är ämnet för artikeln I, där vi undersöker en parallell dubbel kvantprick och möjliga tillämpningar som en laddningssensor.

Hittills har vi inte brytt oss så mycket om vädret. Vilken väg kommer elektronerna att ta om det är mycket varmt på den ena landmassan och mycket kallt på den andra, som i Fig. A? Om vi kan övertyga elektronerna om att hoppa till sidan med fler elektroner har vi använt *värmen* från den varma sidan för att utföra *elektriskt arbete*. Detta är konceptet för en *värmemotor*. Tänk om vi kunde få ön och fastlandet tillräckligt nära varandra så att två elektroner kunde ropa åt varandra och samordna sina hopp, eller så kunde en av dem hoppa två gånger på mycket kort tid? De processer där två koordinerade hopp äger rum kallas för *cotunnelling*-händelser. Om man tillåter dessa avtal mellan elektroner ändras inte bara det genomsnittliga antalet hoppande elektroner, *strömmen*, utan också antalet hoppande elektroner, som fluktuerar runt det genomsnittliga antalet hoppande elektroner. Detta kallas *brus*. Det påverkar också värmemotorns *verkningsgrad*. I artikel II undersöker vi dessa effekter och överväger också en avvägning mellan strömmen, bruset och effektiviteten i de så kallade *termodynamiska obestämbarhetsrelationerna*.

Alla elektroner håller sig naturligtvis inte hela tiden i närheten av denna lilla ö i havet. En del av dem har en fast arbetsplats och måste pendla längs en kustväg, med havet på ena sidan och ett oframkomligt landskap på den andra, som visas i Fig. B. Även på motorvägen gäller särskilda trafikregler: Endast blå bilar får köra i ena riktningen och endast röda bilar i den andra. Denna regel kallas *spinn-rörelsemängd-låsning* och de länder där detta sker kallas *topologiska isolatorer*. I dessa mycket speciella länder är elektronerna också mycket miljövänliga och måste bilda bilpooler. De har också roliga bilar. Beroende på vilka säten i bilen som är upptagna är bilens färg antingen röd eller blå. Denna egenskap kallas *spinn projektion* och bestämmer i vilken riktning elektronerna tillåts röra sig. När bilen stöter på ett farthinder, som kallas *magnetiska orenheter*, kastas elektronerna ibland upp från sina platser. Om de

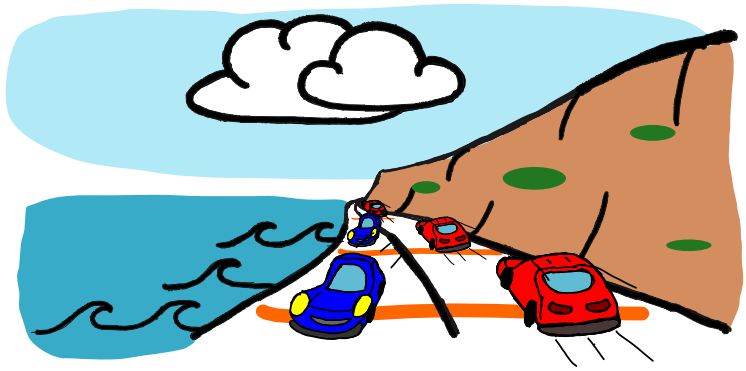

Figur B: Illustration av kustmotorvägen med de märkliga trafikreglerna: röda bilar får bara köra till höger, blå bilar till vänster i motsatt riktning. Farthindren visas i orange.

lägger sig på olika ställen efter denna *spridningshändelse* kan bilen ändra färg. Om de kör på ett farthinder på motorvägen och bilen ändrar färg, måste de naturligtvis vända. Detta kan göra trafiken ganska utmanande. När en bil kör in i ena änden av kustmotorvägen kallas sannolikheten för att den ska ta sig till andra sidan för *transmission*. I artikel III tittar vi på hur farthinder påverkar trafiken och hur troligt det är att elektroner kommer dit de vill. Och eftersom det inte är konstigt nog får vi också farthindren att rotera.

Med det här arbetet hoppas vi kunna bidra till förståelsen av elektronernas resvanor så att de kan användas i den märkliga och underbara kvantvärld som vi och elektronerna lever i. Elektronernas semester- och samåkningsvanor kan komma att användas i många tekniska tillämpningar i framtiden. Från att använda kvanteffekter för att göra befintlig elektronik mer effektiv, till att mäta saker som vi inte kunde mäta tidigare, eller till och med för att utveckla helt nya typer av datorer - mycket verkar möjligt.

Introduction

Electronic transport is the basis of modern semiconductor technology. In many technologies, including computers, chip miniaturization plays a big role. Modern processing methods allow for smaller and smaller structures. Semiconductor companies now routinely fabricate transistors with gate lengths on the scale of tens of nanometers [1]. Also light emitting diodes [2], solar cells [3] and highly sensitive charge sensors [4, 5] can be made from nanoscale structures. Due to the small length scales in these nanostructures quantum mechanic effects start playing a role or are even the reason why they work in the first place. This is the case, e.g., for qubits [6], the basic building blocks of quantum computers. At these tiny length scales electrons start experiencing confinement effects and can no longer move freely. A fitting analogy here is water. A huge, deep body of water, like an ocean, will have drastically different properties compared to a shallow lake, river or a droplet.

Not only for applications, but also for understanding fundamental science aspects, electronic transport plays a big role as transport properties like the current are comparatively easy to access. Measuring transport allows extracting a lot of information about the properties and/or structure of the material [7–11]. Modern processing and measurement methods also allow us to investigate structures at the nanoscale experimentally. To understand the effects that drastically change the properties at small scales and control them the development of accurate theory models is crucial.

1 Nanostructures and transport in the quantum regime with reduced dimensionality

In bulk materials electrons can move freely. Confining them in the spacial dimensions leads to a quantization of their energy due to their wave nature. In semiconductors this happens approximately at the length scale of tens of nanometers when the de Broglie-wavelength of the electrons around the Fermi energy becomes comparable to the size they are confined to.

If the electrons are confined in one spacial direction and can only move freely in a two dimensional plane a two dimensional electron gas is formed. This can be done in heterostructures, e.g., made from GaAs [8, 12, 13], where the two dimensional electron gas can form at the interface between two different materials. In contrast, there are also intrinsically two dimensional systems like, e.g., graphene [14] where the the staring point is an atomically thin layer of material. A two dimensional electron gas can be used to investigate, e.g., the quantum Hall effect [15], form quantum dots (QDs) [16] or has applications in electronics [17, 18]. An important characteristic in low dimensional electronic systems is the density of states [19]. Intuitively the density of states should have a big influence on the transport properties of a system, as it describes how many electrons can exist within a small energy interval around a given energy. For example the density of states of a free electron gas in tree dimensions follows a square root dependence on the energy, two dimensional systems have a flat density of states and one dimensional systems follow a inverse square root dependence for each sub band. If the electrons get confined in all three spacial dimensions discrete energy levels form, i.e., electrons can only exist at specific energies and the density of states becomes a delta function [20].

Some special types of two dimensional systems can form channels on the edge of the system, where the electrons effectively move in a one dimensional channel. Examples for such systems, with rather exotic properties, are quantum Hall systems [15, 21–23] and two dimensional topological insulators with so-called helical edge states [24–26]. Another example of electrons confined in more than one spacial direction are nanowires with diameters on the nanoscale [27]. In such systems the electrons can only move freely along the wire. Nanowires can be grown from semiconductor materials [28, 29] and investigated in a variety of experiments. Particularly relevant to this thesis is the fact that they can be used to form QDs. The QD structures have a discrete energy spectrum that allows, e.g., for the use as solar cells [30], qubits [6, 31], optical [32] and charge sensors [33, 34] and even nanoscopic heat engines [35–38].

2 Quantum dots and quantum thermodynamics

One of the most prominent applications of QDs coupled to electronic reservoirs are currently spin qubits [6, 31, 39–41], one possible basic building block of quantum computers. The realization of spin qubits requires great control of the properties of QDs and it is therefore crucial to understand their transport properties. Also for other applications, e.g., charge sensing [33, 34, 42] or QD heat engines [35–38] understanding the transport properties is important. Last but not least different QD structures are also interesting from a fundamental physics point of view, for example to investigate coherence and entanglement [43].

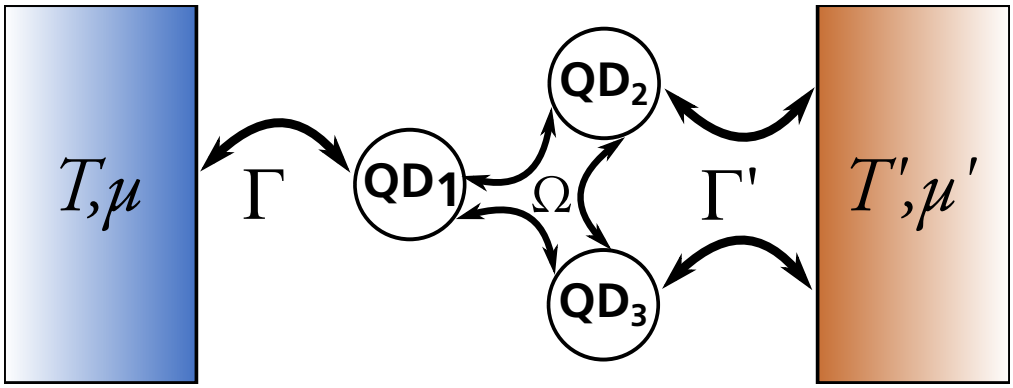

Figure 2.1: Schematic representation of an example transport setup for QDs. The QDs are coupled to each other by Ω and to macroscopic leads described by their respective temperatures T, T' and chemical potential μ, μ'. The coupling between the QD system and the leads is contained in the tunnel rates Γ, Γ'.

QDs have been realized in various ways, e.g., by electrostatically confining electrons in a two dimensional electron gas [16] or in nanowires [44]. In nanowires the barriers confining the electrons along the wire can also be epitaxially defined, i.e., due to a change in crystal structure [45, 46] or material along the wire. For the level of theory description we use here the practical realization is not important.

An important effect in QDs is Coulomb interaction which leads to a repulsive force between electrons. A consequence of that is the so-called Coulomb blockade [47, 48], a regime where the current is blocked by an electron on the QD, that prohibits other electrons from tunneling through. An example for a transport setup where a QD system is coupled to a number of leads is shown in Fig. 2.1. In these setups the leads are described by their respective temperatures T, T' and chemical potential μ, μ'. The QDs are coupled to each other via Ω. The couplings between QD levels and leads are described by the tunnel rates Γ, Γ'.

2.1 Quantum thermodynamics and thermodynamic uncertainty relations

Thermodynamics is branch of physics that emerged long before quantum mechanics. Developed as a tool to improve steam engines it deals with large systems close to equilibrium. In the realm of quantum mechanics we work with very small systems and very small particle numbers. This begs the question of how the large scale theory with the laws of thermodynamics carries over to the quantum world and which adaptations or extensions are needed. To answer these questions, in recent years the field of quantum thermodynamics has emerged. Within this field significant efforts have been made to extend thermodynamics and non-equilibrium statistical physics considering small system sizes and quantum effects [49]. This has been approached in many different ways not only by the statistical

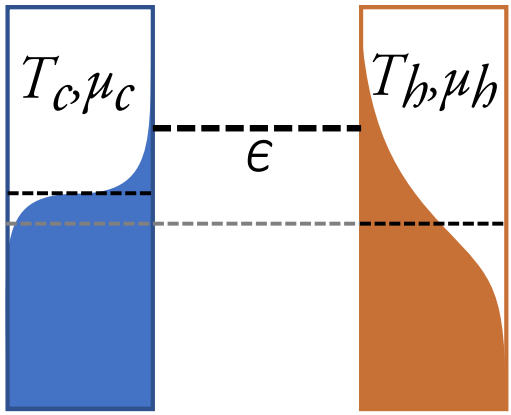

Figure 2.2: Schematic representation of a single level QD heat engine. The QD energy level is denoted by ϵ. The QD level is coupled to a hot/cold lead with temperature T_h/T_c and chemical potential μ_h/μ_c.

physics and many-body theory communities [49], but also from a quantum information theory perspective [50]. It is now possible to describe, e.g., classical engine cycles like the Otto or Carnot cycle or other driving schemes in a quantum thermodynamic process [51, 52]. One can also define thermodynamic properties like heat or entropy on the quantum level and put quantum bounds on these quantities [53]. For a more exhaustive overview we refer to the various reviews and books on the field like, e.g., Refs. [49–51, 53, 54].

Prototypical quantum systems for considering thermodynamic properties are QD heat engines [35, 36, 55–58]. They are both interesting from a fundamental point of view as well as for practical applications. Since QDs can be a building block for quantum computers, operating them as a heat engine can be used for local cooling and potentially improve the performance of quantum computers [59]. Similar applications are heat rectification and refrigeration [60–63].

A typical QD heat engine setup is shown in Fig. 2.2. The working principle is rooted in the energy filtering provided by the QD level [55]. The difference in the lead temperatures leads to energy windows, where the occupation of the hot lead is higher than that of the cold lead. If the energy level of the QD is placed in such a window a thermoelectric current will flow from the hot to the cold lead. This can even happen against the electrical bias given by the difference in the chemical potentials. In that case the thermocurrent can be used to perform electrical work and the QD setup works as a heat engine.

For QD heat engines investigating thermodynamic properties seems natural. Also in the context of biomolecular processes and motors questions with regards to thermodynamics have emerged [64]. The systems studied here are small and therefore fluctuations become important. However, the effects can be described by means of classical statistical physics and no quantum description is needed. In that field the so-called thermodynamic uncertainty

relation (TUR)s [64, 65] have been developed. They are a relation between the mean and fluctuations of a physical observable and the entropy production in the system. Knowing two of the quantities consequently leads to a bound on the third. This physical observable could, e.g., be the power output of a heat engine or the electrical current.

QD heat engines are a good platform for probing these TURs. This can give insights into how to create highly efficient QD heat engines. Moreover, violations of the TURs indicate the presence of quantum effects [66]. It is an interesting questions, whether taking into account different effects results in different bounds. It has been shown that, e.g., in the quantum regime a looser bound holds [67] and that including measurement and feedback can lead to modified relations [68]. The search for performance bounds in quantum thermal engines and other thermal machine is an active area of research, see, e.g., [69–73].

3 Topology and two dimensional topological insulators

Here we want to briefly describe why we are interested in topological systems. Mathematically topology is the branch considering conserved properties of geometric objects under continuous deformations. In our case the deformed objects are typically bandstructures and continuous deformations correspond to deformation of the bands without closing the band gap. The first question that comes to mind is why we should care about such abstract things. To answer this, let us consider a complicated system. If we can deform the bandstructure of the complicated system continuously to a simple toy model where we can easily perform calculations, we can learn properties of very complicated systems from simple calculations. The properties we can learn about are connected to so called topological invariants, i.e., quantities that do not change under continuous deformations of the bandstructure. It is possible to connect the existence of these topological invariants to the symmetries and dimension of the system. This has been done in the Altland-Zirnbauer periodic table of topological phases [74, 75]. That table also directly tells us against which perturbations the properties we found are robust, namely all perturbations that conserve the symmetries considered in the table. The robustness of these properties is connected to the existence of states on the boundary of the finite system, given by the so called bulk-boundary correspondence. It predicts the existence of topological states at the boundaries of systems that are in a non-trivial topological phase [75, 76]. Some examples of topological states are Majorana bound states [77–79] at the edges of a so-called Kitaev-chain [80], quantum Hall edge channels [21–23, 81, 82] at the boundary of two or three dimensional materials and quantum spin Hall states on the boundaries of so called topological insulators [24, 25, 83–85].

These boundary states in topological insulators are dissipationless and protected by time-reversal symmetry. In three dimensional topological insulators the electronic structure of

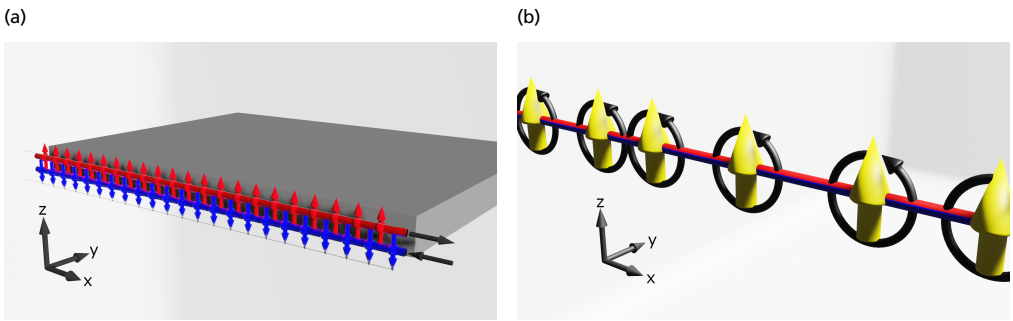

Figure 3.1: Illustration of (a) edge channels carrying different spin species (red/blue) on the edge of a two dimensional material and (b) randomly placed, aligned rotating magnetic impurities (yellow) on the 1D edge channels (red/blue). Adapted from Ref. [100].

the boundary states leads to interesting transport properties [86–89]. If the bulk material is instead a two dimensional system the dissipationless edge states are one dimensional, but still follow a linear dispersion relation. They exhibit so called spin-momentum-locking, i.e. the two counter-propagating states carry opposite spins. For a more extensive review of the topic we refer to Refs. [26, 75, 76].

We can understand the emergence of these edge states in two dimensional systems in a semi-classical picture. The origin of the quantum Hall effect is the movement of electrons in a strong magnetic field. The electrons are forced on circular orbits by the Lorenz force. These orbits are quantized and the emerging discrete energy levels are called Landau levels [90]. The closed electron orbits mean that the bulk of these two dimensional materials are insulating. At the edge of the system the quantized orbits lead to edge states with quantized conductance [21] due to the Landau levels. In the semi-classical picture the electrons cannot complete their orbit at the edge and we can imaging the electrons bouncing along the edge in so-called skipping orbits [19]. In two dimensional topological insulators the effect forcing the electrons onto the circular orbits is not an external magnetic field, but the strong spin-orbit coupling. This also implies that electrons with different spin circulate in different directions. This is called quantum spin hall effect [83] and leads to two counter-propagating helical edge states, illustrated in Fig. 3.1a. The edge channels have been shown to follow a Dirac type dispersion [75, 76].

Two dimensional topological insulators have first been predicted in 2006 [24], and in 2007 they were experimentally confirmed in HgTe/CdTe quantum wells [84, 85]. Subsequently, various measurements on quantum spin Hall systems in HgTe/CdTe wells have been performed [91–94], but also other material systems like InAs/GaSb/AlSb quantum wells have been shown to be two dimensional topological insulators [95–98]. The dissipationless transport through the helical edge states suggests applications in, e.g., low-power information processing and spintronics [94, 99].

Impurities close to the edge states can have an influence on the transport properties [101, 102]. In practice, impurities can rarely be avoided, and are often introduced intentionally via doping to control the properties of the system. In the absence of electron-electron interactions in the case of two dimensional topological insulators only magnetic impurities with a magnetic moment have an influence, e.g., on the density of states. This is due to the fact that purely electric impurities do not enable backscattering in the edge states. For backscattering to occur time-reversal symmetry needs to be broken, i.e., magnetic impurities are necessary. This is due to the aforementioned spin-momentum locking, that only allows the electrons to backscatter if their spin is also flipped. A situation like where magnetic impurities are present on the edge is schematically depicted in Fig. 3.1b. If electron-electron interactions are present, also non-magnetic impurities can lead to backscattering [103]. The effect of static aligned magnetic impurities has been investigated in Ref. [101].

4 Thesis outline

This thesis focuses on theoretical investigations of transport properties in QD systems, connected to papers I and II, and two dimensional topological insulators in the context of paper III.

In the QD transport part we begin by introducing the QD Hamiltonian we use to describe QD systems in Sec. 5. Subsequently, we introduce the main ideas and formalism used in papers I and II, most notably generalized master equations in Sec. 6 and counting statistics in Sec. 7. In Secs. 8 and 9 we introduce two relevant approximations to the generalized master equations. We discuss some details concerning the numerical implementation of counting statistics in Sec. 10. To familiarize ourselves further with QD transport, we discuss some instructive toy models in Sec. 11 using the previously introduced methods. Section 12 provides context on charge sensing relevant for the summary and discussion of paper I in Sec. 13. For the discussion of paper II we provide some context on quantum (dot) thermodynamics and TURs in Sec. 14. The summary and discussion of paper II follows in Sec. 15.

The topological insulator part in a similar fashion covers the most relevant methods for paper III. Section 16 introduces the model Hamiltonian for the topological insulator edge states with impurities. In Sec. 17 background on Floquet theory is provided. Section 18 covers Green's functions and Sec. 19 explains how transport properties are extracted from the Green's functions. Paper III investigates the effect of harmonically rotating magnetic impurities in two-dimensional topological insulators using these methods and is discussed in Sec. 20.

We close with an overview of ongoing research and a brief outlook.

Quantum dot transport

In QD transport setups QDs get coupled to macroscopic leads and currents through the system are investigated. When such a small system gets coupled to a large environment this is referred to as an open quantum system where the density matrix is needed to describe the system. There are several different techniques that are commonly used on open quantum systems. If the, e.g., the electron-electron interactions in the system are small enough to be neglected the transport problem can be solved with exact Landauer-Büttiker theory [104–106]. Non-equilibrium Green's function techniques [107–109] can be used if the interactions are not negligible and the tunnel coupling to the leads is strong. When tunnel couplings and interactions are of the same order typically renormalization group approaches [110, 111] are employed. In the case of strong electron-electron interaction and weak tunnel couplings master equations are a standard tool for transport calculations in QD systems. These systems exhibit for example effects like Coulomb blockade, where the trapping of one electron on the system leads to a blocking of the current.

Generalized master equations, equations of motion for the density matrix [112, 113], give access to many useful quantities like for example occupation probabilities and particle, spin or heat currents. They are typically based around a perturbative expansion in the tunnel couplings and naturally incorporate electron-electron interactions. There are many ways of setting up a master equation for a given system involving different approximations [112, 114–118]. For calculating steady state properties, master equation techniques lead to a matrix equation for the density matrix that can be solved numerically. There are however many approximations one can make in the setup (see, e.g., [116]) and depending on the choice the calculations of the needed matrix elements can become numerically expensive. Another potential pitfall of a master equation approach is that approximations under certain circumstances can lead to unphysical results, like density matrices that are not positive semi-definite [112] or violations of the Onsager relations [119]. Therefore, one needs to carefully select the approach and make sure it is appropriate for the system under investigation.

In this chapter we first introduce the QD Hamiltonian in Sec. 5. Subsequently we outline the theoretical framework of (generalized) master equations (Sec. 6), that we will be using

to calculate different properties of QD systems coupled to reservoirs. Then we give an introduction to electron counting statistics withing the framework of the aforementioned master equations in Sec. 7. Two relevant approximations to the generalized master equation and the combination with counting statistics are introduced in sections 8 and 9. We also discuss numerical implementations of counting statistics in Sec. 10. We then discuss two relevant models, the single resonant level and the spinful single level, in different approximations and contexts, see Sec. 11. With these models at hand we first discuss charge sensing in Sec. 12 and paper I in Sec. 13. Subsequently, we give a brief introduction to quantum thermodynamics and QD thermoelectric engines, see Sec. 14 and discuss paper II in Sec. 15.

5 The quantum dot Hamiltonian

We consider a general QD system of the type shown in Fig. 2.1. The Hamiltonian can be written as [37, 118]

$$H_{QD} = H_{\text{Single}} + H_{\text{Coulomb}}, \tag{5.1}$$

where we have separated the single particle Hamiltonian and the interaction due to Coulomb repulsion

$$H_{\text{Single}} = \sum_i \epsilon_i d_i^\dagger d_i + \sum_{i \neq j} \Omega_{ij} d_i^\dagger d_j, \tag{5.2}$$

$$H_{\text{Coulomb}} = \sum_{mnkl} U_{mnkl} d_m^\dagger d_n^\dagger d_k d_l \qquad \text{with} \quad m < n. \tag{5.3}$$

The single particle Hamiltonian contains the energy levels ϵ_i where i is an orbital and/or spin index and the couplings between QD levels within the system are given by Ω_{ij}. The charging energy due to Coulomb interaction is given by U_{mnkl}. The QD creation/annihilation operators $d_i^\dagger / d_i$ appear in both the single particle and interaction Hamiltonians. This Hamiltonian can be diagonalized in the many-body energy eigenbasis $\{|a\rangle\}$ and together with the reservoir Hamiltonian H_R and the tunneling Hamiltonian H_T we can write the QD coupled to reservoirs as [37, 118]

$$H = H_{QD} + H_R + H_T, \tag{5.4}$$

where

$$H_{QD} = \sum_a E_a \left|a\right\rangle \left\langle a\right|, \tag{5.5}$$

$$H_R = \sum_r H_{R,r} = \sum_{rk\sigma} \omega_{rk\sigma} c_{rk\sigma}^\dagger c_{rk\sigma}, \tag{5.6}$$

$$H_T = \sum_r H_{T,r} = \sum_{rki\sigma} t_{rk\sigma,i} d_i^\dagger c_{rk\sigma} + t_{rk\sigma,i}^* d_i c_{rk\sigma}^\dagger. \tag{5.7}$$

Here we have introduced the many-body energies E_a, the lead energies $\omega_{rk\sigma}$ indexed by the reservoir r, momentum k and spin-index σ, the reservoir creation/annihilation operator $c^\dagger_{rk\sigma}/c_{rk\sigma}$ and the tunneling amplitudes $t_{rk\sigma,i}$ connecting the QD to the leads. From the tunneling amplitudes we can define the tunneling rates as

$$\Gamma_{rk\sigma,i} = 2\pi\nu_r|t_{rk\sigma,i}|^2, \tag{5.8}$$

where we have assumed the wide band limit, i.e., the density of states ν_r of the leads are constant over the relevant energy range in the leads. We assume the leads to be infinitely large and in thermal equilibrium, such that they can be described by their temperatures T_r and their chemical potentials μ_r. The average occupation is then described by the Fermi-Dirac distribution

$$f_r(E) = \frac{1}{e^{(E-\mu_r)/T_r}+1}. \tag{5.9}$$

Note, that throughout the thesis we set $\hbar = e = k_B = 1$. This description of the QD system coupled to leads allows us to investigate the dynamics and stationary state transport properties using generalized master equations.

6 Generalized master equation

The derivation of the generalized master equation in this section follows Refs. [37, 118, 120]. Generalizsed master equations provide an equation of motion for the reduced density matrix of the system of interest, which in this thesis is given by one or several QDs. Here we use the QD Hamiltonian (5.4) to describe the systems we have in mind for these calculations. Explicitly, we think about one or several QDs coupled to electronic leads.

The Liouville-von Neumann equation that governs the time-evolution of the density matrix $\rho(t)$ can be written as (see, e.g., [112, 113])

$$\dot\rho(t) = -\mathrm{i}\,[H, \rho(t)] = -\mathrm{i}L\rho(t), \tag{6.1}$$

where $[\bullet, \bullet]$ is the commutator and we have introduced the superoperator $L = [H, \bullet]$. If we refer to corresponding superoperators for the separate parts of the QD Hamiltonian (5.4) we index it like $L_A = [H_A, \bullet]$, where A is QD, R or T. Note that it is always possible to recast the density matrix into a vector and write Eq. (6.1) as a matrix$\times$vector equation with an appropriate matrix representation of the superoperator L. This is called superoperator space and is often useful for numerical calculations. Working in this matrix representation of superoperator space transforms the equation to what looks like a classical rate-equation, but since transforming to superoperator space does not reduce dimensionality coherence effects can be present.

The Liouville-von Neumann Eq. (6.1) for time-independent L has the formal solution

$$\rho(t) = e^{-\mathrm{i}Lt}\rho(0) \tag{6.2}$$

for the full density matrix. In open systems relevant to us we are usually not interested in the full density matrix, but the reduced density matrix of the QD system. To gain access to that we trace out the degrees of freedom of the reservoirs

$$\rho_{QD} = \mathrm{Tr}_R\, \rho. \tag{6.3}$$

Assuming the leads to be in their equilibrium state ρ_R and the system to be initially uncorrelated, i.e., $\rho(0) = \rho_R \otimes \rho_{QD}(0)$ we can perform a Laplace transform to find

$$\rho_{QD}(z) = \mathrm{Tr}_R \int_0^\infty \mathrm{d}t\, e^{\mathrm{i}zt} e^{-\mathrm{i}Lt}\rho(0) = \mathrm{Tr}_R \frac{\mathrm{i}}{z-L}\rho_{QD}(0) \otimes \rho_R. \tag{6.4}$$

Here z is the Laplace frequency. The fraction in Eq. (6.4) can be expanded in powers of the tunneling part L_T of the Liouvillian $L = L_{QD} + L_R + L_T$. The resulting geometric series in L_T can be re-summed into an effective self-energy. After taking the trace the result is

$$\rho_{QD}(z) = \frac{\mathrm{i}}{z - L_{QD} - \mathrm{i}W(z)}\rho_{QD}(t_0), \tag{6.5}$$

where the effective self energy superoperator $W(z)$ contains the information about the tunneling between the QDs and the lead due to L_T. Note that the expansion and re-summing, that is, e.g., carried out in Refs. [118, 121], is in principle exact. In practice it is usually not possible to calculate the full series and different approximations and simplifications need to be made to find the exact form of $W(z)$. For this work, the relevant approaches are Lindblad master equations [114, 117, 122] and second order perturbation theory based on real-time diagrammatics [118, 121, 123–126]. They will be briefly introduced in Sec. 8 and 9 respectively.

We are usually interested in the stationary state limit, i.e., $t \to \infty$. In Laplace space this corresponds to the limit $z \to 0^+$ resulting in

$$\left(-\mathrm{i}L_{QD} + W(\mathrm{i}0^+)\right)\rho_{QD} = 0. \tag{6.6}$$

Note that before the infinite time limit W has a dependence on the Laplace frequency z, which is going to be important for the counting statistics approach in Sec. 7.

Transforming back to the time-domain Eq. (6.5) turns into the integrodifferential equation

$$\dot{\rho}_{QD}(t) = \int_0^\infty \mathrm{d}t'\, \mathcal{L}(t-t')\rho_{QD}(t'), \tag{6.7}$$

where we introduced the effective Liouvillian or kernel $\mathcal{L}(t-t') = -\mathrm{i}L_{QD} - W(t-t')$.

7 Counting statistics

Since the transport of electrons is a statistical process, the average current does not contain all the information.. Fluctuations, i.e., current noise and higher momenta of the distribution describing the transport have to be taken into account to fully describe the process. In particular, the noise can contain additional information about the transport in the system [106, 127, 128].

Full counting statistics are commonly used to access the current statistics. Counting statistics were originally developed in a transmission function setting [129] and can be used to investigate, e.g., molecular junctions [130] and superconducting systems [131–133]. In the context of rate equations they have also been used [134], e.g., for single QDs [135]. Based on the rate equation approach Ref. [136] describes how higher cumulants can be accessed via master equations. Here we introduce this counting statistics formalism following Refs. [113, 120, 137].

The conditional master equation describes the dynamics of the system keeping track of how many particles have been transferred between the system and a set of leads. This set of leads can be chosen freely, and we refer to them as counting leads. Here, $\rho_{QD}^{(n)}$ is the density matrix of the system, under the condition that it has transferred n electrons to the counting leads. The full density matrix is then the sum over the number of transferred particles, i.e., $\rho_{QD} = \sum_n \rho_{QD}^{(n)}$. The most general form for the reduced density matrix reads [137]

$$\frac{\mathrm{d}}{\mathrm{d}t}\rho_S^{(n)}(t) = \sum_{n'=-\infty}^{\infty} \int_0^{\infty} \mathrm{d}t\,' \mathcal{L}_{n-n'}(t-t')\rho_S^{(n')}(t'), \tag{7.1}$$

where the reduced density matrix and effective Liouvillian now carry an additional index to clarify the condition of having transferred n and transferring $n-n'$ electrons, respectively. A Fourier transform introduces the counting field χ as conjugate variable to the number of transferred particles n. Transforming to Laplace space subsequently results in

$$z\rho_S^{\chi}(z) - \rho_S^{\chi}(t=0) = \mathcal{L}(\chi, z)\rho_S^{\chi}(z). \tag{7.2}$$

From this one can find the cumulant generating function M for large times

$$M(\chi, t) = tz^*(\chi). \tag{7.3}$$

The generating function M describes the distribution of transferred particles. In order to find the current cumulants we need to take the time derivative to go from number of transferred particles to the rate of transferred particles, i.e., the current cumulants. The time derivative is simply $z^*(\chi)$, which is given by the solution of

$$z^* - \Lambda_0(\chi, z^*) = 0, \tag{7.4}$$

where Λ_0 is the eigenvalue of the kernel $\mathcal{L}(\chi, z)$ that develops adiabatically from 0 with χ, i.e., $\Lambda_0(0, z) = 0$. On the one hand, the solution z^* can be expanded in $\mathrm{i}\chi$ which yields

$$z^*(\chi) = \sum_{n=1}^{\infty} \frac{(\mathrm{i}\chi)^n}{n!} \langle\langle I^n \rangle\rangle. \tag{7.5}$$

On the other hand, Λ_0 can be expanded according to Brillouin-Wigner perturbation theory (see, e.g., [136]). Comparing coefficients of the two expansions then gives the current cumulants.

To write them in a compact way we introduce notations used in the Brillouin-Wigner perturbation theory. The left and right eigenvectors of the kernel (in superoperator space) are defined as

$$\mathcal{L}(0, 0^+)|\psi_0\rangle\rangle = 0, \tag{7.6}$$
$$\langle\langle\psi_0|\mathcal{L}(0, 0^+) = 0. \tag{7.7}$$

$|\psi_0\rangle\rangle$ is the stationary density matrix of the system in superoperator space, together with $\langle\langle\psi_0|$ it corresponds to taking the trace, i.e., $\langle\langle\psi_0|A|\psi_0\rangle\rangle = \mathrm{Tr}\,(A\rho_{QD})$. These vectors also define the expectation value

$$\langle\langle \bullet \rangle\rangle = \langle\langle\psi_0| \bullet |\psi_0\rangle\rangle \tag{7.8}$$

and the projection operators

$$P = |\psi_0\rangle\rangle\langle\langle\psi_0|, \tag{7.9}$$
$$Q = 1 - P. \tag{7.10}$$

With these we can, in turn, define the pseudo-inverse

$$R(\epsilon) = Q \frac{1}{\mathrm{i}\epsilon + \mathcal{L}(0, 0^+ - \mathrm{i}\epsilon)} Q \tag{7.11}$$

and

$$J(\chi, \varepsilon) = \mathcal{L}(\chi, z = \varepsilon + i0^+) - \mathcal{L}(\chi = 0, z = i0^+), \tag{7.12}$$

along with the derivatives

$$J' = \partial_\chi J|_{\chi, \varepsilon \to 0}, \tag{7.13}$$
$$\dot{J} = \partial_\varepsilon J|_{\chi, \varepsilon \to 0}. \tag{7.14}$$

Using these conventions the first two current cumulants, namely the average current $\langle I \rangle$ and the current noise S evaluate to [120]

$$\langle I \rangle = \langle\langle I^1 \rangle\rangle = -\mathrm{i}\langle\langle J' \rangle\rangle, \tag{7.15}$$

$$S = \langle\langle I^2 \rangle\rangle = \underbrace{-\langle\langle J'' - 2J'RJ' \rangle\rangle}_{S_m} + \underbrace{2\langle I \rangle \langle\langle \dot{J}' - J'R\dot{J} \rangle\rangle}_{\text{"non-Markovian" contribution}} . \tag{7.16}$$

For Markovian master equations, the kernel $\mathcal{L}$ does not depend on the Laplace frequency z [137]. In that case terms containing $\dot{J}$ are zero. Hence we refer to the first terms S_m in Eq. 7.16 as the Markovian part of the noise and call the second term non-Markovian contributions[1]. Here we only give the first two cumulants, but in principle it is also possible to find higher cumulants, as, e.g., done in Refs. [120, 136, 137].

8 Gorini-Kossakowski-Sudarshan-Lindblad master equation

The so-called Gorini-Kossakowski-Sudarshan-Lindblad (GKSL) form is the most general form of a Markovian quantum master equation that is a trace preserving completely positive map [114, 122]. That means it is mathematically guaranteed to produce physical density matrices, where the diagonals, i.e., the probabilities of the many-body states of the system, are all non-negative and sum to one. Starting from the generalized master equation Eq. (6.1), inserting the QD Hamiltonian Eq. (5.4) and making the Born-Markov approximation one arrives at the so-called Redfield equation. The Born-Markov approximation assumes weak coupling between bath and QD system and that the bath relaxation time is faster than any other time scale present. The Redfield equation is only of GKSL form if one does a secular approximation, i.e., keep off diagonal elements only between degenerate states. However, this is a bad approximation whenever there are states that have a small but finite energy splitting (comparable to Γ). Fortunately, it has been shown in Refs. [117, 138, 139] that the Redfield equation also in this case can be cast in GKSL form by additional approximations. The resulting master equation of GKSL form for a QD system we use takes the form

$$\dot{\rho}_{QD} = -\mathrm{i}\left[H_{QD} + H_{LS}, \rho_{QD}\right] + \sum_{\substack{\alpha=\pm \\ r,i}} \left(A_{ri,\alpha}\rho_{QD}A^\dagger_{ri,\alpha} - \frac{1}{2}\{A^\dagger_{ri,\alpha}A_{ri,\alpha}, \rho_{QD}\} \right), \tag{8.1}$$

with the Lamb-shift Hamiltonian H_{LS} and the jump operators $A_{ri,\alpha}$. $\{\bullet, \bullet\}$ denotes the usual anti-commutator. The Lamb-shift is a renormalization of the many-body energies due

[1] We use a loose notion of (non-)Markovian as explained in Ref. [136]

to the coupling with the bath [138]. The jump operators $A_{ri,\alpha}$ in the many-body energy eigenbasis $\{|a\rangle\}$ of the QD Hamiltonian H_{QD} are [117, 138, 139]

$$A_{ri,+} = \sum_{mn} \sqrt{\Gamma_{r,i} f_r(E_m - E_n)}\, |m\rangle \langle m|\, d_i^\dagger\, |n\rangle \langle n|\,, \tag{8.2}$$

$$A_{r,i-} = \sum_{mn} \sqrt{\Gamma_{r,i}(1 - f_r(E_m - E_n))}\, |m\rangle \langle m|\, d_i\, |n\rangle \langle n| \tag{8.3}$$

with the many-body eigenenergies E_m. The jump operators correspond to the physical processes, where electrons from the lead tunnel into the dot and change the many-body energy state of the system.

If coherences do not play a role, i.e., the off-diagonals of the density matrix in the (many-body) energy eigenbasis for the isolated QD are zero, the system can be fully described by the occupation probabilities $P_a = \langle a|\, \rho_{QD}\, |a\rangle$ of these eigenstates. This is the case, e.g., if all quantum numbers that index the many-body states are conserved in the entire system (QD and reservoirs and tunneling) [121]. Then we can replace the reduced density matrix in the equations above with a probability vector P. In fact, ignoring coherences and the Lamb shift in the Lindblad Eq. (8.1) leads to the so-called classical Pauli rate equation for the occupation probabilities.

$$\dot{P}_a = \sum_b W_{ab} P_b - W_{ba} P_a \tag{8.4}$$

where the rates W_{ab} are given by

$$W_{ab} = \sum_{\substack{\alpha=\pm \\ r,i}} (A_{ri,\alpha})_{ab} (A_{ri,\alpha}^\dagger)_{ba} \tag{8.5}$$

$$= \sum_{ri} \Gamma_{r,i} f_r(E_a - E_b) |\langle a|\, d_i^\dagger\, |b\rangle|^2 + \Gamma_{r,i}(1 - f_r(E_a - E_b)) |\langle a|\, d_i\, |b\rangle|^2 \tag{8.6}$$

8.1 Counting statistics in the sequential tunneling Markovian case

In the conditional master equation (7.1), just like for the generalized master equation (6.1), the time dependence in the kernel is a delta function, i.e., $\mathcal{L}(t, n) = \mathcal{L}(n)\delta(t)$. Thus, the transformation to Laplace space leads to a z-independent master equation. The noise then reduces to

$$S = -\langle\!\langle J'' - 2J'RJ' \rangle\!\rangle. \tag{8.7}$$

In the case of first order Markovian master equations, i.e., perturbation theory of the kernel to leading order in the tunneling rates together with the Markov approximation, the kernel

only contains processes that transfer single electrons between the leads an the dot. That means, the counting field dependent kernel can be decomposed as

$$\mathcal{L}(\chi) = \mathcal{L}_0 + e^{\mathrm{i}\chi}\mathcal{L}_+ + e^{-\mathrm{i}\chi}\mathcal{L}_-, \tag{8.8}$$

where $\mathcal{L}_\pm$ contain rates of all processes adding/removing an electron to/from the system via the counting leads. Note that the exact form depends on the details in the setup of the master equation and also the choice of leads, e.g., for counting at lead r with the GKSL equation Eq. (8.1) $\mathcal{L}_\pm$ will contain the matrix elements of the jump operators $A_r i, \sigma$, i.e,

$$\mathcal{L}_\pm \bullet = \sum_i \left(A_{ri,\pm} \bullet A^\dagger_{ri,\pm} - \frac{1}{2}\{A^\dagger_{ri,\pm} A_{ri,\pm}, \bullet\} \right). \tag{8.9}$$

In sequential tunneling they will necessarily be located on the first off-diagonal of charge blocks, since they can only transfer exactly one electron. Using Eq. (9.6) we can write $J(\chi) = (1 - e^{\mathrm{i}\chi})\mathcal{L}_- + (1 - e^{-\mathrm{i}\chi})\mathcal{L}_+$ and Eqs. (7.15) and (8.7) reduce to

$$\langle I \rangle = \langle\!\langle \mathcal{L}_- - \mathcal{L}_+ \rangle\!\rangle \tag{8.10}$$

$$S = \langle\!\langle (\mathcal{L}_- + \mathcal{L}_+) - 2(\mathcal{L}_- - \mathcal{L}_+) R (\mathcal{L}_- - \mathcal{L}_+) \rangle\!\rangle \tag{8.11}$$

For paper I we use the Lindblad approach described above. If the coherences do not play a role in the system, the Lindblad equation reduces to a classical rate equation. This is for example a good model for a weakly coupled single level, both with and without spin. The counting field resolved kernel and the decomposition Eq. (8.8) is then easy to find analytically. We will treat this explicit example later in Sec. II.1.

9 Second order real time diagrammatic approach

In this section we introduce the real-time-diagrammatic approach to second order [118, 121, 123–126]. It allows for co-tunneling and all other coherent processes involving two tunneling events, including also pair tunneling [140], as well as processes leading to level broadening and renormalization [121]. In paper II we use this theory to investigate the effects of slightly larger tunnel couplings up to $\Gamma = 0.4T$, where the sequential tunneling approximation begins breaking down and regimes where sequential tunneling is suppressed. Note here that the resulting master equation is not of Lindblad form, i.e. it can not be written in the structure of Eq. (8.1). While it is trace preserving it can in principle lead to negative probabilities.

The real-time diagrammatic approach is a systematic expansion of the effective self-energy kernel $W(z)$ in Eq. (6.6) to second order in the tunnel rates[2] Γ

$$W(z) \approx W^{(2)}(z) + W^{(4)}(z). \tag{9.1}$$

Note, that only even orders are present in the expansion, as tracing over the reservoirs eliminates all terms with an odd number of QD creation/annihilation operators. The expansion results in

$$W^{(2)}(z) = -\mathrm{i}\gamma_{21}^{p_2p_1} G_2^{p_2} \frac{1}{z + x_1 - L} G_1^{p_1}, \tag{9.2}$$

$$\begin{aligned} W^{(4)}(z) = &-\mathrm{i}\gamma_{32}^{p_3p_2}\gamma_{41}^{p_4p_1} G_4^{p_4} \frac{1}{z + x_1 - L} G_3^{p_3} \frac{1}{z + x_1 + x_2 - L} G_2^{p_2} \frac{1}{z + x_1 - L} G_1^{p_1} \\ &+ \mathrm{i}\gamma_{42}^{p_4p_2}\gamma_{31}^{p_3p_1} G_4^{p_4} \frac{1}{z + x_2 - L} G_3^{p_3} \frac{1}{z + x_1 + x_2 - L} G_2^{p_2} \frac{1}{z + x_1 - L} G_1^{p_1}. \end{aligned} \tag{9.3}$$

Terms of the type $(z + x - L)^{-1}$ are free propagators between the vertices $G_i^{p_i}$ and the energies x_j are implicitly integrated over. The vertices $G_i^{p_i}$ correspond to creation/annihilation operators in superoperator space. They can be expressed in a diagrammatic language. For more details see Refs. [118, 120, 121]. Here, we are mainly interested in the contraction functions $\gamma_{ij}^{p_ip_j}$. First we note that the indices $p_1, \ldots, p_4 \in \{\pm\}$ in Eqs. (9.2) and (9.3) are Keldysh-indices, for more details see Refs. [118, 121]. Second, the lower indices on $\gamma_{ij}^{p_ip_j}$ are a multi-indices, $j = (\eta_j, k_j, r_j)$ where $\eta_j \in \{\pm\}$ denotes whether the corresponding lead operator is a creation or annihilation operator, k_j denotes its momentum and r_j labels the lead. These are implicitly summed over in Eqs. (9.2) and (9.3). The standard bath contraction function reads

$$\gamma_{21}^{p_2p_1} = \delta_{2\bar{1}} p_1 f_{r_1}(-\eta_1 p_1 \omega_1) \tag{9.4}$$

where f_r is the Fermi function Eq. 5.9 and ω_1 the energy of lead r_1.

Physically the first order kernel corresponds to single coherent tunneling processes. The second order kernel represent coherent processes with two tunneling events within a short time interval. This, for example, allows for transport through a virtual intermediate state which can lead to an effective level broadening and finite currents in the Coulomb blockade regime.

The matrix elements of a superoperator S are evaluated according to

$$S_{ab}^{a'b'} = \langle a| \left(S\,|a'\rangle\,\langle b'|\right) |b\rangle\,. \tag{9.5}$$

[2]This is equivalent to fourth order in the tunnel amplitudes. We follow the convention of Refs. [118, 120, 121] and index the kernel by the order in tunnel amplitudes. In the text we refer to the expansion in orders of tunnel rates.

For more details, see [121, 141, 142]. Calculating the matrix elements of the kernels Eqs. (9.2) and (9.3) one has to evaluate several integrals that are given for example in Refs. [118, 120, 121]

9.1 Second order counting statistics

When including coherent tunneling of two electrons, the n-resolved master equation (7.1) can contain terms that transfer up to two electrons. Similar to Eq. (8.8) the kernel can then be decomposed as

$$\mathcal{L}(\chi) = \mathcal{L}_0 + e^{\mathrm{i}\chi}\mathcal{L}_+ + e^{-\mathrm{i}\chi}\mathcal{L}_- + e^{2\mathrm{i}\chi}\mathcal{L}_{2+} + e^{-2\mathrm{i}\chi}\mathcal{L}_{2-}. \tag{9.6}$$

Looking at the second order kernel Eq. (9.3) it is not straight forward to assign the terms to the corresponding $\mathcal{L}_{0,1\pm,2\pm}$. The second order terms can in principle transfer any number of electrons up to two at one specific lead. If exactly two electrons at the counting lead are transferred in the same direction, the term is contained in $\mathcal{L}_{2\pm}$. If they are transferred in opposite directions, they should be assigned to $\mathcal{L}_0$. Finally, there are also processes that only transfers one electron at the observed lead, and an additional one at another lead. These terms should be assigned to $\mathcal{L}_\pm$.

Modifying the bath contraction functions γ_{ij} to [120]

$$\gamma_{21}^{p_2p_1}(\chi) = \gamma_{21}^{p_2p_1} \exp\left[\mathrm{i}s_{\alpha_1}\eta_1\left(\frac{p_1-p_2}{2}\right)\chi_{\alpha_1}\right], \tag{9.7}$$

assigns the counting field correctly to the physical processes. Here, s_{α_1} is a sign that sets the convention for the current direction for each lead, i.e., whether going onto the QD or the lead is positive current. In practice this means that calculating the "counting index" $\eta_1\left(\frac{p_1-p_2}{2}\right)$ for every contraction function and assigning the term to the corresponding parts of the counting kernel results in the correct decomposition.

Similar to Eqs. (8.10),(8.11) we can find expressions for the current and noise up to second order. Due to the ϵ-derivative $\dot{J}$ Eq. (7.14) in Eq. (7.16) these expressions are lengthy and we omit them here.

10 Transport calculations with QmeQ

There are many software packages for quantum transport calculations, e.g., *QuTiP* [143, 144] that focuses on simulating the dynamics of open systems using various different master equation solvers, Monte Carlo, stochastic solvers and many more. It contains a large variety of methods and can be used to simulate many different types of quantum systems. Other

packages like *kwant* [145] are made for quantum transport calculations in tight binding models. Naturally, that means kwant can only deal with non-interacting systems. We use and develop the python package *QmeQ* [116], that is specialized on master equation transport calculations in QD systems. Given the Hamiltonians of a QD system, leads and tunneling, QmeQ can set up the master equation using various different approximations and methods. The different methods to set up the master equation in QmeQ are called approaches. The standard QmeQ implementation calculates stationary electronic and heat currents for a given QD system. Large parts of this thesis involve calculations performed with an extended version of QmeQ that has been adapted to perform the counting statistics calculations described in sections 7,8,9 [3]. Developing this extended QmeQ version was a central part of the thesis work with the big benefit that it can be used by others on different systems as well. As this was a central part of the work and an important tool for the results presented here, we will in this chapter describe the basics of how QmeQ operates and how it was adapted to perform counting statistics calculations.

The first order approaches in QmeQ are classical rate equations, also referred to as the Pauli approach [47], Bloch-Redfield master equations [112] and Lindblad master equations [114, 117, 122]. Additionally, there are the so called first and second order von-Neumann approaches [146, 147], that are based on taking the full correlation between up to one and two electrons, respectively, into account. Finally, the second order perturbation theory based on real time diagrammatics discussed in Sec. 9 was implemented in QmeQ as described in [37].

Fig. 10.1 schematically shows the standard procedure and the counting statistics implementation in QmeQ. The main difference is the separation of the kernel into the counting field resolved parts. Once this is done the current and noise can directly be calculated according to Eqs. (7.15) and (7.16). In contrast to the original QmeQ implementation we do not get the lead resolved current, i.e., the current at *every* lead separately, but only the current through a set of leads, the counting leads, that we pass as a model parameter. This is mainly done to reduce overhead, however, a generalization is straightforward. The current working version has the counting statistics implementation running alongside the regular calculations for the convience of immediate cross checking. In the case of the first order approaches the additional counting statistics calculations are included in the original approach class. In the future they could be separated into completely separate approaches to optimize performance and clearly differentiate from the standard approaches. The real time diagrammatic (RTD) implementation has been moved to a separate approach, that inherits many functions and properties from the original RTD implementation. Additionally, an extended kernel handler class has been implemented to deal with the counting kernel.

[3] The extended version is available on a fork of QmeQ at `https://github.com/si8881wo/qmeq`. Note that the extension is work in progress and while the core functions will presumably not change much, details could still be adapted. When we refer to QmeQ we mean (a branch) of this repository, unless stated otherwise.

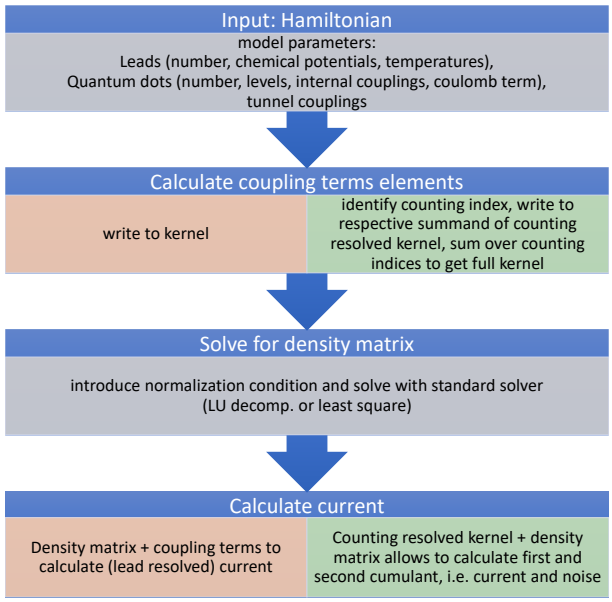

Figure 10.1: Schematic of the procedure to calculate the current in QmeQ with the steps specific to standard QmeQ (orange), the counting statistics implementation (green) and common procedures (gray). All steps except the first one (setting model parameters and from them building the Hamiltonian) are defined and performed in the *approach* class, that defines in which way the Master equation is set up.

The practical difficulty lies in finding the counting field dependence of the kernel $\mathcal{L}$ in Eq. (7.1). For the first order approaches in QmeQ, finding the different parts of the counting field resolved kernel is straightforward. QmeQ assumes that charge is a good quantum number and in the process of building the kernel it loops over the different charge states as well as the leads. This implementation is very convenient to identify kernel matrix elements that change the charge state due to the transfer of a single charge between the QD and the chosen leads. Currently all first order approaches in QmeQ work with this method. Since paper 1 is using the Lindblad approach we show a code example in Listing 1 with source code from the Lindblad approach. The additional lines that write the elements of $\mathcal{L}_+$ into the correct matrix (*kh.set_matrix_element_lpm(...)*) are highlighted in green. Here we use the fact that in sequential tunneling the processes transferring a lead to/from the leads are on the off-diagonal of the charge blocks. Building the kernel QmeQ loops over these charge blocks and the leads, so we can easily identify in which part of the counting field resolved kernel Eq. (8.8) the matrix element needs to be written. The original approach does, at this point, not differentiate between the leads and simply adds the summed up coupling terms to the full kernel matrix (*kh.set_matrix_element(...)*, highlighted in blue). In addition to identifying the elements to write into the correct part of the counting field resolved kernel, the implementation in QmeQ involves setting up necessary infrastructure including additional matrices, parser functions, etc., that we will not discuss further here.

```
def generate_coupling_terms(self, b, bp, bcharge):
  tLba = self.tLba
  si, kh = self.si, self.kernel_handler
  nleads, statesdm = si.nleads, si.statesdm
  Lpm = self.Lpm
  countingleads = self.funcp.countingleads

  acharge = bcharge-1
  ccharge = bcharge+1

  for a, ap in itertools.product(statesdm[acharge], statesdm[acharge]):
    if kh.is_included(a, ap, acharge):
      fct_aap = 0
      for l in range(nleads):
        fct_aap += tLba[l, b, a]*tLba[l, bp, ap].conjugate()
        if l in countingleads:
          kh.set_matrix_element_lpm(1j*tLba[l, b, a]*tLba[l, bp, ap].conjugate(), 0, b, bp, bcharge, a,
              ap, acharge)
      kh.set_matrix_element(1j*fct_aap, b, bp, bcharge, a, ap, acharge)
  # ------------------------------------------------
  for bpp in statesdm[bcharge]:
    if kh.is_included(bpp, bp, bcharge):
      fct_bppbp = 0
      for a in statesdm[acharge]:
        for l in range(nleads):
          fct_bppbp += -0.5*tLba[l, a, b].conjugate()*tLba[l, a, bpp]
      for c in statesdm[ccharge]:
        for l in range(nleads):
          fct_bppbp += -0.5*tLba[l, c, b].conjugate()*tLba[l, c, bpp]
      kh.set_matrix_element(1j*fct_bppbp, b, bp, bcharge, bpp, bp, bcharge)
    # ------------------------------------------------
    if kh.is_included(b, bpp, bcharge):
      fct_bbpp = 0
      for a in statesdm[acharge]:
        for l in range(nleads):
          fct_bbpp += -0.5*tLba[l, a, bpp].conjugate()*tLba[l, a, bp]
      for c in statesdm[ccharge]:
        for l in range(nleads):
          fct_bbpp += -0.5*tLba[l, c, bpp].conjugate()*tLba[l, c, bp]
      kh.set_matrix_element(1j*fct_bbpp, b, bp, bcharge, b, bpp, bcharge)
  # ------------------------------------------------
  for c, cp in itertools.product(statesdm[ccharge], statesdm[ccharge]):
    if kh.is_included(c, cp, ccharge):
      fct_ccp = 0
      for l in range(nleads):
        fct_ccp += tLba[l, b, c]*tLba[l, bp, cp].conjugate()
        if l in countingleads:
          kh.set_matrix_element_lpm(1j*tLba[l, b, c]*tLba[l, bp, cp].conjugate(), 1, b, bp, bcharge, c,
              cp, ccharge)
      kh.set_matrix_element(1j*fct_ccp, b, bp, bcharge, c, cp, ccharge)
  # ------------------------------------------------
```

Listing 1: Code example from the Lindblad approach in QmeQ. This function generates one column of the kernel and gets called for all charge states during the kernel generation.

Currently, in the first order approaches, the reduced density matrix is calculated with the kernel from the original QmeQ routine for convenience. In principle it is exactly the same matrix as the counting field resolved kernel evaluated at $\chi = 0$ and the redundancy of storing two kernels could be removed when optimizing performance. The counting field resolved kernel is currently only used for calculating the current and noise according to Eqs. (7.15) and (7.16) *additionally* to the standard method.

10.1 Real time diagrammatics implementation

For the second order implementation we follow Ref. [120], that provides a simple way to find the counting field resolved kernel for the real-time diagrammatic approach [118, 121]. This procedure has been described in Sec. 9. Once the counting field resolved kernel is found the full non-Markovian formula for the cumulants Eqs. (7.15) and (7.16) can be applied.

To find the current and Markovian part of the noise it is enough to find the "counting index", as the ε-derivative from Eq. (7.14) does only appear in the "non-Markovian" part of Eq. (7.16). Taking this derivative numerically requires solving the integrals for the matrix elements with a modification of the many-body energy level spacing.

The standard real-time diagrammatics implementation in QmeQ exploits the so-called "mirror rule" [121]

$$\begin{aligned} \mathrm{Re}W^{a_1+a_1-}_{a_2+a_2-} &= \mathrm{Re}W^{a_1-a_1+}_{a_2-a_2+}, \\ \mathrm{Im}W^{a_1+a_1-}_{a_2+a_2-} &= -\mathrm{Im}W^{a_1-a_1+}_{a_2-a_2+}, \end{aligned} \tag{10.1}$$

in order to reduce number of times the numerically expensive integrals have to be calculated when evaluating the kernel. It follows from the general kernel property $(W(z))^{a_1+a_1-}_{a_2+a_2-} = (W(-z*))^{a_1+a_1-}_{a_2+a_2-}*$ that guarantees a hermitian stationary state density matrix. In particular, using the mirror rule in Eq. (10.1) halves the number of integrations. That is because the mirror rule corresponds to flipping all indices. However, the mirror rule is only valid in the limit $z \to i0^+$. We need to evaluate the kernel at finite $z = \varepsilon + i0^+$ in order to take the numerical derivative $\dot{J}$. A finite ε in the kernel $W(\varepsilon + i0^+)$ corresponds to a system with a slight shift in the many-body eigenenergies.

The diagrams that need to be calculated are implemented explicitly in QmeQ. We have added the required additional diagrams with flipped indices in order to be able to calculate the numerical derivative. Note that the finite difference is used for the numerical derivative. The step length is set explicitly (but can be changed like a model parameter) and it is in principle not guaranteed to be small enough. One could iterate over decreasing step lengths until convergence, but for each step the integral has to be evaluated again. That comes at a large numerical cost and we choose to leave it up to the users discretion to change it appropriately if needed. To set the standard value and check for implementation errors we compared to the results of Ref. [120]. We have also implemented the "O(4) trunc." approach from Ref. [120] alongside second order RTD, as it uses the same counting kernels. It is a rigorous expansion of the transport quantities to second order in the tunnel couplings. The density matrix, projectors and pseudoinverse in Eqs. (7.15) and (7.16) need to be expanded in orders of Γ as well and subsequently all terms $O(\Gamma^3)$ are neglected. Details on this expansions can be found in Refs. [148, 149].

11 Single resonant level and Anderson dot

In this section we want to make use of the formalism and tools we have introduced in Secs. 5-10. We give a simple example of using counting statistics on the single resonant level in Sec. 11.1 and use it briefly illustrate the working principle of a QD thermoelectric engine and a simple QD charge sensor. In Sec. 11.2 we then discuss the effects of interactions and second order tunneling.

11.1 Counting statistics with rate equations on a single resonant level

The simplest model of a QD system is a single resonant level. We can think of it as a QD with a single level without spin. The full Hamiltonian is

$$H_{SRL} = \varepsilon d^\dagger d + \sum_{r,k} t_{k,r} c_{r,k}^\dagger d + h.c. + \sum_{r,k} t_{k,r} c_{r,k}^\dagger c_{r,k}. \tag{11.1}$$

With this Hamiltonian the energy eigenbasis is simply $\{|0\rangle, |1\rangle\}$, where the states are numbered by their occupation. We can insert this in the Pauli rate equation (8.4) and with the rates in Eq. (8.6) find the rate equation

$$\dot{P}_0 = -(\Gamma_L f_L + \Gamma_R f_R) P_0 + (\Gamma_L (1 - f_L) + \Gamma_R (1 - f_R)) P_1 \tag{11.2}$$

$$\dot{P}_1 = (\Gamma_L f_L + \Gamma_R f_R) P_0 - (\Gamma_L (1 - f_L) + \Gamma_R (1 - f_R)) P_1 \tag{11.3}$$

for the occupation probabilities $P_1 = 1 - P_0$ of the QD. Note that in a single level there are no off-diagonals of the density matrix, so this is a full description in the sequential tunneling regime. From here we can set up the conditional rate equation by keeping track of the number of transferred electrons n at, for example, the left lead as

$$\dot{P}_0(n) = -(\Gamma_L f_L + \Gamma_R f_R) P_0(n) + \Gamma_L (1 - f_L) P_1(n+1) + \Gamma_R (1 - f_R) P_1(n) \tag{11.4}$$

$$\dot{P}_1(n) = \Gamma_L f_L P_0(n-1) + \Gamma_R f_R P_0(n) - (\Gamma_L (1 - f_L) + \Gamma_R (1 - f_R)) P_1(n). \tag{11.5}$$

Note that this is an very simple version of the conditional master equation (7.1). Introducing the counting field χ as conjugate variable to n via $\dot{\tilde{P}}(\chi) = \sum_n e^{in\chi} P(n)$ we find the counting field resolved rate equation in matrix form

$$\dot{\tilde{P}} = \begin{pmatrix} -\Gamma_L f_L - \Gamma_R f_R & \Gamma_L (1 - f_L) e^{-i\chi} + \Gamma_R (1 - f_R) \\ \Gamma_L f_L e^{i\chi} + \Gamma_R f_R & -\Gamma_L (1 - f_L) - \Gamma_R (1 - f_R) \end{pmatrix} \tilde{P}. \tag{11.6}$$

Here we relabeled the sum index when converting to the counting field dependent probabilities. In this simple case it is possible to obtain an analytical expression for the needed eigenvalue of the counting field resolved Liouvillian

$$z(\chi) = \frac{(\Gamma_L + \Gamma_R)}{2} \cdot \left(\sqrt{1 + \frac{4\Gamma_L \Gamma_R}{(\Gamma_L + \Gamma_R)^2} \left(f_L \left(1 - f_R\right) \left(e^{i\chi} - 1\right) + f_R \left(1 - f_L\right) \left(e^{-i\chi} - 1\right)\right)} - 1 \right) \tag{11.7}$$

and take the first and second derivative in the expansion Eq. (7.5) to arrive at

$$I = -iz'(0) = \frac{\Gamma_L \Gamma_R}{(\Gamma_L + \Gamma_R)} \left(f_L - f_R\right) \tag{11.8}$$

$$S = -z''(0) = \frac{\Gamma_L \Gamma_R}{(\Gamma_L + \Gamma_R)} \frac{\left(\Gamma_L^2 + \Gamma_R^2\right) \left(f_L + f_R - 2 f_L f_R\right) + 2\Gamma_L \Gamma_R \left(f_L(1 - f_L) + f_R(1 - f_R)\right)}{\left(\Gamma_L + \Gamma_R\right)^2}. \tag{11.9}$$

Alternatively can easily identify

$$\mathcal{L}_- = \begin{pmatrix} 0 & \Gamma_L(1 - f_L) \\ 0 & 0 \end{pmatrix}, \quad \mathcal{L}_+ = \begin{pmatrix} 0 & 0 \\ \Gamma_L f_L & 0 \end{pmatrix}. \tag{11.10}$$

and arrive at the same expressions for I and S via Eqs. (8.10) and (8.11).

In Fig. 11.1 we show an example of the current I, differential conductance $^{dI}/_{dV}$, noise S and Fano factor $F = |^{S}/_{I}|$ according to Eqs. 11.8 and 11.9. In this case we show a system with symmetric tunnel couplings $\Gamma_L = \Gamma_R = \Gamma$ and a temperature bias $T_L > T_R$ between the leads. We see that $I = \pm 0.5\Gamma$ for large positive/negative biases Additionally, the effect of the temperature bias is visible in the different broadening of the current steps/conductance lines.

We now focus on the current, Eq. (11.8), that depends on a the difference between the Fermi functions at the left and right leads, i.e.

$$I \propto f_L - f_R = \frac{1}{e^{(\varepsilon - \mu_L)/T_L} + 1} - \frac{1}{e^{(\varepsilon - \mu_R)/T_R} + 1}. \tag{11.11}$$

In the large bias limit with $\mu_L < \mu_R$ we have $f_L = 0$ and $f_R = 1$ and find a negative current for all QD levels ε, that corresponds to electrons flowing from the left lead to the right lead. Similarly, if the bias is finite but significantly bigger than temperature $\mu_L -$

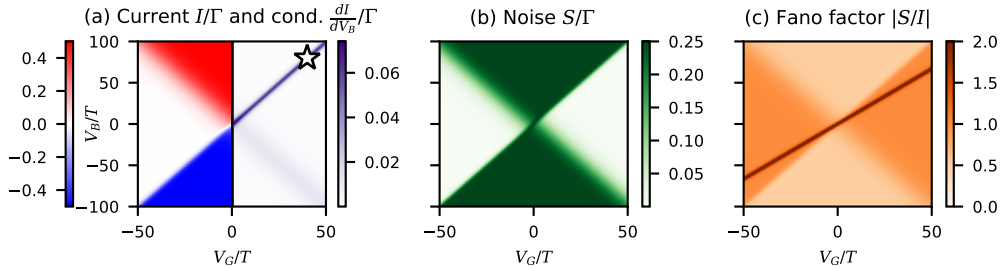

Figure 11.1: (a) Current I (red-blue, left), differential conductance $^{dI}/_{dV}$ (purple, right), (b) noise S and (c) Fano factor $F = |^{S}/_{I}|$ as functions of a symmetrically applied bias $V_b = \mu_L - \mu_R$ and gate voltage $V_g = -\varepsilon$, where $T_L = 5T$ and $T_R = T$ sets the temperature bias and $\Gamma_L = \Gamma_R = 0.25T$. The star in (a) indicates a reasonable point to operate the QD as a sensor, c.f. Sec. 12.

$\mu_R \gg T$, then if the QD level is in the so-called bias window $\mu_L < \varepsilon < \mu_R$, we get the same current as in the infinite bias case. Outside the bias window the current will drop to zero. This can be utilized as a charge sensor, by coupling to the QD level [150–152]. The current through the QD can then be used as the signal when switching between two configurations. The sensitivity of such a sensor is then tied to the temperature, which determines how well the current reacts to changes in the QD level. This can clearly be seen in the width of the conductance lines. The line associated with the hotter left lead is broader than the one associated with the colder right lead. We will discuss this in more detail in the context of paper I in sections 12 and 13.

Given the temperature difference $T_L > T_R$ between the leads, for biases with $\mu_L < \mu_R$ it is possible to find an ε resulting in a current from right to left, against the bias. The system then operates as a heat engine. The QD levels where electrons are transported against a bias in this case will lie above the bias window. We will discuss this in more detail in sections 14.2 and 15 in the context of paper II.

11.2 Interaction and second order effects in an Anderson dot

If one includes also the spin in the QD we call the system an Anderson dot. It exhibits rich physics like, e.g, the Kondo effect [153–156] and Coulomb blockade. The former only becomes relevant for large tunnel couplings and requires a type of theory that is beyond the scope of this thesis. The Anderson dot can also be operated in a heat engine regime similar to the single resonant level. In this subsection we want to briefly show effects of Coulomb interactions and second order perturbation theory in the tunnel couplings on the transport

through such an Anderson dot. The Hamiltonian reads

$$\begin{aligned} H_{AD} =& H_{QD} + H_T + H_R \\ =& \sum_\sigma \varepsilon_\sigma d_\sigma^\dagger d_\sigma + U d_\uparrow^\dagger d_\uparrow d_\downarrow^\dagger d_\downarrow \\ &+ \sum_{r,k,\sigma} t_{rk\sigma} c_{rk\sigma}^\dagger d_\sigma + h.c. \\ &+ \sum_{r,k,\sigma} \omega_{rk\sigma} c_{rk\sigma}^\dagger c_{rk\sigma}. \end{aligned} \tag{11.12}$$

Compared to the single resonant level introduced before, we have added a spin index σ to the level and a charging energy U between electrons on the dot. Note that due to the charging energy U it is not easily possible to find an analytical solutions for this system. We can however make use of the numerical machinery introduced in Sec. 7 and calculate transport quantities. In particular we here want to show the difference between the sequential tunneling case and the second order approximation introduced in Sec. 9. In Fig. 11.2 we show various transport quantities as functions of V_B and V_G calculated using the Pauli (a-c) and RTD (d-f) approaches.

The introduction of the second spin state and the Coulomb interaction leads to the emergence of so-called Coulomb diamonds. When an electron occupies the dot and the bias is not large enough to overcome the charging energy U no current can flow. This can be seen in the current and differential conductance in Figs. 11.2(a) and (d) for both first and second order, where in the central region the current is suppressed. The height of the Coulomb diamond is determined by the charging energy U and the magnetic field $B = \varepsilon_\uparrow - \varepsilon_\downarrow$ that splits the spin levels. In sequential tunneling, the current is exponentially suppressed in the Coulomb diamond. Second order processes lead to a finite conductance and additional structure inside the Coulomb diamond. Note that the structure is not visible in the current on a linear scale, and only becomes apparent in the differential conductance on a logarithmic color scale. Similarly, on the linear scale used here, there is no obvious difference between the noise S in first and second order. When looking at the Fano factor $F = |S/I|$ however, the difference between the first and second order results becomes apparent also on a linear scale.

Figure 11.2 clearly highlights the effects of second order tunneling processes in the regions where current is suppressed. Given a temperature bias on the leads of a spinful single level QD, this blockaded region is precisely where the system can be operated as a heat engine. That means that for a proper analysis of a the heat engine we need to take second order effects into account. This and more will be discussed in more detail in sections 14 and 15 in the context of paper II.

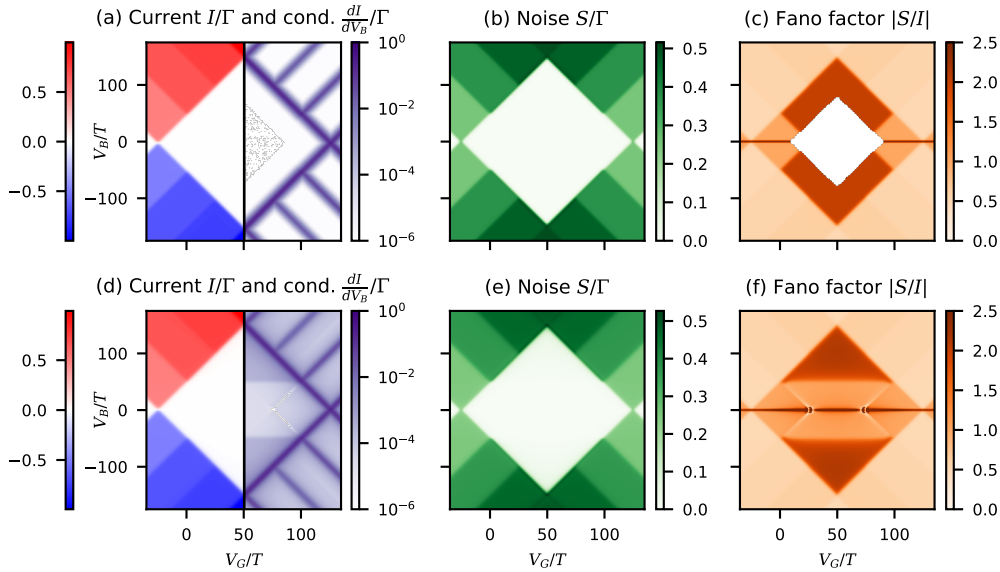

Figure 11.2: (a) Current(red-blue, left) and differential conductance (purple, right), (b) noise and (c) Fano factor for the Anderson dot in first (upper row (a-c)) The lower row (d-f) shows the same quantities in the second order RTD approach. The parameters are $\Gamma = 0.25T$, $U = 100T$ and a magnetic field $B = 25T$ that detunes the spin levels $\varepsilon_{\uparrow/\downarrow} = -V_G \pm B$. Note that far inside the Coulomb diamond the sequential tunneling current is exponentially suppressed. This can lead to numerical problems when calculating the Fano factor and hence the center in (a) and (c) have been left blank. The implementation of the RTD approach can lead to artifacts related to higher order tunneling processes, which can be seen origination from points at zero bias in the Coulomb diamond in (d) and (f).

12 Charge sensing

A sensor is a device that measures the properties of an adjacent system. Here we want to detect small changes in the electrostatic environment of our sensor. More specifically, we think about detecting single charges, e.g., electrons on a QD or charge island, close to the sensor system. To achieve this we want to use an observable that is easy to measure and sensitive to changes in the electrostatic environment. Our observable of choice is the charge current through a QD system, as we have easy access to it not only in our theoretical description, but it also is a standard measurement in transport setups.

To illustrate the principle we will make use of a standard setup for charge sensing [150–152], the single resonant level model[4] as described in Sec. 11.1. The changes in the electrostatic environment will be reflected in changes to the energy level ε of the QD. In principle it would also be possible to use a change in the tunnel couplings, but in practice that is much less sensitive to changes to nearby charges.

[4]The same arguments apply if, e.g., an Anderson type setup described in Sec. 11.2 is used.

We formalize the signal as a derivative of the current with respect to a change the QD level

$$\partial_{\delta\varepsilon} I = \frac{dI}{d\delta_\varepsilon}|_{\delta_\varepsilon=0}. \tag{12.1}$$

In practice that means we want to tune the gate and bias voltage of the QD, such that we are positioned on the conductance line at the border between a high and low current regime, as indicated by the star in Fig. 11.1(a). At that point we find $\mu_R = -\varepsilon$ and if we are far enough from the crossing point of the conduction lines the current according to Eq. (11.8) reduces to

$$I \approx \frac{\Gamma_L \Gamma_R}{(\Gamma_L + \Gamma_R)} \left(1 - \frac{1}{e^{\delta_\varepsilon / T_R} + 1}\right). \tag{12.2}$$

At $\delta_\varepsilon = 0$ we then find the signal

$$\partial_{\delta\varepsilon} I = -\frac{\Gamma_L \Gamma_R}{4\,(\Gamma_L + \Gamma_R)} \frac{1}{T} \propto \frac{1}{T}. \tag{12.3}$$

Optimizing only the signal is not sufficient for a good sensor. If the noise is too big, then no signal can be extracted from a measurement in a reasonable time. The performance can be formalized in the error

$$\sigma^2_{\delta\varepsilon} = \frac{1}{\tau} \frac{S}{(\partial_{\delta\varepsilon} I)^2}, \tag{12.4}$$

obtained by the standard error propagation formula [157, pp.366]. Here, τ is the measurement time. The error reflects the trade-off between large signal and acceptable noise. We will use it as is our measure for the quality of a sensor.

At the operation point, where $\mu_R = -\varepsilon$, and far enough from the crossing we find $f_L = 1$ and $f_R = 1/2$, such that the noise according to Eq. (11.9) is constant with respect to temperature. That means the temperature dependence of the error here is due to the scaling behavior of the signal. Overall we find

$$\sigma^2_{\delta\varepsilon} \propto T_R^2 \tag{12.5}$$

for the error of the single resonant level model operated as a charge sensor.

13 Summary and discussion of paper 1

We investigate the dynamics of an interacting parallel double QD and its possible application as a charge sensor in paper 1. The parallel double QD system can exhibit metastable

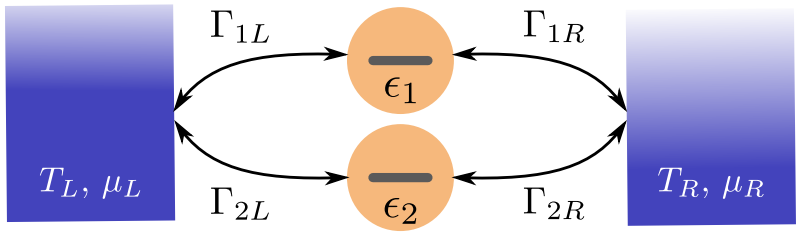

Figure 13.1: Schematic representation of the parallel QD setup. The QD energy levels are denoted by ϵ_i and are coupled to macroscopic leads s via the tunnel couplings Γ_{is}. Here $i = 1, 2$ is the QD level index and $s = L, R$ is the lead index. The leads are characterized by temperatures T_L and T_R and chemical potentials μ_L and μ_R, respectively. Adapted from paper I.

behavior, i.e., it can evolve through a quasi stationary state before relaxing into its true stationary state [158–161], giving rise to an additional relaxation time scale that has to be considered for the sensor application. Dynamical and quantum effects may even give rise to advantages for metrology applications [162, 163].

In the specific system we are investigating, two spinless QDs coupled in parallel to macroscopic leads as shown in Fig. 13.1. The Hamiltonian can be written in a form similar to Eq. (5.4)

$$H = H_{\mathrm{PD}} + H_L + H_T, \tag{13.1}$$

where the parallel QD Hamiltonian is

$$H_{\mathrm{PD}} = \sum_{j=1,2} \epsilon_j d_j^\dagger d_j + U d_1^\dagger d_1 d_2^\dagger d_2. \tag{13.2}$$

The two parallel single level QDs are labeled by j and they interact only via Coulomb interaction U. The leads and tunneling parts are

$$H_L = \sum_{s=L,R} \sum_k \omega_{sk} c_{sk}^\dagger c_{sk}. \tag{13.3}$$

$$H_T = \sum_{j=1,2} \sum_{s=L,R} \sum_k \left(t_{jsk} c_{sk}^\dagger d_j + t_{jsk}^* d_j^\dagger c_{sk} \right), \tag{13.4}$$

Importantly, the two QDs couple to the same lead mode.

In the fully symmetric configuration, i.e. $t_{jsk} = t_k$ and $\epsilon_j = \epsilon$ the system is invariant under exchanging electrons on the two dots. If this symmetry is intact, the system supports two distinct stationary states. In the presence of strong Coulomb interaction, these two stationary states carry vastly different currents. Breaking this parity-like symmetry leads to the emergence of an additional slow timescales in the dynamics of the systems relaxation

to the steady state. The stationary state in the so-called metastable regime can be expressed as a probabilistic mixture of the two stationary states of the fully symmetric system. Since the two stationary states in the symmetric case carry such different currents, the current of the stationary state, when the symmetry is broken can be very sensitive with regard to small changes in parameters. This allows for the use of the system as a charge sensor, e.g., by capacitively coupling to the gates controlling the QD levels.

The contributions relevant for this thesis were the numerical steady state noise and signal calculations in chapter V of paper I. The remainder of this chapter will therefore focus on the details and results of these calculations, implications and also a more detailed comparison to the conventional single QD setup for charge sensing. The noise calculations were done using the methods described in Secs. 6-8.

We use the Lindblad approach since coherences play a central role for the physics of the system. In this particular case the Lamb-shift has been taken into account. Interference between the two paths the electrons can take when tunneling from one lead to another, see Fig. 13.1, is encoded in the non-diagonal density matrix elements.

To operate the double QD as a sensor we set the energy levels to be

$$\epsilon_1 = \epsilon - \delta\epsilon, \quad \epsilon_2 = \epsilon + \delta\epsilon, \tag{13.5}$$

i.e., they are equal up to a detuning $\delta\epsilon$. The tunneling rates are chosen as

$$\Gamma_{1L} = \Gamma - \delta\Gamma, \quad \Gamma_{1R} = \Gamma + \delta\Gamma, \tag{13.6}$$

$$\Gamma_{2L} = \Gamma + \delta\Gamma, \quad \Gamma_{2R} = \Gamma - \delta\Gamma, \tag{13.7}$$

with a small perturbation $\delta\Gamma$. We make this specific choice to break the symmetry leading to the metastable behavior, but that the qualitative physics remains the same for any perturbation that breaks this symmetry.

We assume that the charge we want to sense, e.g., an electron on a nearby QD, impacts the detuning $\delta\epsilon$. The response of the current to a change in the detuning, i.e., $\partial_{\delta\epsilon} I$, is the signal. In Fig. 13.2 (a-c) we show the current, signal and noise for this setup. The current plot, Fig. 13.2(a), shows that regions with greatly different currents emerge when changing the detunings. If we choose the detuning in between these two regions any small change due to close by charges will lead to a big signal.

We can also see that the signal increases if we close in on the high-symmetry point where all tunnel couplings are equal and there is no detuning, see Fig. 13.2(b). For some parameter choices (small $\delta\varepsilon$ and $\delta\Gamma$) the system exibits a metastable regime due to an emerging small time scale set by the small perturbations. The relevant time scales in this case are given λ_2 and λ_3 that are the eigenvalues with largest non-zero real part of the Liouvillian, where $0 > \mathrm{Re}\lambda_2 > \mathrm{Re}\lambda_3$. If $\mathrm{Re}\lambda_2 \gg \mathrm{Re}\lambda_3$ then there is an additional relaxation timescale

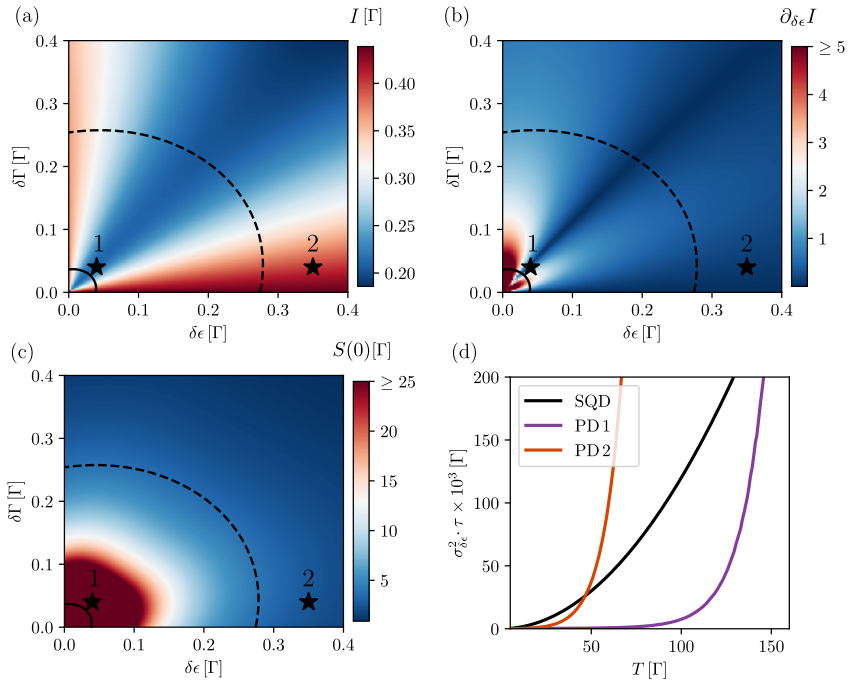

Figure 13.2: (a) Current, (b) signal, (c) noise as a function of detuning $\delta\epsilon$ and $\delta\Gamma$ and (d) temperature dependence of the error of the double QD set-up operated at the points 1 and 2 indicated by the stars in (a-c). Here $U = 250\Gamma$ and $T_L = T_R = 10\Gamma$. The gate voltage controlling the QD level ($\epsilon_i = -eV_G$) is set to $V_G = 0$ and the chemical potentials of the leads are set to result in a symmetric bias of $V_B = 30\Gamma$. This operation point is also indicated in the stability diagrams 13.3. Adapted from paper 1.

present and we identify the regime where metastability occurs by the somewhat arbitrarily picked condition $\mathrm{Re}\lambda_3/\mathrm{Re}\lambda_2 > 20$. The outer border of this region is indicated by the dashed line in Figs. 13.2(a-c). To make use of the metastable behavior for the sensor we need to be in inside this border.

The slowest timescale in the system also gives a lower limit on the choices for $\delta\varepsilon$. The dynamics have to be fast enough for the system to reach the steady state on a much smaller timescale than the measurement time τ. In that case we can calculate all quantities in the steady state. Requiring $-\mathrm{Re}\lambda_2/\Gamma > 10^3$ to ensure fast enough relaxation results in the solid line in Figs. 13.2(a-c).

In Fig. 13.2(c) we see that the noise is strongly enhanced for small detunings. As this is also the region where the signal is large, finding a good operation point is a trade off between large enough signal and acceptable noise. In Fig. 13.2(d) we show the error for the two parameters indicated in the other plots of Fig. 13.2 along with the error for a single QD operated as a sensor. We see that the double QD setup by far outperforms the single-QD sensor. This is due to the fact that the two different current regimes in Fig. 13.2(a) are caused

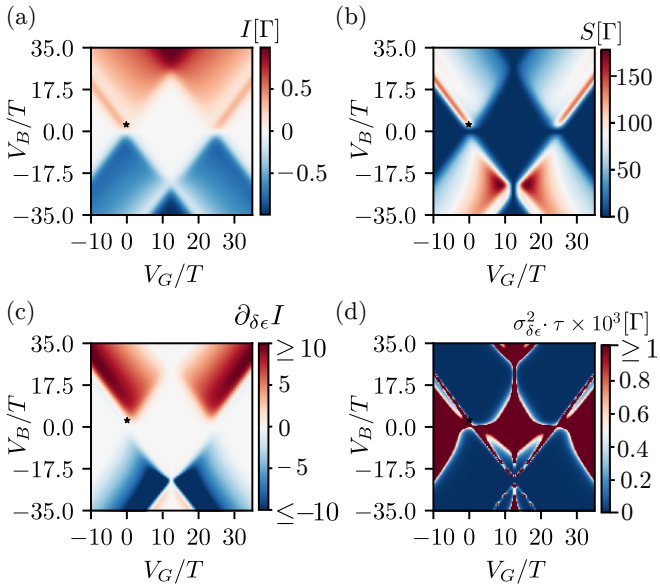

Figure 13.3: (a) Stationary current, (b) noise, (c) signal and (d) error for the parallel double QD system plotted as a function of V_G and V_B. The star indicates the parameters used in Fig. 13.2. Adapted from paper I.

by coherences in the system that are not limited by the lead temperature.

In the stability diagrams shown in Fig. 13.3 the parameter point used in Fig. 13.2 is indicated by a star. Note that the structure inside the Coulomb diamond in Fig. 13.3(d) is due to the current and noise not being exactly zero, but exponentially suppressed. In this area higher order processes dominate the transport and the Lindblad approach is not a good description of the system so we do not consider this area further. The operation point in the stability diagram has not been fine tuned to achieve the optimal error. Comparing Figs. 13.3(b,c) or directly looking at the error Fig. 13.3(d) we can see that most of the area between the conductance lines can result in a good sensor. The fact that the operation point and detunings in Fig. 13.2(d) were not optimized shows the double QD setups potential as a charge sensor.

14 Quantum dot thermoelectric engines and quantum thermodynamics

On the one hand, driving current through a QD does not only transfer particles from one lead to the other, but also energy and heat flow between the leads. On the other hand, applying different temperatures to leads coupled to a QD system can lead to a thermoelectric

current driven by the temperature gradient. With the help of quantum master equations we can calculate the relevant thermodynamic quantities and investigate thermodynamic properties at the quantum level.

14.1 Additional transport quantities

In the context of quantum thermal machines, the particle current and noise are not the only relevant transport quantities. In order to define efficiencies, we need to additionally define for example the produced power, heat current and efficiency. In this section we follow [54], in particular section 3, to formulate the first law of thermodynamics in the context of the QD Hamiltonian Eq. (5.4) in order to motivate the heat current. The relevant quantity is the time derivative of the average of the total Hamilatonian, i.e. the total energy in the system and baths,

$$\begin{aligned} \partial_t \langle H(t)\rangle &= \mathrm{Tr}(\partial_t H(t)\rho_{tot}(t)) + \underbrace{\mathrm{Tr}(H(t)\partial_t\rho_{tot}(t))}_{=0, \text{ see Ref. [54]}} && (14.1)\\ &= \partial_t\langle H_{QD}(t)\rangle + \partial_t\sum_r\langle H_{R,r}\rangle + \partial_t\langle H_{T,r}\rangle. && (14.2)\end{aligned}$$

Here we assumed that the reservoir and tunneling Hamiltonians are time independent, i.e. $\partial_t H(t) = \partial_t H_{QD}(t)$. Note that this does not imply $\partial_t\langle H_{R,t}\rangle = 0$ since the average contains the time dependence of the total density matrix. Writing the power provided to the system by an external drive as $\langle\partial_t H_{QD}(t)\rangle = P_s$ we can rearrange this to

$$\partial_t\langle H_{QD}(t)\rangle = P_s - \partial_t\sum_r\langle H_{R,r}\rangle - \partial_t\sum_r\langle H_{T,r}\rangle. \tag{14.3}$$

This is an energy balance for the QD or in other words a first law of thermodynamics for our QD. Here $\partial_t\sum_r\langle H_{R,r}\rangle$ is the energy flowing out of the reservoirs, i.e. energy current from reservoirs and the last term $\partial_t\sum_r\langle H_{I,r}\rangle$ corresponds to some energy, stored in the coupling barriers between system and bath. The latter is typically small and can be neglected in weak coupling [54]. The energy current out of reservoir r typically gets further separated into

$$\partial_t\langle H_{R,r}\rangle = Q_r + \mu_r I_r, \tag{14.4}$$

where $I_r = \partial_t\langle N_r\rangle$ is the particle current. The heat current

$$Q_r = \partial_t\langle H_{R,r}\rangle - \mu_r I_r \tag{14.5}$$

can in this way be seen as the energy flowing out of reservoir r due to particles flowing out of the reservoir at energies above its chemical potential μ_r or electrons entering the

reservoir r below the its chemical potential. In summary, when we assume no driving on the QD and weak coupling we find that the energy change on the QD

$$\partial_t \langle H_{QD}(t) \rangle = -\sum_r (Q_r + \mu_r I_r) \tag{14.6}$$

is due to heat and electrons flowing from the leads into the QD or vice versa. This is consistent with a classical thermodynamic view of energy conservation.

Note here that we have not made any approximations up until this point and have not set up a master equation. It is also worth noting that finding the heat current in this way (i.e. via the energy current) with, e.g., a master equation of Lindblad form does not necessarily ensure that the thermodynamic laws hold (see Refs [54, 164] for example with Lindblad). This is due to the various approximations like Markov or secular approximation that are often made when deriving master equations. Large violations typically indicate that one operates outside the regime of validity of one or more or the approximations.

In the context of QD thermoelectric engines the heat current is an important quantity since it can be used to calculate the efficiency. In particular the efficiency is the ratio of produced electrical power P to the heat flowing out of the hot lead Q_H

$$\eta = P/Q_H. \tag{14.7}$$

For the details of how the energy and heat current are calculated we refer to Refs. [37, 116].

14.2 Quantum dot thermoelectric engines

As mentioned for the simple model in Sec. 11, QD devices can be operated as heat engines. To do this we make use of their energy filtering properties. For two leads at different temperatures, the Fermi function describing their population is broadened differently. This can lead to situations, where in an energy range the occupation probability in the lead with lower chemical potential is greater than in the lead with higher chemical potential lead. Using QDs to create a narrow transmission window between two leads allows one to restrict electron exchange to this energy window and generate an overall current against the external potential difference. One can even show that a narrow transmission window, like a single QD level in the sequential tunneling limit described by rate equations, is the most efficient [165, 166]. It can in principle reach Carnot efficiency, but in that case the process needs to be reversible and no power can be extracted.

For two leads, there are two configurations where the occupation probabilities are inverted. When the hot lead has lower chemical potential, the occupation inversion lies above the bias window. If the cold leads chemical potential lies lower, then the inversion happens below

the bias window. These two situations are sketched in Fig. 14.1(a) and (b), respectively. The electrical power of a heat engine is simply the current times the bias

$$P = -IV_b, \tag{14.8}$$

where the minus sign comes from our convention for current and bias directions.

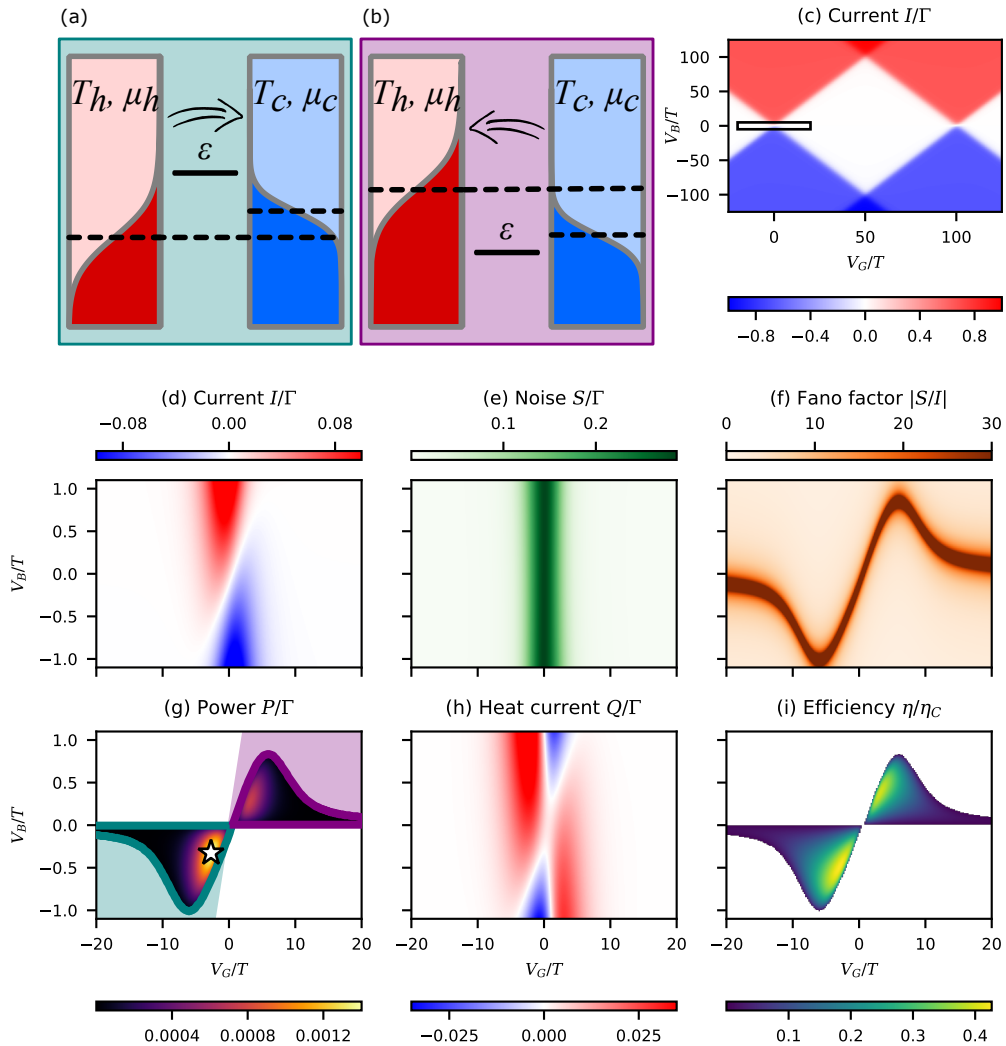

Figure 14.1: (a) and (b) indicate the possible configurations of energy levels and chemical potential for operation as a heat engine (adapted from paper II). The arrow indicates the direction of the (particle) thermocurrent. Figures (c-i) show transport quantities for a Anderson dot with $T_h = 1.3T_c$, $\Gamma = 0.25T_c$ and $U = 100T_c$. In (c) the current is shown over a wide range in V_B and V_g with the box indicating the region displayed in (d-i). In the smaller area we show (d) the current, (e) the noise and (f) the Fano factor. Figure (g) shows the power output where the QD operates as a heat engine and the star indicating the maximum, (h) the heat current at the hot lead and (i) the efficiency.

In Figs. 14.1(c-i) we show the transport quantities for an Anderson type QD described by the Hamiltonian H_{AD} in Eq. (11.12) calculated with the second order RTD approach outlined in Sec. 9. Figure 14.1(c) shows the full current Coulomb diamond, where the rectangle around the left crossing indicates the area where it operates as a heat engine. The current and noise in that area are shown in Fig. 14.1(d) and (e) respectively. With that, the Fano factor can be calculated, shown in Fig. 14.1(f). Note here that the large increase around zero current clearly indicates the edge of the positive power regime, where the setup operates as a heat engine.

The power is shown in Fig. 14.1(g), where only areas of positive power have been drawn and the remaining areas are left blank. The star indicates the maximum power. The shape of the positive power lobes is a result of the second order approach and is due to the effective broadening of the level due to cotunneling. In sequential tunneling the positive power area would extend to the teal and purple shaded areas. The color indicates the configuration of the QD as shown in 14.1(a) and (b).

Figure 14.1(h) shows the heat current at the hot lead. When the power is positive, the heat current is also positive, i.e. heat is flowing out of the lead. In Fig. 14.1(i) the efficiency is shown. Note that the maximum efficiency point does not line up with the maximum power point.

While transporting electrons against an externally applied bias shows the thermoelectric current we wish to use in a heat engine, it is not possible to extract electrical work in this setup. An external load, where the power is developed can be modeled by connecting the leads via a resistor R. This situation is shown in Fig. 14.2(a) and (b).

To find the voltage and current through the load resistor we use Ohms law

$$I(U, V_g) - \frac{U}{R} = 0, \tag{14.9}$$

where $I(U, V_g)$ is the current through the QD with bias U at gate voltage V_g. Due to Kirchhoffs law this is exactly the voltage drop U over the resistor R and current going through it. We can numerically solve this equation for the bias U at a given gate and resistance.

For a given resistor, sweeping the gate results in a cut through the positive power lobe. At infinite resistance, i.e. an open circuit, the resulting cut is exactly the outline of the positive power lobes, while the short circuit power will be zero. If one wishes to operate at the maximum power point, is possible to calculate the needed load resistor. To do that one can simply find the maximum power point in gate-bias space and rearrange Eq. (14.9) for the resistance R. Similarly, one can find a load resistance corresponding to any other operating point in the heat engine regime.

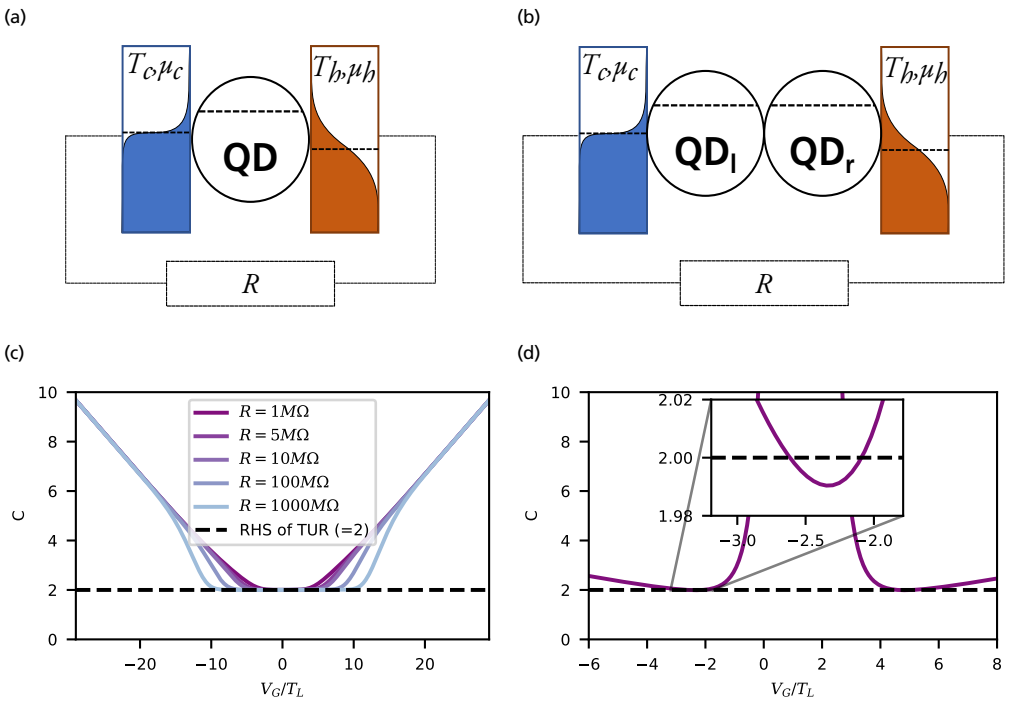

Figure 14.2: Schematic of (a) a single spinful QD (Anderson model) and (b) a serial double QD operated as a heat engine coupled to a load resistor. (c) shows the left hand side of the TUR (14.12) for the Anderson model using Pauli rate equations. The parameters used for the calculations correspond to $\Gamma_L = 5.0$GHz, $\Gamma_R = 1.1$GHz, $T_L = 1$K, $T_R = 1.5K$, $U = 100$meV which is motivated by preliminary measurements taken in a lab. (d) shows the hand side of the TUR (14.12) for serial double QD operated as a heat engine coupled to a load resistor with inter dot coupling $\Omega = 50\Gamma$, Coulomb interaction strength $U = 250\Gamma$ and temperatures $T_L = 100\Gamma$, $T_R = 150\Gamma$ using the Lindblad approach. The inset shows the violations, where the value of the left hand side clearly goes below 2, which is the value given by the TUR.

14.3 Thermodynamic uncertainty relations in thermoelectric engines

The general form of the TUR is [64, 167, 168]

$$\frac{\langle\langle \Phi^2 \rangle\rangle}{\langle \Phi \rangle^2}\sigma \geq 2, \tag{14.10}$$

where $\langle \Phi \rangle$ and $\langle\langle \Phi^2 \rangle\rangle$ are mean and fluctuations, respectively, of a physical observable Φ and σ is the entropy production. It can be derived in the context of classical rate equations. That means it can in principle be violated when quantum effects are taken into account and play a role in the system. In fact, violations are expected and have been shown in a non-interacting setting in Refs. [169, 170], specifically in the presence of coherences and for higher order tunneling contributions. Previous works showed that even in a single QD operating as a heat engine at high efficiencies second order contributions become important

for modeling the current accurately [35–37]. It seems likely that second order contributions will have a notable effect also on the noise, which could lead to violations of the TURs.

The TURs in thermoelectric engines can be expressed in terms of transport quantities, namely the current I, noise S and efficiency η. In particular, the entropy production σ in thermoelectric engines can be written as [170]

$$\sigma = \langle j_p \rangle \frac{1}{T_c} \frac{\eta_c - \eta}{\eta}, \tag{14.11}$$

where $\langle j_p \rangle = P = -I \cdot V$ is the power output of the engine, $\eta_{(c)}$ the (Carnot) efficiency and T_c the temperature of the cold reservoir. The efficiency can be calculated from the heat current Q via $\eta = {}^{P}/_{Q} = {}^{IV}/_{Q}$ and the Carnot efficiency $\eta_c = 1 - {}^{T_c}/_{T_h}$ depends on the ratio of the temperatures of the cold and hot bath. The setups we investigate here are for example the ones sketched in Fig. 14.2, where the energy filtering property of the QD(s) is used to create a thermocurrent against the potential bias due to a load resistor.

Inserting Eq. (14.11) into the general TUR in Eq. (14.10) and choosing the current as observable Φ we get

$$C = \frac{S}{I^2}\sigma = \frac{S}{I} V \frac{1}{T_c} \frac{\eta_c - \eta}{\eta} \geq 2, \tag{14.12}$$

Where we have introduced the variable C to refer to the left hand side of the inequality.

We can investigate the TUR, e.g., for the Anderson model (single spinfull QD) coupled to a load resistor, see Fig. 14.2a. Since in this systems there are no coherences present we can use Pauli rate equations for first order calculations in tunneling rate and we do not expect any TUR violations. Indeed, if we plot the left hand side of Eq. (14.12) for a system with experimentally relevant parameters we see that while we get very close to saturating the inequality we never violate it, see Fig. 14.2c.

In Refs. [169, 170] it has been theoretically shown that serial double QD heat engines can violate the TUR. While the presence of coherences does not guarantee violations, we can find regimes where violations occur. An example system where coherences play a significant role is a serial double QD, see Fig. 14.2b. Fig. 14.2d shows calculations using the Lindblad approach (that was also used in paper 1) for Coulomb interaction strength $U = 250\Gamma$ and temperatures $T_L = 100\Gamma$, $T_R = 150\Gamma$. For a large range of gate voltages the TUR is clearly fulfilled, i.e., the left hand side is clearly bigger than two. There are, however, two intervals where the relations are close to saturated and the inset clearly shows, that they are in fact violated. Note that the violations here are small. We have not tuned the system for maximal violations, so it is possible, that the model parameters can be optimized for bigger violations. In contrast to Refs. [169, 170], that use non-interacting transmission functions, we have included electron-electron interactions. A comparison of different ap-

proaches and investigation of the TURs in a serial double QD system without temperature bias has recently been done [171].

15 Summary and discussion of paper II

Coherences are not the only effect that can lead to violations of the TURs. Another effect that is not considered in the original derivations [64, 167, 168] is higher order tunneling contributions. Refs. [169, 170] show that including them can lead to violations. In paper II the aim was to investigate the TURs using the second order RTD approach outlined in Sec. 9, where processes up to cotunneling order are considered.

Figure 14.1 shows the transport properties of the Anderson dot heat engine described by the Hamiltonian H_{AD} in Eq. (11.12). In previous works [35, 36] the optimal efficiency and power of such a heat engine has been investigated, with the result that second order is necessary to accurately model this system as a heat engine. This gives the motivation for paper II to investigate the noise and the TURs. In Fig. 15.1 we plot the the left hand side C of the TUR Eq. (14.12) for the same parameters and in the same regime as earlier in Fig. 14.1. The minima of C in the two heat engine lobes indicated by the stars are close to zero bias, where the power output is approaching 0. For the chosen parameters the minima are far from saturating the TUR, in contrast to the sequential tunneling results from Fig. 14.2c(c). The parameters in either case are not optimized to minimize C.

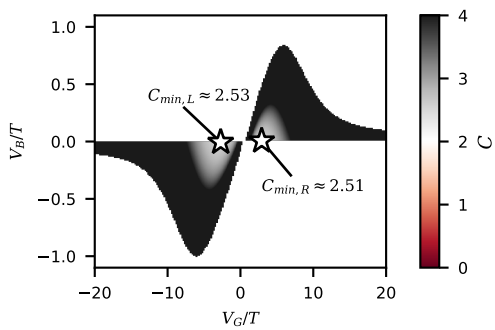

Figure 15.1: Left hand side C of the TUR for the same parameters as in Fig. 14.1. The stars indicate the minima $C_{min,L} \approx 2.53$ in the left and $C_{min,R} \approx 2.51$ in the right power lobe.

In paper II, instead of the minima of the TUR we focus on the maximum power point in the heat engine regime, as this is where one would realistically want to operate. This point is not necessarily fixed in gate-bias space when varying parameters. Here, we vary the tunnel couplings Γ and the temperature bias ΔT. In Fig. 15.2(a) and (b) we show the position of the maximum power point in gate-bias space for varying Γ and ΔT respectively. Note that for varying Γ, see Fig. 15.2(a), the maximum power point for the first order results does not

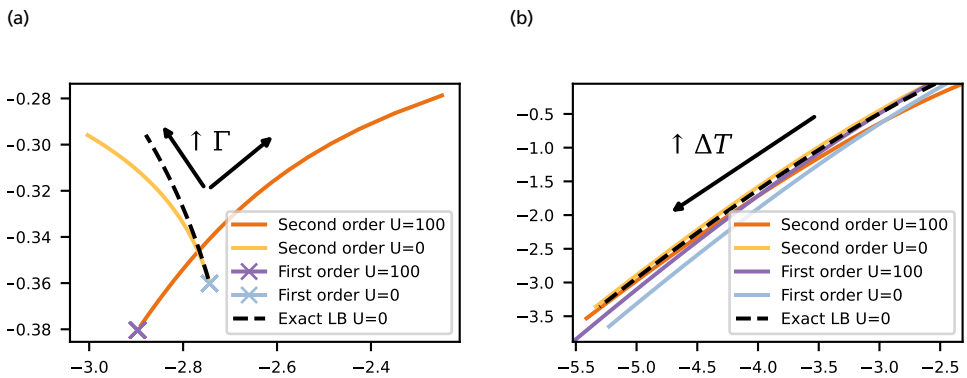

Figure 15.2: Position of the maximum power point in gate-bias space when varying (a) the tunnel coupling $0 < \Gamma \leq 0.4$ and (b) temperature difference $0 < \Delta T \leq 3$. The arrows indicate the change in position when increasing the Γ and ΔT respectively. Adapted from paper II.

move. This is due to the fact that the current in first order simply scales with Γ. Here, also the difference between Coulomb interaction being present or not can clearly be seen. For varying temperature difference there is no large difference in the overall trend between the different parameters and approaches. In all cases the maximum power point moves towards larger bias and gate voltages, see Fig. 15.2(b)

Using an appropriate resistance to cross through the maximum power when sweeping the gate voltage at fixed Γ and ΔT we find two important results. First, the Fano factor $F = |S/I|$, which is directly proportional to C, for this sweep is increased for second order. While in the heat engine regime second order tunneling processes decrease both current and noise, the current is affected more strongly, leading to an enhanced Fano factor. Second, the efficiency is also decreased. This is due to the decoupling of particle and heat current leading to a non-vanishing heat current at the current inversion point [35]. While in sequential tunneling the QD heat engine can in principle reach Carnot efficiency (at vanishing power output) the decoupling in second order prevents that. These two effects of second order prevent us from saturating (as well as from breaking) the TUR in this configuration. The gate sweeps are shown in Figs. 15.3(a) and (b). Both effects are also visible when comparing the transport quantities at the maximum power point for different tunnel couplings, as shown in Fig. 15.3(c) and (d). The Fano factor increases and the efficiency decreases with increasing tunnel couplings Γ. The opposite happens when the temperature bias is increased, i.e., the Fano factor decreases while the efficiency increases, as can be seen in Fig. 15.3(e) and (f). However, this is not enough to counteract the effects of second order. The bounds appear generally closer to saturation for sequential tunneling.

Additionally to the comparison with sequential tunneling we also investigate the effect of Coulomb interaction on the quantities. We compare master equation results for no

interaction $U = 0$ and $U = 100T \gg T, \Gamma$ with non-interacting scattering theory (for $U = 0$ only). The results for $U = 0$ reproduce the non-interacting scattering theory results well for a large range of parameters. Increasing Γ leads to larger deviations, as expected. In particular the comparison between the non-interacting cases shows that it is important to go to second order, even for relatively small Γ, especially around the blockaded regimes where sequential tunneling processes are exponentially suppressed.

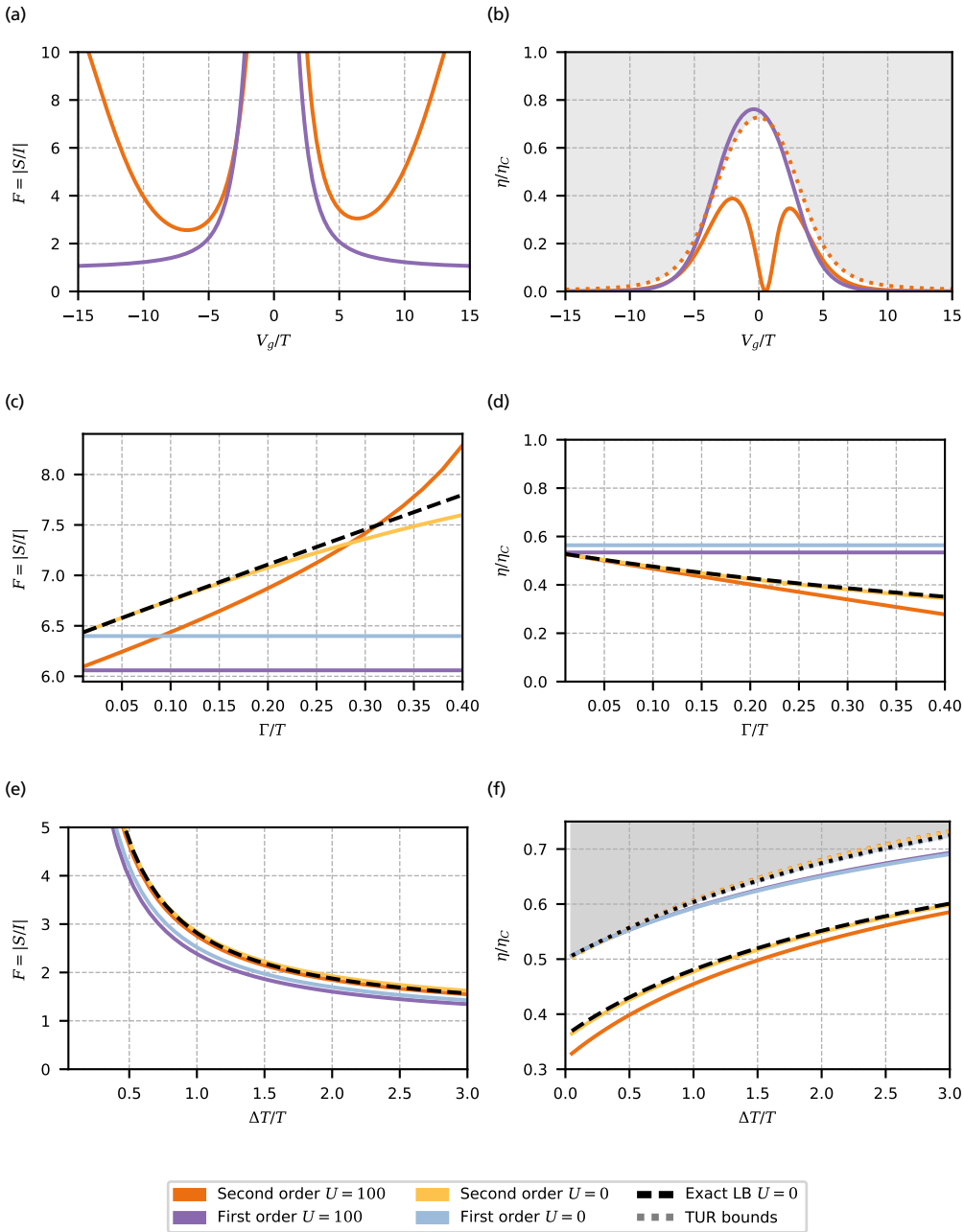

Figure 15.3: (a) Fano factor F and (b) efficiency η/η_C for a gate sweep with fixed resistance, $\Gamma = 0.25$ and temperature bias $\Delta T = 0.3T$. (c) and (d) show the Fano factor and efficiency, respectively, for varying Γ at fixed $\Delta T = 0.3$. (e) and (f) show the Fano factor and efficiency, respectively, for varying ΔT at fixed $\Gamma = 0.25$. Adapted from paper II.

Topological insulators and transport through edge states

In the following we give a short introduction to some concepts that are important for the understanding of paper III. We start with introducing the Bernevig-Hughes-Zhang (BHZ) Hamiltonian. Subsequently we briefly introduce some fundamental theoretical tools we use, namely Floquet theory following Refs. [172–174] and the general concept of Green's functions. The application of Green's functions to periodically driven systems will connect to Floquet theory and result in the main equations we are using in paper III to access the Green's function. We then outline how we can extract information about the spectral and transport properties from the Green's function and finally discuss some aspects of paper III more closely.

16 The BHZ Hamiltonian

The BHZ model is a theoretical description of quantum spin Hall insulators proposed in 2006 [24]. The full Hamiltonian for an infinite two dimensional plane reads [76]

$$H_{\mathrm{BHZ}} = \begin{pmatrix} h\left(\vec{k}\right) & 0 \\ 0 & h^*(-\vec{k}) \end{pmatrix}, \tag{16.1}$$

$$h\left(\vec{k}\right) = \epsilon\left(\vec{k}\right) + \sum_i d_i\left(\vec{k}\right)\sigma_i, \tag{16.2}$$

$$\epsilon\left(\vec{k}\right) = C - D(k_x^2 + k_y^2), \tag{16.3}$$

$$d_i\left(\vec{k}\right) = \left[Ak_x, -Ak_y, M\left(\vec{k}\right)\right], \tag{16.4}$$

$$M\left(\vec{k}\right) = M - B(k_x^2 + k_y^2), \tag{16.5}$$

with the Pauli matrices σ_i. The material parameters A, B, C, D and M depending on the specific quantum well geometry [76]. This Hamiltonian is expressed in the basis $\{|E_+\rangle, |H_+\rangle, |E_-\rangle, |H_-\rangle\}$, where $E_\pm$ and $H_\pm$ are the relevant electron and hole bands in the quantum well, respectively. The states $|E_\pm\rangle$ and $|H_\pm\rangle$ are degenerate Kramers pairs, leading to the block-diagonal structure. The two blocks are related by time-reversal symmetry and are essentially two copies of the massive Dirac Hamiltonian. In the form of Eq. (16.4) we can see that $M(\vec{k})$ plays the role of a mass term, that determines the splitting of electron and hole bands, composed of a static (Dirac) part M and a momentum dependent (Newtonian) part $B(k_x^2 + k_y^2)$. The system is in a topological state supporting edge states if the ratio $M/B > 0$ [76]. Figure 16.1(a) shows a typical bulk bandstructure for the BHZ Hamiltonian in a topological regime with the edge states with different spin polarization indicated in different colors. At the phase transition point, see Fig. 16.1(b), the gap is closed when transitioning from the topological into the trivial state. The trivial bandstructure is shown in Fig. 16.1(c).

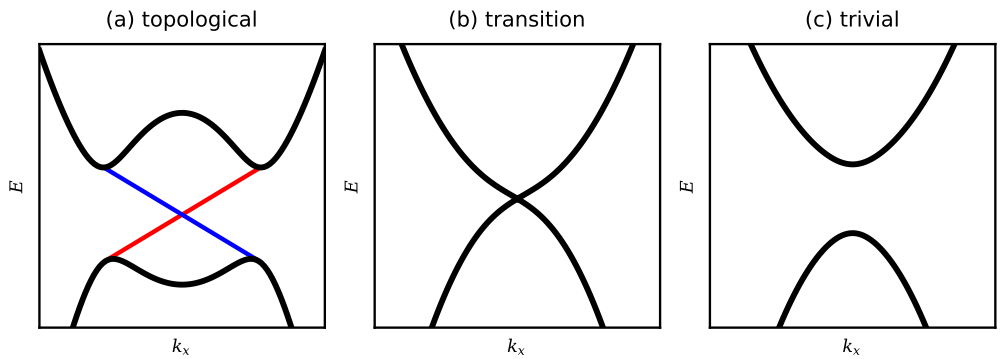

Figure 16.1: Typical bulk bandstructure of the BHZ Hamiltonian (a) in the topological regime, (b) at the transition and (c) in the trivial regime. The edge states in the topological case (a) are indicated in red and blue, where the colors correspond to the two different spin polarizations. Note, that the bulk bands are doubly degenerate.

The 4×4 effective Hamiltonian (16.1) describes the bulk properties of two dimensional topological insulators. If one is interested in the properties of the edge states it is possible to find an effective description for those as well. Solving this Hamiltonian on an infinite half-plane yields two states $\Psi_\uparrow$, $\Psi_\downarrow$ that are localized at the edge [76, 85, 175–177]. As illustrated earlier these two states have opposite spin projection and momentum orientation, so different spins travel in different directions, as illustrated in Fig. 3.1a. This is called spin momentum locking. The direction of spin polarization of the edge states is determined by the sign of A/B [76].

To find the effective edge Hamiltonian the full Hamiltonian (16.1) can be projected onto the edge states $\Psi_\uparrow$, $\Psi_\downarrow$ via $H_{edge}^{\alpha,\beta}(k) = \langle \Psi_\alpha | H_{\mathrm{BHZ}} | \Psi_\beta \rangle$. Assuming a symmetric bulk band

structure, this results in the effective edge Hamiltonian [76]

$$H_{\text{edge}} = Ak_x\sigma_z = \hbar\nu_F k_x\sigma_z. \tag{16.6}$$

This Dirac type Hamiltonian describes two one-dimensional edge states with opposite Fermi velocities on the edge of the half plane and can be applied if the considered energies lie within the bulk band gap of the full BHZ Hamiltonian (16.1). The edge state dispersion is indicated in red and blue in the bulk band gap in Fig. 16.1.

17 Floquet theory

Floquet theory is a formalism developed to solve time-periodic differential equations. As such it is very useful to treat time-periodic Hamiltonians $H(t+T) = H(t)$. The foundation of Floquet theory is the Floquet theorem, that similar to the Bloch theorem [178] for space-periodic functions, predicts the existence of solutions for the time-periodic case. A main advantage is that it avoids so-called secular terms, that are not periodic in time. Secular terms frequently appear when applying Raighley-Schrödinger perturbation theory [172] and are artifacts of the perturbation theory. Since they are not present in Floquet theory, it intrinsically respects the time-periodicity of the system.

Here we briefly introduce the core concepts of this formalism. More details can be found in Refs. [172–174]. To solve the time dependent Schrödinger equation we can invoke the Floquet theorem, which states that there exist solutions of the form

$$\psi_\alpha(t) = \exp\left(-\mathrm{i}\frac{\epsilon_\alpha}{\hbar}t\right)\Phi_\alpha(t). \tag{17.1}$$

These are called Floquet-state solutions and consist of the quasi-energy exponential $\exp(-\mathrm{i}\epsilon_\alpha/\hbar t)$ and the time-periodic Floquet modes $\Phi_\alpha(t) = \Phi_\alpha(t+T)$. The Floquet-state solutions live in a composite Hilbert space $\mathcal{R}\otimes\mathcal{T}$, composed of the space $\mathcal{R}$, spanned by the eigenfunctions of the time-independent part of the Hamiltonian and the T-periodic functions $\mathcal{T}$. We can solve for the Floquet modes in the composite space, where the difference is essentially that we decomposed the time-dependence of the system into Fourier components and get a block of the dimension of the original system for each Fourier component. In practice this blows up the matrix dimension in calculations, which means it comes at a numerical cost. As long as we can truncate at small enough Fourier indices this poses no problem for numerical simulations.

With the Floquet modes, we can calculate the time evolution of any initial state $|\psi(0)\rangle$ as

$$|\psi(t)\rangle = \sum_\alpha c_\alpha \exp(-i\varepsilon_\alpha t/\hbar)\,|\Phi_\alpha(t)\rangle\,, \tag{17.2}$$

where $c_\alpha = \langle\Phi_\alpha(0)|\psi(0)\rangle$ [172].

18 Green's function formalism

Green's functions are a mathematical tool to solve differential equations[179]. They can be applied in many fields of physics, e.g., geophysics [180], acoustics [181], particle physics [182], and many more. We are interested in their application in solid state systems, where they can be used to solve the Schrödinger equation. In the transport setups we are thinking about, we are often interested in the response of the system to an excitation, such as an incoming electron. The Green's function describes exactly this response of the system [183]. The single particle Green's function approach we use here is conceptually simple and connects naturally to scattering theory [8]. In particular, the retarded Green's function [8, 183] is often called a propagator since a physical interpretation of it is that it "propagates" the wave function [184] in space and/or time. Given a basis of incoming wave functions the scattering matrix containing transmission and reflection coefficients can readily be extracted [185]. In contrast to master equations that we introduce in section 6 to analyze transport in QD systems, the approach we use here does not contain interactions between electrons. The propagator simply describes how a single electron moves in the system. While it is in principle possible to also include interactions [179] and write scattering-type expressions for the transmission, in practice it quickly becomes impossible to find the Green's function and approximations need to be made. In this section we introduce the basic concept of non-interacting Green's functions and extend it to time-periodic systems. We also highlight the connection to wave functions and outline how to extract transport properties from them.

18.1 Green's functions

Green's functions are a well know method in solid state physics. More detailed introductions can, e.g., be found in Refs. [183, 184], on which this short introduction is based.

Mathematically, Green's functions are fundamental solution to the Schrödinger equation

$$(H - \mathrm{i}\hbar\partial_t)\psi(t) = 0. \tag{18.1}$$

For the non-interacting case the so-called retarded Green's function can be defined as a solution of the equation of motion,

$$[i\hbar\partial_t - H(\vec{r})]\, G^R(\vec{r}, t; \vec{r}', t') = \delta(t - t')\delta(\vec{r} - \vec{r}'). \tag{18.2}$$

If the Hamiltonian has matrix structure due to, e.g., spin, the Green's function will inherit this matrix structure. We can explain the name *retarded* Green's function by looking at the effect of it on a known wave function ψ at time t' via the integral equation

$$\psi(\vec{r}, t) = \int \mathrm{d}t'\ \mathrm{d}\vec{r}'\, G^R(\vec{r}, t; \vec{r}', t')\psi(\vec{r}', t'). \tag{18.3}$$

We see that G^R propagates the wave function forward in time to t depending on the wave function at time t', hence the name. In the following chapters we will omit the superscript and simply refer to it as the Green's function. On the one hand, this relation to the propagation of states explains why the Green's function is interesting for calculations of transport properties. It is therefore also closely related to the scattering matrix as we will discuss later in this section. On the other hand, this relation also explains the similarities between the Floquet theory discussed earlier and the Green's functions for time-periodic Hamiltonians we will discuss now.

18.2 Green's functions for time periodic Hamiltonians

Here we give a short overview of a procedure closely related to Floquet theory to calculate the Fourier components of the Green's function for a time-periodic Hamiltonian. It has been used in paper III and a detailed description can be found in Ref. [100].

For a general time dependent Hamiltonian $H(t) = H_0 + V(t)$ we can write the integral equation of motion for the Green's function

$$G(t,t') = g(t-t') + \int \mathrm{d}t_1\, g(t-t_1)V(t_1)G(t_1,t'), \tag{18.4}$$

where $g(t-t')$ is the free Green's function. The free Green's function $g(t-t')$ is determined by the free equation of motion

$$[i\hbar\partial_t - H_0]g(t-t') = \delta(t-t'). \tag{18.5}$$

Note, that for convenience we suppress the spatial dependence. If $V(t)$ is periodic, i.e. $V(T+t) = V(t)$, the Green's function $G(t,t')$ can be shown to be periodic in t' and t. That allows us to Fourier transform to the energy domain in t' and expand as a Fourier series in t. As a result the Green's function can be written as

$$\tilde{G}(t,E) = \sum_{n\in\mathbb{Z}} e^{in\frac{2\pi}{T}t}\tilde{G}_n(E), \tag{18.6}$$

where the Fourier components $\tilde{G}_n(E)$ can be calculated as

$$\tilde{G}_n(E) = \tilde{g}(E)\delta_{n,0} + \tilde{g}(E-n\hbar\Omega)\sum_m V_m\tilde{G}_{n-m}(E). \tag{18.7}$$

Here $\tilde{g}(E)$ is the Fourier transform of the free Green's function $g(t-t')$. This general set of coupled equations can be written as a matrix equation and solved numerically. We then have access to the Fourier components of the Green's function.

19 Extracting transport properties from the Green's function

The nature of the Green's function as a propagator for the wave function suggests an underlying connection to the transport properties of the system. Indeed we can extract useful information from the Green's function, as outlined in the following subsections.

19.1 Density of states

The density of states is an experimentally accessible property of mesoscopic systems. It describes the number of states in an infinitesimal interval around a given energy [8, 19, 184] and can be found from the Green's function via taking the trace

$$\mathcal{D}(E,t) = -\frac{1}{\pi}\mathrm{Im}\,\mathrm{Tr}\,\tilde{G}(t,E). \tag{19.1}$$

For practical purposes we are interested in the time-averaged density of states. When taking the time average over Eq. (18.6) all Fourier components except $\tilde{G}_0(E)$ will average out due to the complex exponentials, so the time-averaged density of states can be calculated as

$$\bar{\mathcal{D}}(E) = -\frac{1}{\pi}\mathrm{Im}\,\mathrm{Tr}\,\tilde{G}_0(E). \tag{19.2}$$

For a system without impurities, the density of states turns out to be flat.

19.2 Transmission

In addition to the previous topics that were covered in more detail in Ref. [100], paper III also investigates transport properties of the system. While Ref. [186] describes the procedure to get the scattering matrix from the Green's function by propagating an initial state from one lead of a multi-terminal system to another, Ref. [185] introduces the Floquet-scattering matrix, which is the appropriate scattering matrix for driven systems. Paper III (specifically section IID) describes how to combine these two building blocks into a scattering theory similar to Baranger and Stone [186] for time periodic driving to extract the transmission via the Floquet-scattering matrix calculated from the Fourier expansion of the Green's function.

The cornerstones of the derivation are the propagation of a basis of initial states via the space-dependent Green's function. Decomposing the outgoing state into the appropriate basis states results in Floquet-scattering matrix elements $S^F_{RL}(E',E)$ for scattering from the *left* to the *right* lead. The energy arguments play an important role here, as these matrix elements describe the scattering amplitude for an incoming mode with energy E' to the outgoing mode at the other lead with energy E. In the case of a harmonically driven system

the energy difference $\Delta E = E - E'$ will correspond to energy quanta of the driving absorbed during transmission, i.e., if the system is driven harmonically with frequency Ω, then $\Delta E = n\hbar\Omega$ with an integer n.

The transmission is simply the absolute square of the Floquet scattering matrix, but depends on the absorbed energy as well according to

$$T_{RL}^{(n)}(E) = |S_{RL}^{F}(E', E)|^2 \qquad \text{with} \qquad E' - E = n\hbar\Omega. \tag{19.3}$$

With this we can calculate the current and assuming low temperature and small bias extract the total transmission

$$T(E) = \sum_n T_{RL}^{(n)}(E). \tag{19.4}$$

However, that this simplification is only possible if $T_{RL}^{(n)}(E) = T_{LR}^{(n)}(E)$. We can in this approximation interpret the transmission as the sum over transmission channels indexed by the number of absorbed energy quanta n.

19.3 Impurity averaging

In realistic systems we often encounter large amounts of randomly distributed impurities. One can imagine, that a real sample the size of millimeters, even at low doping densities contains a huge number of impurities. In contrast to real systems in a lab, theoretical calculations are restricted by computing power and we can only perform calculations for a much smaller number of impurities. We can get around the numerical limitations by dividing the system into smaller subsystems, that only contain a numerically viable number of impurities, perform the calculations for the smaller subsystems and then average over all subsystems. In general this is possible, if the coherence length of the particles in the system is smaller than the size of the subsystems, i.e., the subsystems need to be uncorrelated [184]. In practice that means that we perform the calculations for many randomly generated impurity distributions and analyze the average of those.

20 Summary and discussion of paper III

In paper III we investigate the behavior of helical edge states of a two dimensional topological insulator in the presence of impurities on the edge. The impurities have a scalar electrical potential as well as a time-reversal symmetry breaking magnetic moment. This breaking of time-reversal symmetry enables backscattering from one of the counter-propagating

edge states into the other and can thus open a gap in the density of states and also impact the transmission. The effective edge Hamiltonian including the delta impurities reads

$$H(t) = \hbar v_F k_x \sigma_z + \sum_j (V\sigma_0 + \boldsymbol{M}(t)\cdot\boldsymbol{\sigma})\delta(x - x_j), \tag{20.1}$$

where v_F is the Fermi velocity, V is the static potential and the magnetic part of the delta impurities can be expressed as

$$\begin{aligned}
\frac{\boldsymbol{M}(t)\cdot\boldsymbol{\sigma}}{|\boldsymbol{M}|} =& M_s\sigma_y && (20.2)\\
&+ \sqrt{1-M_s^2}(\sin(\Omega t)\sigma_x + \cos(\Omega t)\sigma_z) && (20.3)\\
=& M_s\sigma_y + \frac{\sqrt{1-M_s^2}}{2i}(\sigma_x + i\sigma_z)e^{i\Omega t} && (20.4)\\
&- \frac{\sqrt{1-M_s^2}}{2i}(\sigma_x - i\sigma_z)e^{-i\Omega t}. && (20.5)
\end{aligned}$$

For static impurities this has been investigated previously [101]. The results there show, that orienting the magnetic moment of aligned impurities in the x-y-plane leads to a gap opening in the density of states, that is closed by sufficiently large electric potential of the impurities. For impurities pointing along the z-direction there is no gap.

We now look at impurities that are are aligned and their magnetic moment rotates in the x-z-plane, i.e., from a direction that results in a gap in the static case to one that doesn't and back. Depending on the drive speed we find and explain different gaps in the time averaged density of states and reduced transmissions that, similar to the static case, close with increasing scalar potential.

To calculate the Green's functions describing propagation between arbitrary $\bar{x}_1$ and $\bar{x}_N$ positions on the edge we start from the matrix Eq. 18.7 which for harmonic driving can be written out as

$$\begin{pmatrix}
\ddots & \ddots & & & \\
\ddots & 1-\tilde{g}(E+\hbar\Omega)V_0 & -\tilde{g}(E+\hbar\Omega)V_+^\dagger & & \\
& -\tilde{g}(E)V_+ & 1-\tilde{g}(E)V_0 & -\tilde{g}(E)V_+^\dagger & \\
& & -\tilde{g}(E-\hbar\Omega)V_+ & 1-\tilde{g}(E-\hbar\Omega)V_0 & \ddots \\
& & & \ddots & \ddots
\end{pmatrix}
\begin{pmatrix} \vdots \\ \tilde{G}_{-1}(E) \\ \tilde{G}_0(E) \\ \tilde{G}_1(E) \\ \vdots \end{pmatrix}
=
\begin{pmatrix} \vdots \\ 0 \\ \tilde{g}(E) \\ 0 \\ \vdots \end{pmatrix}. \tag{20.6}$$

Explicitly including the spacial dependence we get

$$\tilde{G}_n(E;\bar{x}_1,\bar{x}_N) = \tilde{g}(E;\bar{x}_1,\bar{x}_N)\delta_{n,0} + \sum_{m=0,\pm1}\sum_{k=1}^{N_{imp}} \tilde{g}(E_n;\bar{x}_1,x_k)U_m\tilde{G}_{n-m}(E;x_k,\bar{x}_N). \tag{20.7}$$

We can substitute $\bar{x}_1 = x_k$ in Eq. (20.7) and use the explicit form of the free Green's function [101],

$$\tilde{g}(E;x,x') = U_V(x,x')g_0(x-x',E), \tag{20.8}$$

$$U_V(x,x') = e^{i\frac{\sigma_z}{\hbar\nu_F}\sum_l V_l(\theta(x-x_l)-\theta(x'-x_l))} \tag{20.9}$$

$$g_0(x-x',E) = \frac{-i}{2\hbar\nu_F}\left[e^{\frac{E(x-x')}{\hbar\nu_F}}\theta(x-x')(1+\sigma_z) + e^{-\frac{E(x-x')}{\hbar\nu_F}}(1-\theta(x-x'))(1-\sigma_z)\right], \tag{20.10}$$

to find the $\tilde{G}_{n-m}(E;x_k,\bar{x}_N)$ numerically for each k. With those we can finally calculate $\tilde{G}_n(E;\bar{x}_1,\bar{x}_N)$.

Note here that the free Green's function has dimension 2×2 due to spin, so in total the blocks of Eq. (20.6) have dimension $2N_{imp}\times 2N_{imp}$. This makes it very clear that the number of Fourier components has a large influence on the computational cost, since for each additional component we increase the size of the matrix equation by four times the number of impurities.

In paper III we consider N_{imp} impurities in the region $x=0$ to $x=L$. On the one hand, if we set $\bar{x}_1,\bar{x}_N = L/2$ to be the center of the impurity region we can already directly calculate the density of states via Eq. (19.2) On the other hand if we set $\bar{x}_1,\bar{x}_N$ to be the left and tight end of the impurity region, respectively, we calculate the scattering solution as described in paper III and project out the Floquet scattering matrix elements and find the partial transmissions

$$T^{(n)}_{RL}(E) = |S^F_{RL}(E_n,E)|^2 = (\hbar\nu_F)^2\left|\left[\tilde{G}_n(E;L,0)\right]_{\uparrow\uparrow}\right|^2. \tag{20.11}$$

Note here that the transmission is essentially the diagonal matrix elements of the 2×2 Green's function corresponding to one spin polarization, in this case $\uparrow$. This reflects the helicity of the edge states, since outside the impurity region, and in fact also in between the impurities, due to the spin-momentum locking a spin species can only travel in one direction.

Another aspect is that the effective transmission Eq. (19.4) only holds for symmetric partial transmissions. Due to the structure of Green's function this is not necessarily given

for a single impurity distribution, in fact it only holds for impurity distributions symmetric around the center of the impurity region. On the other hand the impurity averaging results in symmetric partial transmission, due to the large number of random impurity distributions.

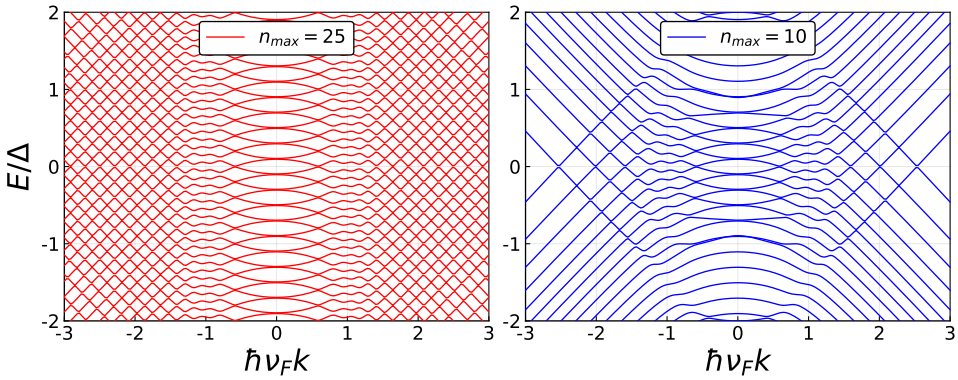

Figure 20.1: Band structure calculated directly from the Floquet-Hamiltonian for a homogeneous dynamic magnetic barrier. Floquet parameters: $\hbar\Omega/\Delta = 0.2$, $n_{max} = 25$ (red) and $n_{max} = 10$ (blue). Adapted from [100]

An important question for the numerical calculations is where to cut of the Fourier series, as this has a big influence on the computation time. On the one hand one can estimate the involved time scales by comparing to relaxation times in a static system, i.e., looking at the time evolution operator for a static system. This estimation is carried out in Ref. [100] and results in $2\Delta/\hbar\Omega \lesssim n_{max}$, where Δ is the expected gap for a average magnetic field corresponding to the impurities, Ω is the driving frequency and n_{max} is the cut-off Fourier index. This also motivates the scaling of energies in terms of the driving frequency we use. On the other hand we can also use intuition from Floquet theory, see section 17. The quasi energies of the Floquet state solutions have to be equally spaced. We can diagonalize the Floquet Hamiltonian for a homogeneous rotating magnetic field exactly to find the "quasi bandstructure". Using a magnetic field strength corresponding to the average over the impurity region, we can determine whether the quasi energy bands are periodic. In Fig. 20.1 we show the band structure for different cut offs n_{max}, where we can clearly see that the energy levels are not periodic for the smaller cut off. This has also been discussed in some detail in Ref. [100] and together these two methods should provide a reliable way to determine a good cut off.

In paper III we calculate the density of states and transmission in different driving regimes and for different scalar potential strength. We find that the time-reversal symmetry breaking impurities lead to gaps opening in the density of states and the transmission. The position and shape of the gap depend on the driving frequency. Specifically in the fast driving case shown in Fig. 20.2c we can see the gaps being formed at half the driving frequency. This can be understood in the context of the Floquet band structures discussed earlier. The

gaps close with increasing scalar potential and similar to the static impurity case [101] a flat density of states is recovered. The transmission shown in Fig. 20.2 for three different driving frequencies flattens slower than the density of states. Note here how the transmission does not approach unity, so the potential part cannot screen the magnetic impurities in a way that fully prevents backscattering.

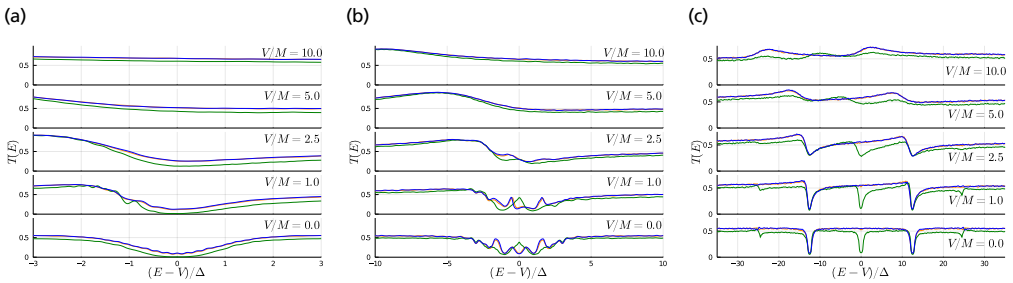

Figure 20.2: Transmission T for (a) slow driving ($\hbar\Omega/M = 0.2$, $n_{max} = 20$), (b) resonant driving ($\hbar\Omega/M = 2$, $n_{max} = 6$) and (c) fast driving ($\hbar\Omega/M = 25$, $n_{max} = 2$) as a function of energy. We show results for different ratios of potential and magnetic part V/M and $M_S = 0.0$ (blue), $MS = 0.1$ (orange), $MS = 0.5$ (green), i.e., 0%/10%/50% of the magnetic part statically pointing along the edge. The remaining model parameters are $|M|/\hbar\nu_F = 0.2$, and $L/l_\Delta = 8.0$ and we averaged over $N_{runs} = 1000$ impurity configurations. Adapted from paper III

Outlook

In this thesis we investigated two very different low dimensional systems using different methods. As paper I and II are the more recent work, this outlook naturally focuses around topics and methods addressed in these works. Specifically, the general implementation of the counting statistics for noise calculations in the QmeQ package can be used for many other things in the future. Here it is worth noting that the implementation of the real time diagrammatics counting statistics at the moment neglects coherences (which were not present in the model we studied in this thesis). This limits the type of systems we can investigate with this approach, but the inclusion of the off-diagonal corrections should be straight forward.

The counting statistics implementation allows for easy access to the zero frequency noise for QD systems. We have used this in the context of a single QD thermoelectric engine in paper II. QmeQ is well suited to aid experimental efforts by modeling data. The general implementation in QmeQ means we could perform calculations on more complicated heat engine systems and investigate the TURs there. Setups one could think of would for example be more complicated multi terminal heat engine devices [57, 187] or the double QD setup from paper I operated as a heat engine. Furthermore, investigating the TURs in a strong coupling regime or even in the Kondo regime, where higher order tunneling plays an important role in the transport, is an interesting topic. In general TURs are a very active topic of research within the quantum thermodynamics community, for example in the search for bounds on the performance of thermal machines [71, 72].

In paper I we also investigated the dynamics of a QD system. Easy access to the kernel in QmeQ also allows us to look at dynamics of noise and TURs for example in the metastable regime, which could be a future direction. Another active area of research is quantum reservoir computing [188, 189], where the dynamic of a complicated quantum system is used to perform calculations. One idea for the realization of such a reservoir is a network of QDs with random parameters. Using for example the chemical potentials as inputs and (transient) currents as outputs, together with a single linear layer of artificial neurons, this system can for example perform memory tasks. We have started to investigate this idea, but

it is not part of this thesis. One could even go one step further and think about tuning the system parameters in order to train the QD network to perform these tasks. This idea is then closer to quantum neuromorphic computing and quantum extreme learning machines.

All in all, the developments in quantum thermodynamics and on QD systems promise a better understanding of fundamental physics in the quantum regime and also possible applications for quantum systems. With this thesis and the contained papers we aim to contribute to this development.

References

[1] D. K. Ferry, *Transport in semiconductor mesoscopic devices* (Institute of Physics Publishing, 12th Aug. 2015), 316 pp.

[2] E. Barrigón, M. Heurlin, Z. Bi, B. Monemar and L. Samuelson, "Synthesis and applications of III–V nanowires", Chem. Rev. **119**, 9170 (2019).

[3] G. Otnes and M. T. Borgström, "Towards high efficiency nanowire solar cells", Nano Today **12**, 31 (2017).

[4] L. M. K. Vandersypen, J. M. Elzerman, R. N. Schouten, L. H. W. van Beveren, R. Hanson and L. P. Kouwenhoven, "Real-time detection of single-electron tunneling using a quantum point contact", Appl. Phys. Lett. **85**, 4394 (2004).

[5] C. Barthel, M. Kjærgaard, J. Medford, M. Stopa, C. M. Marcus, M. P. Hanson and A. C. Gossard, "Fast sensing of double-dot charge arrangement and spin state with a radio-frequency sensor quantum dot", Phys. Rev. B **81**, 161308 (2010).

[6] D. Loss and D. P. DiVincenzo, "Quantum computation with quantum dots", Phys. Rev. A **57**, 120 (1998).

[7] G. Binnig and H. Rohrer, "Scanning tunneling microscopy—from birth to adolescence", Rev. Mod. Phys. **59**, 615 (1987).

[8] S. Datta, *Electronic transport in mesoscopic systems* (Cambridge Univ. Press, Cambridge : 1997).

[9] B. C. Stipe, M. A. Rezaei and W. Ho, "Single-molecule vibrational spectroscopy and microscopy", Science **280**, 1732 (1998).

[10] L. P. Kouwenhoven, D. G. Austing and S. Tarucha, "Few-electron quantum dots", Rep. Prog. Phys. **64**, 701 (2001).

[11] S. M. Reimann and M. Manninen, "Electronic structure of quantum dots", Rev. Mod. Phys. **74**, 1283 (2002).

[12] H. Störmer, R. Dingle, A. Gossard, W. Wiegmann and M. Sturge, "Two-dimensional electron gas at a semiconductor-semiconductor interface", Solid State Commun. **29**, 705 (1979).

[13] D. C. Tsui and R. A. Logan, "Observation of two-dimensional electrons in LPE-grown GaAs-$Al_xGa_{1-x}As$ heterojunctions", Appl. Phys. Lett. **35**, 99 (1979).

[14] C. Berger, Z. Song, T. Li, X. Li, A. Y. Ogbazghi, R. Feng, Z. Dai, A. N. Marchenkov, E. H. Conrad, P. N. First and W. A. de Heer, "Ultrathin epitaxial graphite: 2D electron gas properties and a route toward graphene-based nanoelectronics", J. Phys. Chem. B **108**, 19912 (2004).

[15] Y. Kozuka, A. Tsukazaki, D. Maryenko, J. Falson, S. Akasaka, K. Nakahara, S. Nakamura, S. Awaji, K. Ueno and M. Kawasaki, "Insulating phase of a two-dimensional electron gas in $Mg_xZn_{1-x}O$/ZnO heterostructures below $\nu = 1/3$", Phys. Rev. B **84**, 033304 (2011).

[16] A. T. Johnson, L. P. Kouwenhoven, W. de Jong, N. C. van der Vaart, C. J. P. M. Harmans and C. T. Foxon, "Zero-dimensional states and single electron charging in quantum dots", Phys. Rev. Lett. **69**, 1592 (1992).

[17] T. Mimura, S. Hiyamizu, T. Fujii and K. Nanbu, "A new field-effect transistor with selectively doped GaAs/n-$Al_xGa_{1-x}As$ heterojunctions", Jpn. J. Appl. Phys. **19**, L225 (1980).

[18] P. Grosse, ed., *Festkörperprobleme 23* (Springer Berlin Heidelberg, 1983).

[19] H. Ibach and H. Lüth, *Solid-state physics* (Springer, 2010).

[20] C. Kittel, *Introduction to solid state physics*, 8. ed., [repr.] (Wiley, Hoboken, NJ, 2013), 680 pp.

[21] R. E. Prange and S. M. Girvin, eds., *The quantum hall effect* (Springer New York, 1990).

[22] Q.-Z. Wang, X. Liu, H.-J. Zhang, N. Samarth, S.-C. Zhang and C.-X. Liu, "Quantum anomalous hall effect in magnetically doped InAs/GaSb quantum wells", Phys. Rev. Lett. **113**, 147201 (2014).

[23] C.-X. Liu, S.-C. Zhang and X.-L. Qi, "The quantum anomalous hall effect: theory and experiment", Annu. Rev. Condens. Matter Phys. **7**, 301 (2016).

[24] B. A. Bernevig, T. L. Hughes and S.-C. Zhang, "Quantum spin hall effect and topological phase transition in HgTe quantum wells", Science **314**, 1757 (2006).

[25] J. E. Moore, "The birth of topological insulators", Nature **464**, 194 (2010).

[26] B. A. Bernevig and T. L. Hughes, *Topological insulators and topological superconductors* (Princeton, 2013), p. 247.

[27] R. S. Wagner and W. C. Ellis, "VAPOR-LIQUID-SOLID MECHANISM OF SINGLE CRYSTAL GROWTH", Appl. Phys. Lett. **4**, 89 (1964).

[28] W. Lu and C. M. Lieber, "Semiconductor nanowires", J. Phys. D: Appl. Phys. **39**, R387 (2006).

[29] M. Law, J. Goldberger and P. Yang, "SEMICONDUCTOR NANOWIRES AND NANOTUBES", Annu. Rev. Mater. Res. **34**, 83 (2004).

[30] A. Nozik, "Quantum dot solar cells", Physica E **14**, 115 (2002).

[31] C. Kloeffel and D. Loss, "Prospects for spin-based quantum computing in quantum dots", Annu. Rev. Condens. Matter Phys. **4**, 51 (2013).

[32] F. P. G. de Arquer, D. V. Talapin, V. I. Klimov, Y. Arakawa, M. Bayer and E. H. Sargent, "Semiconductor quantum dots: technological progress and future challenges", Science **373**, eaaz8541 (2021).

[33] M. J. Biercuk, D. J. Reilly, T. M. Buehler, V. C. Chan, J. M. Chow, R. G. Clark and C. M. Marcus, "Charge sensing in carbon-nanotube quantum dots on microsecond timescales", Phys. Rev. B **73**, 201402 (2006).

[34] G. J. Podd, S. J. Angus, D. A. Williams and A. J. Ferguson, "Charge sensing in intrinsic silicon quantum dots", Appl. Phys. Lett. **96**, 082104 (2010).

[35] M. Josefsson, A. Svilans, A. M. Burke, E. A. Hoffmann, S. Fahlvik, C. Thelander, M. Leijnse and H. Linke, "A quantum-dot heat engine operating close to the thermodynamic efficiency limits", Nat. Nanotechnol. **13**, 920 (2018).

[36] M. Josefsson, A. Svilans, H. Linke and M. Leijnse, "Optimal power and efficiency of single quantum dot heat engines: theory and experiment", Phys. Rev. B **99**, 235432 (2019).

[37] M. Josefsson, "Quantum-dot heat engines", PhD thesis (Lund University, 2020).

[38] J. B. Brask, F. Clivaz, G. Haack and A. Tavakoli, "Operational nonclassicality in minimal autonomous thermal machines", Quantum **6**, 672 (2022).

[39] A. Chatterjee, P. Stevenson, S. De Franceschi, A. Morello, N. P. de Leon and F. Kuemmeth, "Semiconductor qubits in practice", Nat. Rev. Phys. **3**, 157 (2021).

[40] S. Miladić, P. Stipsić, E. Dobardžić and M. Milivojević, "Electrical control of a spin qubit in InSb nanowire quantum dots: strongly suppressed spin relaxation in high magnetic field", Phys. Rev. B **101**, 155307 (2020).

[41] J. Yoneda, K. Takeda, T. Otsuka, T. Nakajima, M. R. Delbecq, G. Allison, T. Honda, T. Kodera, S. Oda, Y. Hoshi, N. Usami, K. M. Itoh and S. Tarucha, "A quantum-dot spin qubit with coherence limited by charge noise and fidelity higher than 99.9%", Nat. Nanotechnol. **13**, 102 (2017).

[42] C. Bäuerle, D. C. Glattli, T. Meunier, F. Portier, P. Roche, P. Roulleau, S. Takada and X. Waintal, "Coherent control of single electrons: A review of current progress", Rep. Prog. Phys. **81**, 056503 (2018).

[43] M. Josefsson and M. Leijnse, "Double quantum-dot engine fueled by entanglement between electron spins", Phys. Rev. B **101**, 081408 (2020).

[44] C. Fasth, A. Fuhrer, M. T. Björk and L. Samuelson, "Tunable double quantum dots in InAs nanowires defined by local gate electrodes", Nano Lett. **5**, 1487 (2005).

[45] M. Nilsson, L. Namazi, S. Lehmann, M. Leijnse, K. A. Dick and C. Thelander, "Single-electron transport in InAs nanowire quantum dots formed by crystal phase engineering", Phys. Rev. B **93**, 195422 (2016).

[46] I. Geijselaers, N. Vainorius, S. Lehmann, C. E. Pryor, K. A. Dick and M.-E. Pistol, "Atomically sharp, crystal phase defined GaAs quantum dots", Appl. Phys. Lett. **119**, 263102 (2021).

[47] C. W. J. Beenakker, "Theory of coulomb-blockade oscillations in the conductance of a quantum dot", Phys. Rev. B **44**, 1646 (1991).

[48] P. McEuen, N. S. Wingreen, E. Foxman, J. Kinaret, U. Meirav, M. Kastner, Y. Meir and S. Wind, "Coulomb interactions and energy-level spectrum of a small electron gas", Physica B **189**, 70 (1993).

[49] S. Vinjanampathy and J. Anders, "Quantum thermodynamics", Contemp. Phys. **57**, 545 (2016).

[50] J. Goold, M. Huber, A. Riera, L. del Rio and P. Skrzypczyk, "The role of quantum information in thermodynamics—a topical review", J. Phys. A: Math. Theor. **49**, 143001 (2016).

[51] J. Gemmer, M. Michel and G. Mahler, *Quantum thermodynamics* (Springer Berlin Heidelberg, 2009).

[52] B. Bhandari, P. T. Alonso, F. Taddei, F. von Oppen, R. Fazio and L. Arrachea, "Geometric properties of adiabatic quantum thermal machines", Phys. Rev. B **102**, 155407 (2020).

[53] F. Binder, L. A. Correa, C. Gogolin, J. Anders and G. Adesso, eds., *Thermodynamics in the quantum regime* (Springer International Publishing, 2018).

[54] P. P. Potts, "Quantum thermodynamics", 10.48550/ARXIV.2406.19206 (2024).

[55] T. E. Humphrey, R. Newbury, R. P. Taylor and H. Linke, "Reversible quantum Brownian heat engines for electrons", Phys. Rev. Lett. **89**, 116801 (2002).

[56] A. N. Jordan, B. Sothmann, R. Sánchez and M. Büttiker, "Powerful and efficient energy harvester with resonant-tunneling quantum dots", Phys. Rev. B **87**, 075312 (2013).

[57] B. Sothmann, R. Sánchez and A. N. Jordan, "Thermoelectric energy harvesting with quantum dots", Proc. Spie. **26**, 032001 (2014).

[58] G. Jaliel, R. K. Puddy, R. Sánchez, A. N. Jordan, B. Sothmann, I. Farrer, J. P. Griffiths, D. A. Ritchie and C. G. Smith, "Experimental realization of a quantum dot energy harvester", Phys. Rev. Lett. **123**, 117701 (2019).

[59] O. Arısoy and Ö. E. Müstecaplıoğlu, "Few-qubit quantum refrigerator for cooling a multi-qubit system", Sci. Rep. **11**, 12981 (2021).

[60] P. A. Erdman, B. Bhandari, R. Fazio, J. P. Pekola and F. Taddei, "Absorption refrigerators based on coulomb-coupled single-electron systems", Phys. Rev. B **98**, 045433 (2018).

[61] Y. Zhang and S. Su, "Thermal rectification and negative differential thermal conductance based on a parallel-coupled double quantum-dot", Physica A **584**, 126347 (2021).

[62] L. Tesser, B. Bhandari, P. A. Erdman, E. Paladino, R. Fazio and F. Taddei, "Heat rectification through single and coupled quantum dots", New J. Phys. **24**, 035001 (2022).

[63] K. I. Wysokiński, "Four-terminal quantum dot as an efficient rectifier of heat and charge currents", Phys. Rev. B **107**, 155409 (2023).

[64] A. C. Barato and U. Seifert, "Thermodynamic uncertainty relation for biomolecular processes", Phys. Rev. Lett. **114**, 158101 (2015).

[65] J. M. Horowitz and T. R. Gingrich, "Thermodynamic uncertainty relations constrain non-equilibrium fluctuations", Nat. Phys. **16**, 15 (2019).

[66] A. A. S. Kalaee, A. Wacker and P. P. Potts, "Violating the thermodynamic uncertainty relation in the three-level maser", Phys. Rev. E **104**, l012103 (2021).

[67] G. Guarnieri, G. T. Landi, S. R. Clark and J. Goold, "Thermodynamics of precision in quantum nonequilibrium steady states", Phys. Rev. Research **1**, 033021 (2019).

[68] P. P. Potts and P. Samuelsson, "Thermodynamic uncertainty relations including measurement and feedback", Phys. Rev. E **100**, 052137 (2019).

[69] F. Taddei and R. Fazio, "Thermodynamic uncertainty relations for systems with broken time reversal symmetry: the case of superconducting hybrid systems", Phys. Rev. B **108**, 115422 (2023).

[70] L. Tesser and J. Splettstoesser, "Out-of-equilibrium fluctuation-dissipation bounds", Phys. Rev. Lett. **132**, 186304 (2024).

[71] Y. Hasegawa, "Ultimate precision limit of quantum thermal machines", 10.48550/ARXIV.2412.07271 (2024).

[72] K. Brandner and K. Saito, "Thermodynamic uncertainty relations for coherent transport", 10.48550/ARXIV.2502.07917 (2025).

[73] D. Palmqvist, L. Tesser and J. Splettstoesser, "Combining kinetic and thermodynamic uncertainty relations in quantum transport", 10.48550/ARXIV.2504.04980 (2025).

[74] A. Altland and M. R. Zirnbauer, "Nonstandard symmetry classes in mesoscopic normal-superconducting hybrid structures", Phys. Rev. B **55**, 1142 (1997).

[75] M. Z. Hasan and C. L. Kane, "Colloquium: topological insulators", Rev. Mod. Phys. **82**, 3045 (2010).

[76] X.-L. Qi and S.-C. Zhang, "Topological insulators and superconductors", Rev. Mod. Phys. **83**, 1057 (2011).

[77] J. Alicea, "New directions in the pursuit of majorana fermions in solid state systems", Rep. Prog. Phys. **75**, 076501 (2012).

[78] M. Leijnse and K. Flensberg, "Introduction to topological superconductivity and majorana fermions", Semicond. Sci. Tech. **27**, 124003 (2012).

[79] F. Wilczek, "Majorana returns", Nat. Phys. **5**, 614 (2009).

[80] A. Y. Kitaev, "Unpaired majorana fermions in quantum wires", Phys. Usp. **44**, 131 (2001).

[81] K. v. Klitzing, G. Dorda and M. Pepper, "New method for high-accuracy determination of the fine-structure constant based on quantized hall resistance", Phys. Rev. Lett. **45**, 494 (1980).

[82] B. I. Halperin, "Quantized hall conductance, current-carrying edge states, and the existence of extended states in a two-dimensional disordered potential", Phys. Rev. B **25**, 2185 (1982).

[83] B. A. Bernevig and S.-C. Zhang, "Quantum spin hall effect", Phys. Rev. Lett. **96**, 106802 (2006).

[84] M. König, S. Wiedmann, C. Brüne, A. Roth, H. Buhmann, L. W. Molenkamp, X.-L. Qi and S.-C. Zhang, "Quantum spin hall insulator state in HgTe quantum wells", Science **318**, 766 (2007).

[85] M. König, H. Buhmann, L. W. Molenkamp, T. Hughes, C.-X. Liu, X.-L. Qi and S.-C. Zhang, "The quantum spin hall effect: theory and experiment", J. Phys. Soc. Jpn. **77**, 031007 (2008).

[86] J. H. Bardarson and J. E. Moore, "Quantum interference and aharonov–bohm oscillations in topological insulators", Rep. Prog. Phys. **76**, 056501 (2013).

[87] E. Rossi, J. H. Bardarson, M. S. Fuhrer and S. D. Sarma, "Universal conductance fluctuations in dirac materials in the presence of long-range disorder", Phys. Rev. Lett. **109**, 096801 (2012).

[88] J. Fransson, A. M. Black-Schaffer and A. V. Balatsky, "Engineered near-perfect backscattering on the surface of a topological insulator with nonmagnetic impurities", Phys. Rev. B **90**, 241409 (2014).

[89] A. M. Black-Schaffer, A. V. Balatsky and J. Fransson, "Filling of magnetic-impurity-induced gap in topological insulators by potential scattering", Phys. Rev. B **91**, 201411 (2015).

[90] L. Landau, "Diamagnetismus der metalle", Zeitschrift für Physik **64**, 629 (1930).

[91] G. Grabecki, J. Wróbel, M. Czapkiewicz, Ł. Cywiński, S. Gierałtowska, E. Guziewicz, M. Zholudev, V. Gavrilenko, N. N. Mikhailov, S. A. Dvoretski, F. Teppe, W. Knap and T. Dietl, "Nonlocal resistance and its fluctuations in microstructures of band-inverted HgTe/(hg,cd)te quantum wells", Phys. Rev. B **88**, 165309 (2013).

[92] G. M. Gusev, Z. D. Kvon, E. B. Olshanetsky, A. D. Levin, Y. Krupko, J. C. Portal, N. N. Mikhailov and S. A. Dvoretsky, "Temperature dependence of the resistance of a two-dimensional topological insulator in a HgTe quantum well", Phys. Rev. B **89**, 125305 (2014).

[93] K. C. Nowack, E. M. Spanton, M. Baenninger, M. König, J. R. Kirtley, B. Kalisky, C. Ames, P. Leubner, C. Brüne, H. Buhmann, L. W. Molenkamp, D. Goldhaber-Gordon and K. A. Moler, "Imaging currents in HgTe quantum wells in the quantum spin hall regime", Nat. Mater. **12**, 787 (2013).

[94] A. Roth, C. Brüne, H. Buhmann, L. W. Molenkamp, J. Maciejko, X.-L. Qi and S.-C. Zhang, "Nonlocal transport in the quantum spin hall state", Science **325**, 294 (2009).

[95] I. Knez, R.-R. Du and G. Sullivan, "Evidence for helical edge modes in Inverted-InAs/GaSbQuantum wells", Phys. Rev. Lett. **107**, 136603 (2011).

[96] I. Knez, C. T. Rettner, S.-H. Yang, S. S. Parkin, L. Du, R.-R. Du and G. Sullivan, "Observation of edge transport in the disordered regime of topologically InsulatingInAs/GaSbQuantum wells", Phys. Rev. Lett. **112**, 026602 (2014).

[97] E. M. Spanton, K. C. Nowack, L. Du, G. Sullivan, R.-R. Du and K. A. Moler, "Images of edge current inInAs/GaSbQuantum wells", Phys. Rev. Lett. **113**, 026804 (2014).

[98] K. Suzuki, Y. Harada, K. Onomitsu and K. Muraki, "Edge channel transport in the InAs/GaSb topological insulating phase", Phys. Rev. B **87**, 235311 (2013).

[99] M. He, H. Sun and Q. L. He, "Topological insulator: spintronics and quantum computations", Front. Phys. **14**, 43401 (2019).

[100] S. Wozny, "Gap properties of helical edge states in two-dimensional topological insulators with time-dependent magnetic impurities", MA thesis (Lund University, 2020).

[101] S. Wozny, K. Vyborny, W. Belzig and S. I. Erlingsson, "Gap formation in helical edge states with magnetic impurities", Phys. Rev. B **98**, 165423 (2018).

[102] S. Pradhan and J. Fransson, "Time-dependent potential impurity in a topological insulator", Phys. Rev. B **100**, 125163 (2019).

[103] P. Novelli, F. Taddei, A. K. Geim and M. Polini, "Failure of conductance quantization in two-dimensional topological insulators due to nonmagnetic impurities", Phys. Rev. Lett. **122**, 016601 (2019).

[104] R. Landauer, "Spatial variation of currents and fields due to localized scatterers in metallic conduction", IBM J. Res. Dev. **1**, 223 (1957).

[105] M. Büttiker, "Four-terminal phase-coherent conductance", Phys. Rev. Lett. **57**, 1761 (1986).

[106] Y. Blanter and M. Büttiker, "Shot noise in mesoscopic conductors", Phys. Rep. **336**, 1 (2000).

[107] Y. Meir and N. S. Wingreen, "Landauer formula for the current through an interacting electron region", Phys. Rev. Lett. **68**, 2512 (1992).

[108] A.-P. Jauho, N. S. Wingreen and Y. Meir, "Time-dependent transport in interacting and noninteracting resonant-tunneling systems", Phys. Rev. B **50**, 5528 (1994).

[109] J. Fransson, O. Eriksson and I. Sandalov, "Transport through quasi-degenerate states in coupled quantum dots", Photonics Nanostruct. Fundam. Appl. **2**, 11 (2004).

[110] T. A. Costi, A. C. Hewson and V. Zlatic, "Transport coefficients of the anderson model via the numerical renormalization group", J. Phys. Condens. Matter **6**, 2519 (1994).

[111] W. Metzner, M. Salmhofer, C. Honerkamp, V. Meden and K. Schönhammer, "Functional renormalization group approach to correlated fermion systems", Rev. Mod. Phys. **84**, 299 (2012).

[112] H.-P. Breuer and F. Petruccione, *The theory of open quantum systems* (Oxford University PressOxford, Jan. 2007).

[113] G. Schaller, *Open quantum systems far from equilibrium* (Springer London, Limited, 2014), p. 207.

[114] G. Lindblad, "On the generators of quantum dynamical semigroups", Commun. Math. Phys. **48**, 119 (1976).

[115] D. Manzano, "A short introduction to the lindblad master equation", AIP Advances **10**, 025106 (2020).

[116] G. Kiršanskas, J. Nyvold Pedersen, O. Karlström, M. Leijnse and A. Wacker, "Qmeq 1.0: an open-source python package for calculations of transport through quantum dot devices", Comput. Phys. Commun. **221**, 317 (2017).

[117] G. Kiršanskas, M. Franckié and A. Wacker, "Phenomenological position and energy resolving Lindblad approach to quantum kinetics", Phys. Rev. B **97**, 035432 (2018).

[118] M. Leijnse and M. R. Wegewijs, "Kinetic equations for transport through single-molecule transistors", Phys. Rev. B **78**, 235424 (2008).

[119] K. M. Seja, G. Kiršanskas, C. Timm and A. Wacker, "Violation of onsager's theorem in approximate master equation approaches", Phys. Rev. B **94**, 165435 (2016).

[120] C. Emary, "Counting statistics of cotunneling electrons", Phys. Rev. B **80**, 235306 (2009).

[121] M. Leijnse, "Transport spectroscopy and control of molecular quantum dots", PhD thesis (Aachen, 2009).

[122] V. Gorini, A. Kossakowski and E. C. G. Sudarshan, "Completely positive dynamical semigroups of N-level systems", J. Math. Phys. **17**, 821 (1976).

[123] J. König, H. Schoeller and G. Schön, "Cotunneling at resonance for the single-electron transistor", Phys. Rev. Lett. **78**, 4482 (1997).

[124] H. Schoeller and G. Schön, "Mesoscopic quantum transport: resonant tunneling in the presence of a strong coulomb interaction", Phys. Rev. B **50**, 18436 (1994).

[125] C. Timm, "Tunneling through molecules and quantum dots: master-equation approaches", Phys. Rev. B **77**, 195416 (2008).

[126] I. Weymann, J. König, J. Martinek, J. Barnaś and G. Schön, "Tunnel magnetoresistance of quantum dots coupled to ferromagnetic leads in the sequential and cotunneling regimes", Phys. Rev. B **72**, 115334 (2005).

[127] D. C. Glattli, "Quantum shot noise of conductors and general noise measurement methods", Eur. Phys. J. Special Topics **172**, 163 (2009).

[128] S. Pradhan and J. Fransson, "Shot noise as a probe of spin-correlated transport through single atoms", Phys. Rev. B **97**, 115409 (2018).

[129] L. S. Levitov, H. Lee and G. B. Lesovik, "Electron counting statistics and coherent states of electric current", J. Math. Phys. **37**, 4845 (1996).

[130] R. S. Souto, R. Avriller, R. C. Monreal, A. Martín-Rodero and A. L. Yeyati, "Transient dynamics and waiting time distribution of molecular junctions in the polaronic regime", Phys. Rev. B **92**, 125435 (2015).

[131] W. Belzig and Y. V. Nazarov, "Full counting statistics of electron transfer between superconductors", Phys. Rev. Lett. **87**, 197006 (2001).

[132] R. S. Souto, A. Martín-Rodero and A. L. Yeyati, "Quench dynamics in superconducting nanojunctions: metastability and dynamical Yang-Lee zeros", Phys. Rev. B **96**, 165444 (2017).

[133] R. S. Souto, A. Martín-Rodero and A. L. Yeyati, "Andreev bound states formation and quasiparticle trapping in quench dynamics revealed by time-dependent counting statistics", Phys. Rev. Lett. **117**, 267701 (2016).

[134] Y. V. Nazarov and M. Kindermann, "Full counting statistics of a general quantum mechanical variable", Eur. Phys. J. B **35**, 413 (2003).

[135] A. O. Gogolin and A. Komnik, "Towards full counting statistics for the Anderson impurity model", Phys. Rev. B **73**, 195301 (2006).

[136] C. Flindt, T. Novotný, A. Braggio and A.-P. Jauho, "Counting statistics of transport through coulomb blockade nanostructures: high-order cumulants and non-markovian effects", Phys. Rev. B **82**, 155407 (2010).

[137] C. Flindt, "Electrons in nanostructures– coherent manipulation and counting statistics", PhD thesis (Technical University of Denmark, Aug. 2007).

[138] K. Ptaszyński and M. Esposito, "Thermodynamics of quantum information flows", Phys. Rev. Lett. **122**, 150603 (2019).

[139] F. Nathan and M. S. Rudner, "Universal Lindblad equation for open quantum systems", Phys. Rev. B **102**, 115109 (2020).

[140] M. Leijnse, M. R. Wegewijs and M. H. Hettler, "Pair tunneling resonance in the single-electron transport regime", Phys. Rev. Lett. **103**, 156803 (2009).

[141] S. Mukamel, "Superoperator representation of nonlinear response: unifying quantum field and mode coupling theories", Phys. Rev. E **68**, 021111 (2003).

[142] V. E. Tarasov, "Pure stationary states of open quantum systems", Phys. Rev. E **66**, 056116 (2002).

[143] J. Johansson, P. Nation and F. Nori, "QuTiP: an open-source python framework for the dynamics of open quantum systems", Comput. Phys. Commun. **183**, 1760 (2012).

[144] J. Johansson, P. Nation and F. Nori, "QuTiP 2: a python framework for the dynamics of open quantum systems", Comput. Phys. Commun. **184**, 1234 (2013).

[145] C. W. Groth, M. Wimmer, A. R. Akhmerov and X. Waintal, "Kwant: a software package for quantum transport", New J. Phys. **16**, 063065 (2014).

[146] J. N. Pedersen and A. Wacker, "Tunneling through nanosystems: combining broadening with many-particle states", Phys. Rev. B **72**, 195330 (2005).

[147] J. N. Pedersen, B. Lassen, A. Wacker and M. H. Hettler, "Coherent transport through an interacting double quantum dot: beyond sequential tunneling", Phys. Rev. B **75**, 235314 (2007).

[148] A. Thielmann, M. H. Hettler, J. König and G. Schön, "Cotunneling current and shot noise in quantum dots", Phys. Rev. Lett. **95**, 146806 (2005).

[149] J. Aghassi, "Electronic transport and noise in quantum dot systems", 43.02.01; LK 01; Wissenschaftliche Berichte, FZKA-7343 (September 2007) Dissertation, Universität Karlsruhe 2007, PhD thesis (2007).

[150] Y. Hu, H. O. H. Churchill, D. J. Reilly, J. Xiang, C. M. Lieber and C. M. Marcus, "A Ge/Si heterostructure nanowire-based double quantum dot with integrated charge sensor", Nat. Nanotechnol. **2**, 622 (2007).

[151] H. Kiyama, A. Korsch, N. Nagai, Y. Kanai, K. Matsumoto, K. Hirakawa and A. Oiwa, "Single-electron charge sensing in self-assembled quantum dots", Sci. Rep. **8**, 13188 (2018).

[152] D. Barker, M. Scandi, S. Lehmann, C. Thelander, K. A. Dick, M. Perarnau-Llobet and V. F. Maisi, "Experimental verification of the work fluctuation-dissipation relation for information-to-work conversion", Phys. Rev. Lett. **128**, 040602 (2022).

[153] N. S. Wingreen and Y. Meir, "Anderson model out of equilibrium: noncrossing-approximation approach to transport through a quantum dot", Phys. Rev. B **49**, 11040 (1994).

[154] S. M. Cronenwett, T. H. Oosterkamp and L. P. Kouwenhoven, "A tunable Kondo effect in quantum dots", Science **281**, 540 (1998).

[155] W. G. van der Wiel, S. D. Franceschi, T. Fujisawa, J. M. Elzerman, S. Tarucha and L. P. Kouwenhoven, "The kondo effect in the unitary limit", Science **289**, 2105 (2000).

[156] Y. Cheng, Z. Li, J. Wei, Y. Nie and Y. Yan, "Transient dynamics of a quantum-dot: from Kondo regime to mixed valence and to empty orbital regimes", J. Chem. Phys. **148**, 134111 (2018).

[157] H. Cramér, *Mathematical methods of statistics (pms-9), volume 9* (Princeton University Press, 2016).

[158] A. Bovier, M. Eckhoff, V. Gayrard and M. Klein, "Metastability and Low Lying Spectra in Reversible Markov Chains", Commun. Math. Phys. **228**, 219 (2002).

[159] L. D. Contreras-Pulido, J. Splettstoesser, M. Governale, J. König and M. Büttiker, "Time scales in the dynamics of an interacting quantum dot", Phys. Rev. B **85**, 075301 (2012).

[160] J. Schulenborg, J. Splettstoesser, M. Governale and L. D. Contreras-Pulido, "Detection of the relaxation rates of an interacting quantum dot by a capacitively coupled sensor dot", Phys. Rev. B **89**, 195305 (2014).

[161] K. Wrześniewski, B. Baran, R. Taranko, T. Doma ński and I. Weymann, "Quench dynamics of a correlated quantum dot sandwiched between normal-metal and superconducting leads", Phys. Rev. B **103**, 155420 (2021).

[162] K. Macieszczak, M. Guță, I. Lesanovsky and J. P. Garrahan, "Dynamical phase transitions as a resource for quantum enhanced metrology", Phys. Rev. A **93**, 022103 (2016).

[163] V. Giovannetti, S. Lloyd and L. Maccone, "Advances in quantum metrology", Nat. Photonics **5**, 222 (2011).

[164] P. P. Potts, A. A. S. Kalaee and A. Wacker, "A thermodynamically consistent markovian master equation beyond the secular approximation", New J. Phys. **23**, 123013 (2021).

[165] R. S. Whitney, "Most efficient quantum thermoelectric at finite power output", Phys. Rev. Lett. **112**, 130601 (2014).

[166] R. S. Whitney, "Finding the quantum thermoelectric with maximal efficiency and minimal entropy production at given power output", Phys. Rev. B **91**, 115425 (2015).

[167] T. R. Gingrich, J. M. Horowitz, N. Perunov and J. L. England, "Dissipation bounds all steady-state current fluctuations", Phys. Rev. Lett. **116**, 120601 (2016).

[168] J. M. Horowitz and T. R. Gingrich, "Proof of the finite-time thermodynamic uncertainty relation for steady-state currents", Phys. Rev. E **96**, 020103 (2017).

[169] B. K. Agarwalla and D. Segal, "Assessing the validity of the thermodynamic uncertainty relation in quantum systems", Phys. Rev. B **98**, 155438 (2018).

[170] J. Liu and D. Segal, "Thermodynamic uncertainty relation in quantum thermoelectric junctions", Phys. Rev. E **99**, 062141 (2019).

[171] K. Prech, P. Johansson, E. Nyholm, G. T. Landi, C. Verdozzi, P. Samuelsson and P. P. Potts, "Entanglement and thermo-kinetic uncertainty relations in coherent mesoscopic transport", 2022.

[172] M. Grifoni and P. Hänggi, "Driven quantum tunneling", Phys. Rep. **304**, 229 (1998).

[173] H. Sambe, "Steady states and quasienergies of a quantum-mechanical system in an oscillating field", Phys. Rev. A **7**, 2203 (1973).

[174] J. H. Shirley, "Solution of the schrödinger equation with a hamiltonian periodic in time", Phys. Rev. **138**, B979 (1965).

[175] B. Zhou, H.-Z. Lu, R.-L. Chu, S.-Q. Shen and Q. Niu, "Finite size effects on helical edge states in a quantum spin-hall system", Phys. Rev. Lett. **101**, 246807 (2008).

[176] J. Linder, T. Yokoyama and A. Sudbø, "Anomalous finite size effects on surface states in the topological insulatorBi2se3", Phys. Rev. B **80**, 205401 (2009).

[177] H.-Z. Lu, W.-Y. Shan, W. Yao, Q. Niu and S.-Q. Shen, "Massive dirac fermions and spin physics in an ultrathin film of topological insulator", Phys. Rev. B **81**, 115407 (2010).

[178] F. Bloch, "Über die quantenmechanik der elektronen in kristallgittern", Zeitschrift für Physik **52**, 555 (1929).

[179] H. Haug and A.-P. Jauho, *Quantum kinetics in transport and optics of semiconductors (springer series in solid-state sciences)* (Springer, 2007), p. 362.

[180] E. Pan, "Green's functions for geophysics: a review", Rep. Prog. Phys. **82**, 106801 (2019).

[181] M. A. Jensen, "A recursive green's function technique for acoustic scattering from heterogeneous objects", The Journal of the Acoustical Society of America **103**, 713 (1998).

[182] M. M. Broido, "Green functions in particle physics", Rep. Prog. Phys. **32**, 493 (1969).

[183] S. Doniach and E. H. Sondheimer, *Green's functions for solid state physicists* (Imperial College Press, 9th Jan. 1998), 336 pp.

[184] H. Bruus and K. Flensberg, *Many-body quantum theory in condensed matter physics* (OUP Oxford, 2nd Sept. 2004), 464 pp.

[185] M. V. Moskalets, *Scattering matrix approach to non-stationary quantum transport* (Imperial College Press, London, 2012).

[186] H. U. Baranger and A. D. Stone, "Electrical linear-response theory in an arbitrary magnetic field: a new fermi-surface formation", Phys. Rev. B **40**, 8169 (1989).

[187] J. Monsel, M. Acciai, R. Sánchez and J. Splettstoesser, "Autonomous demon exploiting heat and information at the trajectory level", Phys. Rev. B **111**, 045419 (2025).

[188] K. Fujii and K. Nakajima, "Harnessing disordered-ensemble quantum dynamics for machine learning", Phys. Rev. Applied **8**, 024030 (2017).

[189] K. Nakajima, "Physical reservoir computing—an introductory perspective", Jpn. J. Appl. Phys. **59**, 060501 (2020).

Scientific publications

Paper 1

Metastability and quantum coherence-assisted sensing in interacting parallel quantum dots

S. Matern, K. Macieszczak, **S. Wozny**, M. Leijnse

Physical Review B 107, 125424 (2023)

To access the paper online scan the QR code:

Paper II

Current noise in quantum dot thermoelectric engines
S. Wozny, M. Leijnse
Physical Review B 111, 075422 (2025)

To access the paper online scan the QR code:

Paper III

Dynamic impurities in two-dimensional topological-insulator edge states
S. Wozny, M. Leijnse, S. I. Erlingsson
Physical Review B 104, 205418 (2021)

To access the paper online scan the QR code: